Master Thesis in Reservoir Chemistry

Mechanistic Modeling of Combined Low Salinity Waterflood and Surfactant-Polymer Flooding

Diderik Olav Jarlsby

Centre for Integrated Petroleum Research

Department of Physics and Technology

University of Bergen

June 2018

Acknowledgement

The work presented in this thesis was carried out at the Centre for Integrated Petroleum Research (UNI Research CIPR) at the University of Bergen during the period August 2017 to June 2018.

I would like to express my sincerest gratitude to my supervisor Arne Skauge for his guidance, support and positive attitude throughout the year.

I would also like to thank Nematollah Zamani and Iselin Salmo for all the help regarding the STARS simulator.

Furthermore, I would like to thank my fellow students Trude Sætnan Sæther, Vilde Loug Pedersen and Sivert Mordal Nerbøvik for the numerous discussions and conversations. You created an unforgettable work environment that I will miss dearly.

Last, but not least, I would like to thank my mom and dad for their constant support and encouragement.

Diderik Olav Jarlsby

Bergen, June 2018

Abstract

Flooding experiments have been made to investigating the effects of low salinity brine injection and the combined injection of low salinity surfactant and low salinity polymer solutions. These experiments have shown a large increase in oil recovery compared to traditional, high salinity brine injection. This thesis is a study into the modeling of these hybrid EOR experiments.

The thermal & advanced process simulator STARS from CMG was utilized in mechanistic modeling of low salinity, surfactant and polymer flooding. A history match of differential pressure and oil production was performed to evaluate the functionality of STARS. Wettability alteration was modeled through salinity dependent water/oil relative permeability curves while capillary number was utilized as an interpolation parameter for surfactant relative permeability curves. Due to issues handling a third interpolation parameter, polymer could not be rendered with a dedicated relative permeability set. Instead, its effects were modeled through viscosity, adsorption and inaccessible pore volume.

A new approach to modeling multi- dimensional relative permeability interpolation was investigated. Several aspects were deemed viable, but the presented way of modeling relative permeability of a third component was found to be unusable for the current approach to history matching.

The results showed that the underlying mechanisms of low salinity injection are more complex than wettability alteration alone. Additionally, the low salinity polymer flood and subsequent low salinity waterflood were insufficiently rendered by the current model.

Nomenclature

A	Area	[cm^2]
dA	Infinitesimal change of area	[cm^2]
dP	Differential pressure	[Pa]
dP/dx	Pressure drop over distance x	[cm]
dv/dy	Shear rate	[1/s]
dW	Work	[Nm]
$f_w(S_w)$	Fractional flow of water	Dimensionless
K	Absolute permeability	[mD]
k_i	Effective permeability of phase i	[mD]
k_{ri}	Relative permeability of phase	Dimensionless
$k_{ro}(S_{wi})$	End- point relative permeability of oil	Dimensionless
$k_{rw}(S_{orw})$	End- point relative permeability of water	Dimensionless
M	Mobility ratio	Dimensionless
M°	End- point mobility ratio	Dimensionless
N_c	Capillary number	Dimensionless
P	Pressure	[Pa]
P_c	Capillary pressure	[Pa]
PV	Pore volume	Dimensionless
Q	Volumetric flow	[cm^3/min]
r	Radius	[cm]
S	Saturation	Dimensionless
S_{or}	Residual oil saturation	Dimensionless
S_{wi}	Irreducible water saturation	Dimensionless
u	Darcy velocity	[cm/min]
V	Volume	[cm^3]
θ	Contact angle	[°]
λ	Mobility	[mD/cP]
μ	Viscosity	[cP]
σ	Interfacial tension	[dyne/cm]
τ	Shear stress	[Pa]
φ	Porosity	Dimensionless

Subscripts

abs	Absolute
B	Bulk
c	capillary
g	Gas
c	Capillary
j	component/phase
I	Irreducible/initial/component/phase
o	Oil
p	Pore
r	residual
tot	Total
vol	Volumetric
w	Water
*	Normalized

Abbreviations

LS	Low salinity (-flood)
HS	High salinity (-flood)
SSW	Synthetic sea water (-flood)
LSP	Low salinity, polymer (-flood)
LSS	Low salinity, surfactant (-flood)
LSSP	Low salinity, surfactant and polymer (-flood)
CDC	Capillary desaturation curve
Na^+	Sodium ion
Cl^-	Calcium ion
CIPR	Centre for Integrated Petroleum Research
EOR	Enhanced Oil Recovery
NaCl	Sodium chloride (salt)
STARS	Steam, Thermal and Advanced Processes Reservoir Simulator

STARS Keywords

ADMAXT	Maximum adsorption capacity	[gmol/cm^3]
ADRT	Residual adsorption level	[gmol/cm^3]
ADSCOMP	Indicates component of adsorption function	Name
ADSLANG	Langmuir isotherm coefficients tad1, tad2 and tad3	[gmol/cm^3] Dimensionless
AVISC	Liquid viscosities	[cP]
COMP	Interpolation component name and phase	Name
DISPI/J/K_WAT	Total dispersion coefficients in water phase	[cm/min.m/day?
DTRAPW/N	Wetting or non-wetting phase interpolation parameter	Dimensionless
IFTTABLE	Interfacial tension table input	[dyne/cm]
INTCOMP	Indicate interpolation component	Name
KRINTRP	Interpolation set number	Dimensionless
KRTYPE	Assigns rock- fluid rock type number to each grid block	Dimensionless
LOWER_BOUND	Lower bound of interpolation parameter RPT_INTRP	Dimensionless
PORFT	Accessible pore volume	Dimensionless
RPT	Rock type number	Dimensionless
RPT_INTRP	Specifies interpolation between two rock types	Dimensionless
TUBE-END	Specifies linear flow model of well indices	Dimensionless
UPPER_BOUND	Upper bound of interpolation parameter RPT_INTRP	Dimensionless
VSMIXCOMP	Component using nonlinear viscosity mixing	Dimensionless
VSMIXENDP	Minimum and maximum mole fraction of component	Dimensionless

Table of Contents

List of Figures

List of Tables

1. Introduction

Traditionally oil fields have been flooded with water to maintain reservoir pressure and to displace oil towards the production well. This is a cheap and practical method of oil production. However, due to a low oil recovery factor, and several oil field on the NCS operating at tail production[1], investigations into enhanced oil recovery (EOR) techniques have become of great importance.

In the petroleum industry, there has been a growing interest in low salinity brine injection as an enhanced recovery technique. It has been shown that low salinity brine injection potentially has a positive effect when combined with well-established EOR methods, like surfactant and polymer flooding.

An experimental investigation into the hybrid EOR processes of low salinity, surfactant and polymer flooding, has been conducted at the Centre for Integrated Petroleum Research, CIPR, at the University of Bergen. In this thesis, an attempt was made to simulate this experimental coreflood by utilizing recent developments of modeling multiple component injection. Simulations were performed using the thermal & advanced processes simulator STARS, developed by Computer Modeling Group (CMG).

Chapter 2 contains the theoretical background of general reservoir properties and concepts that this thesis is based on. Chapter 3 presents an introduction of the relevant EOR methods and an accompanying literature study. Chapter 4 contains a wettability study conducted to verify the effects of relative permeability alteration. In chapter 5, a new multiple interpolation routine is reviewed. Chapter 6 presents the approach utilized during modeling and subsequent history match of the aforementioned hybrid EOR experiment. Lastly, chapter 7 contains the final summary and conclusion of this thesis.

2. Theory

In this chapter, the background needed to understand concepts discussed in this thesis is presented.

2.1. Petrophysical properties

2.1.1. Porosity

Porosity is the fraction of void space to bulk volume of a rock. This space, in which reservoir fluids may reside, is called pores and a reservoir rock is therefore also characterized as a porous medium. Porosity depends on grain size, grain shape, grain orientation, packing, cementation and sorting. This is called primary porosity. Porosity that develops through chemical leaching of minerals or a fracture system is called secondary porosity[2].

$$\varphi = \frac{V_p}{V_b} \tag{2,1}$$

Interconnectivity of pores, in a porous medium, is important with regards to fluid flow. Porosity of interconnected pores is called effective porosity.

$$\varphi_{eff} = \frac{V_{p,eff}}{V_b} \tag{2,2}$$

2.1.2. Sautration

Occupying the void space in reservoir rock is reservoir fluid. This pore volume can be represented as the combined volumes of water, oil and gas[2].

$$V_p = V_w + V_o + V_g \tag{2,3}$$

In many cases it is more useful to relate the volume of a given fluid to the total fluid volume. This is called saturation.

$$S_i = \frac{V_i}{V_p}, \ i = w, o, g \tag{2,4}$$

Summing up the fluid saturations, in a given volume, always equates to 1.

$$\sum S_i = 1 \tag{2,5}$$

This implies that to reduce a given saturation there needs to be an increase in the other saturations and/or a decrease in pore volume, e.g. compaction. Hence saturation is a dynamic variable during oil production. As a result of capillary forces, a residual oil saturation is always left in the reservoir, even after production finishes. The amount of this immobile oil is dependent on wettability, recovery methods and reservoir quality/characteristics, some of which will be explained further in this thesis.

2.1.3. Permeability

The capability of flow in a porous medium is called permeability and can be calculated using Darcy's law. The absolute permeability, a constant of the porous medium, is calculated by performing single phase, flow experiments on a core sample. Darcy's law relates volumetric flow rate, Q, cross sectional area perpendicular to flow, A, pressure drop over distance x, dP/dx, fluid viscosity, μ, to absolute permeability, K. The unit of permeability is Darcy, D, and equals $0.9869 \cdot 10^{-12}$ m^2 [2].

$$Q = -A\frac{K}{\mu}\frac{dP}{dx} \tag{2,6}$$

This is the simplest form of Darcy's law. For the equation to be valid, it is assumed that the flow is stationary, horizontal and laminar. Additionally the core is assumed to be 100% saturated by a single, incompressible, fluid, which does not chemically react or exchange ions with the surface of the core.

When multiple fluid phases are present, each phase is assigned an effective permeability dependent on saturation and wettability. This is because fluid flow is obstructed by the presence of other phases. Hence, an increase in a given saturation will lead to an increase in the associated effective permeability. Effective permeability can be described through a generalization of Darcy's law.

$$Q_i = -A\frac{k_i}{\mu_i}\frac{dP_i}{dx},\ i = w, o, g \tag{2,7}$$

The relation between effective permeability and absolute permeability is called relative permeability. Relative permeability is dependent on wettability, fluid distribution, rock properties and saturation history [3].

$$k_{ri} = \frac{k_i}{K},\ i = w, o, g \tag{2,8}$$

2.2. Fluid properties

2.2.1. Viscosity

Viscosity is defined as a fluids internal resistance to flow. It can be calculated as a function of shear stress, τ and shear rate, dv/dy [4]:

$$\mu = \frac{\tau}{dv/dy} \tag{2,9}$$

It follows that viscosity has SI- unit $N \cdot s/m^2$ also known as Poise. Usually, viscosity is given in centipoise, cP, which equals 10^{-3} $N \cdot s/m^2$.

2.2.2. Interfacial tension

In a reservoir, fluid- fluid and fluid- solid electrostatic forces are constantly acting between each other. These forces can both be repulsive and attractive. Attractive forces within and between fluids are referred to as a cohesive forces, while attractive forces between fluids and solids are referred to as adhesive forces. Fluids are immiscible if the intramolecular cohesion is much stronger than the intermolecular cohesion. Because of these force differences, surface area between the fluids is minimized. Extending this area of contact would require work and interfacial tension (IFT) between the two phases can be describes as:

$$\sigma = \frac{dW}{dA} \tag{2,10}$$

When interfacial tension between two phases is equal to or less than zero, the two phases will mix through diffusion. When this is true, the two fluids are miscible [4].

After a waterflood, residual oil is immobile due to high interfacial tension between the water- and oil phase. Water pressure is unable to overcome the required capillary pressure and mobilize the trapped oil. To decrease residual oil saturation, capillary pressure must be reduced. By injecting a surfactant, interfacial tension between oil and water would decrease and lead to a lower capillary pressure, thus mobilizing trapped oil.

2.2.3. Capillary pressure

Capillary pressure, P_c, is the pressure difference between two immiscible fluids. The Laplace equation [4] for a water- wet system describes P_c between oil and water as:

$$P_c = P_{non-wetting} - P_{wetting} = P_o - P_w \tag{2,11}$$

The pressure difference is a consequence of wettability, pore size, pore geometry and surface- and interfacial tensions between the fluids and reservoir rock. Capillary pressure is an important reservoir parameter as it influences properties such as phase saturation and fluid permeability [5].

By describing pore throats as capillary tubes, capillary pressure can be defined by the Young-Laplace equation [6]:

$$P_c = \frac{2\sigma_{ow}\cos\theta}{r} \tag{2.12}$$

where σ is interfacial tension, θ is contact angle and r is pore throat radius.

2.2.4. Wettability

Wettability can be defined as "the tendency of one fluid to spread on or adhere to a solid surface in the presence of other immiscible fluids [3]. In a reservoir, containing oil, water and/or gas, wettability will affect fluid permeabilities, how fluids occupy the pore space and subsequently residual fluid saturation. It is therefore a parameter of great importance. Wettability can be expressed in terms of contact angle between the fluid-fluid interface and the solid surface using Young's equation [4]:

$$\sigma_{is} = \sigma_{js} + \sigma_{ij}\cos\theta_{ij} \tag{2.13}$$

where i and j denotes the two fluids, e.g. oil, water or gas, and s denotes the solid surface. The contact angle is measured through phase j. In a system containing oil and water, contact angle can then be expressed as:

$$\theta_{ow} = \cos^{-1}\frac{\sigma_{os}-\sigma_{ws}}{\sigma_{ow}} \tag{2.14}$$

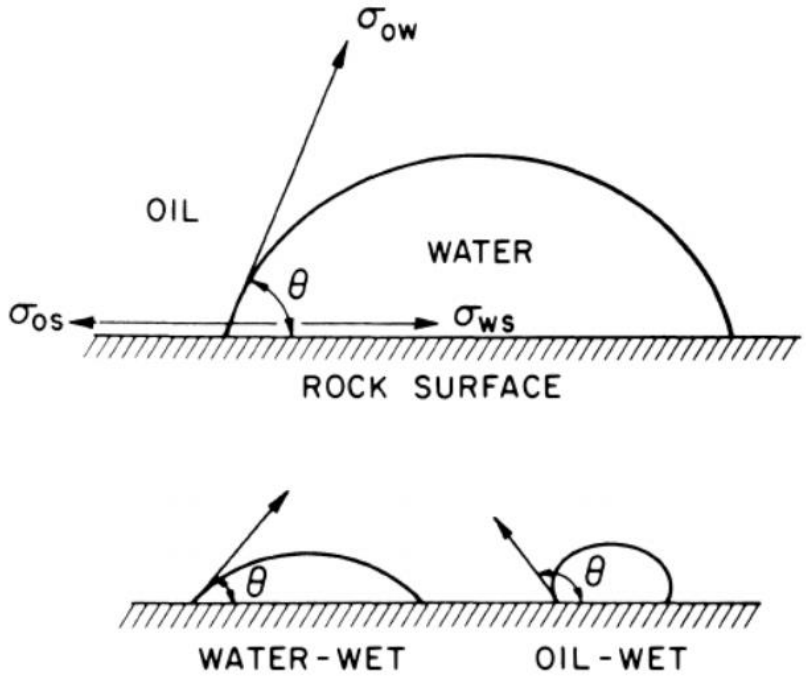

Figure 1.1: Illustration of fluid spreading on a solid surface [7].

As a convention, contact angle is measured over the highest density fluid. Wetting preference of the solid surface is expressed as a function of wetting angle in the following table.

Table 1.1: Wetting preference as a function of wetting angle.

Wetting angle, θ_{ow}	**Wetting preference**
0°- 30°	Strongly water- wet
30°- 90°	Preferentially water- wet
90°	Neutral wet
90°- 150°	Preferentially oil- wet
150°- 180°	Strongly oil- wet

Due to the reservoir rocks affinity to the wetting fluid, said fluid will reside in the smallest pores and against the pore wall. The non- wetting fluid resides in the center of the pores and its flow is therefore less obstructed. When saturation of the wetting fluid rises, the non- wetting fluid might become trapped inside the pore. This can be explained through the pore doublet- and snap- off models where oil is immobilized as a result of capillary forces. From figure 1.2, oil is trapped because water bypasses it in the pore- doublet, leading to a discontinuous oil phase.

From figure 1.3 observe that oil "snaps-off" and becomes discontinuous at the pore throat as water saturation increases.

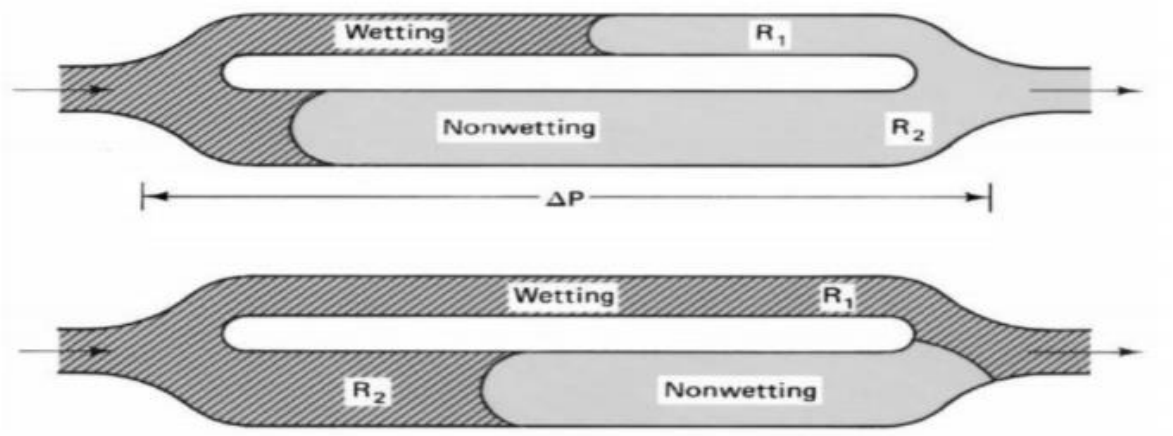

Figure 1.2: Trapping in a pore doublet model [8].

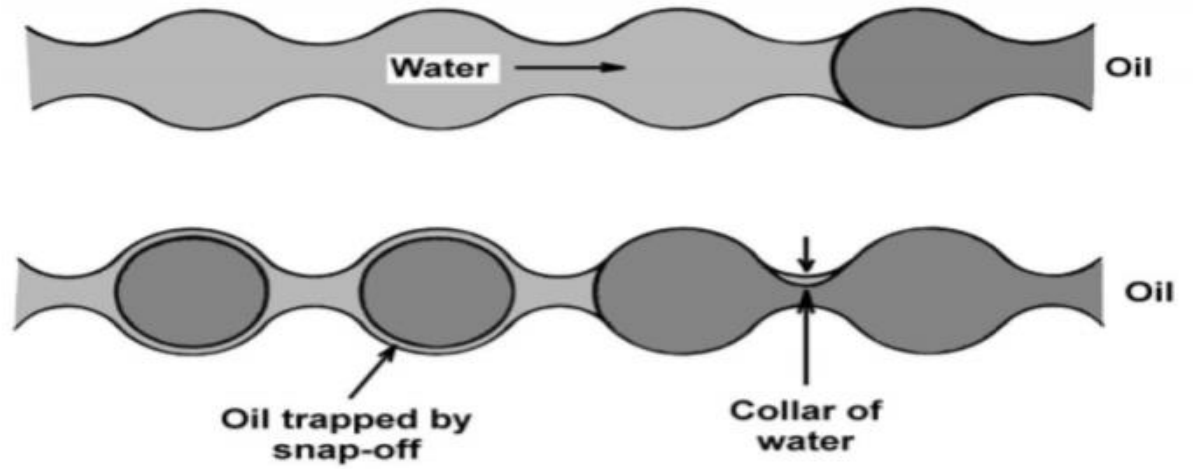

Figure 1.3: Trapping in a snap-off model [8].

These phenomenon lead to a residual oil saturation and also affects the permeability of the mobile, wetting fluid. As can be observed in figure 1.4, relative permeability of the non- wetting fluid will approach 1(absolute permeability) as non- wetting fluid saturation increases.

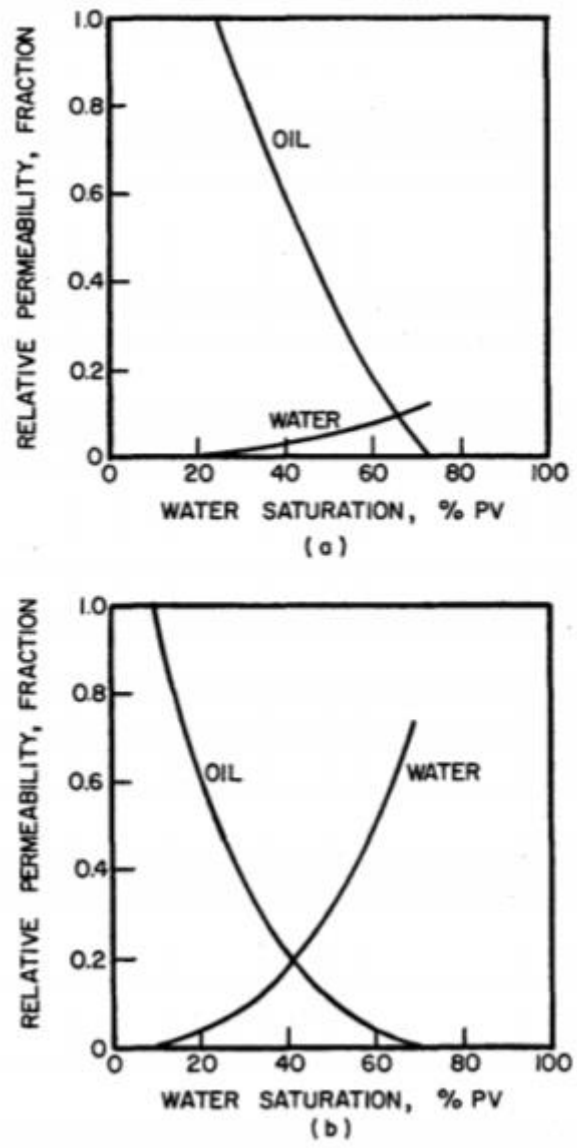

Figure 1.4: Relative permeability curves in a) strongly water- wet cores, and b) strongly oil-wet core [3].

2.2.5. Drainage and Imbibition

Flow processes were fluid saturations change are referred to as either a drainage or an imbibition process. Drainage is when a non- wetting fluid displaces a wetting fluid. The opposite is imbibition, when a wetting fluid displaces a non- wetting fluid. Water injected in an oil- wet system(drainage) has to overcome a threshold capillary pressure in order to invade the largest pores. This can be explained through the Young- Laplace equation. Because of the current wettability and displacement process, the smallest capillary pressures are found in the largest

pores. As water pressure increases, smaller pore sizes are invaded. When an increase in pressure does not lead to more displacement, irreducible oil saturation is reached.

Due to capillary forces, the wetting phase will imbibe into the smallest pores first. For sufficiently small pores, this will happen spontaneously. To invade the larger pores, pressure in the wetting phase must be increased making subsequent imbibition forced.

2.2.6. Mobility and mobility ratio

Mobility of a phase is defined as the ratio between effective permeability and viscosity of the given phase [2]:

$$\lambda_i = \frac{k_i}{\mu_i} = \frac{Kk_{ri}}{\mu_i}, \ i = w, o, g \tag{2,15}$$

Mobility is a measure of fluid flow through a permeable formation.

Mobility ratio, defined as mobility of displacing fluid divided by mobility of displaced fluid, for a waterflood can be represented as:

$$M_{wo} = \frac{\lambda_{displacing}}{\lambda_{displaced}} = \frac{\lambda_w}{\lambda_o} = \frac{k_{rw}\,\mu_o}{k_{ro}\,\mu_w} \tag{2,16}$$

Mobility ratio is generally defined in terms of endpoint relative permeability values. These are relative permeability of water at residual oil saturation (only water is mobile), $k_{rw,or}$, and relative permeability of oil at irreducible water saturation (only oil is mobile), $k_{ro,iw}$.

$$M_{wo}^0 = \frac{\lambda_w^0}{\lambda_o^0} = \frac{k_{rw,or}\,\mu_o}{k_{ro,iw}\,\mu_w} \tag{2,17}$$

During a waterflood, oil is propagated by a waterfront. When the front reaches the production well, the well has a water breakthrough. The oil production will decrease and water production will increase from this point on. The water breakthrough and subsequent oil recovery is dependent on relative permeability and fluid viscosity. Neglecting capillary effects and assuming a horizontal displacement system the fractional flow of water is given by [8]:

$$f_w(S_w) = \frac{1}{1+\frac{k_{rw}\mu_o}{k_{ro}\mu_w}} = \frac{1}{1+\frac{1}{M_{wo}}} \qquad (2,18)$$

Since relative permeability is dependent on wettability, this shows that so too fractional flow.

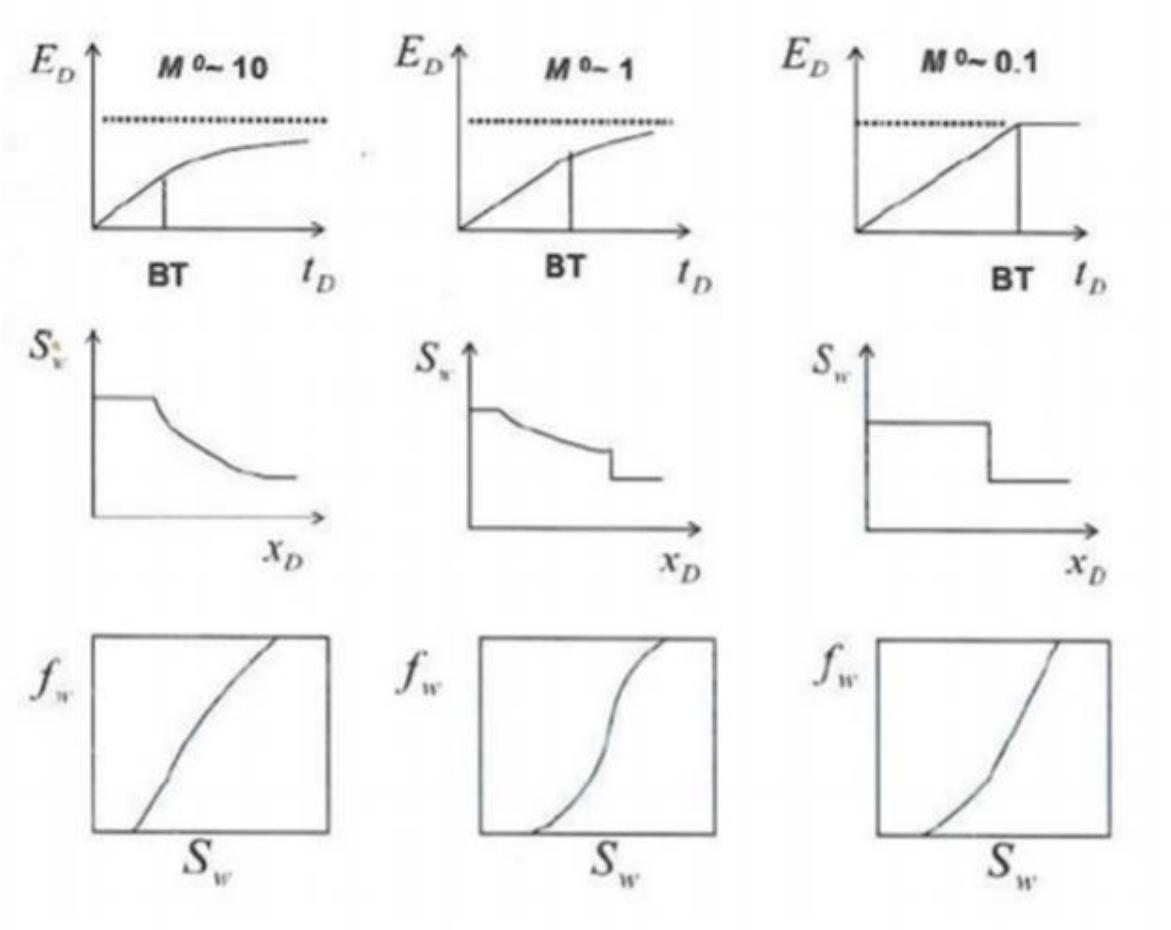

Figure 1.5: The effect of endpoint mobility ratio on displacement efficiency, saturation profile and water fractional flow, dashed lines represents ultimate microscopic recovery efficiency [8].

For high end point mobility ratios, about 10, water breakthrough will come early and lead to a long tail production of oil. In practice, this means that the displacing phase comparatively moves more easily through the reservoir. For end point mobility ratios around 1, water breakthrough happens later. Tail production of oil is shorter. Lastly, the most favorable end point mobility ratio of about 0.1 means that mobility of oil is greater than that of water. Most oil is produced before breakthrough and the tail production is short.

2.2.7. Capillary Number and the Capillary Desaturation Curve

Residual oil saturation is connected to the capillary number, introduced by Brownell et al., 1947) [9],which relates viscous forces to capillary forces. It is often defined as [8]:

$$N_c = \frac{u_w \mu_w}{\sigma_{ow} \cos\theta} \tag{2,19}$$

where N_c is capillary number, u_w is Darcy velocity (u=Q/A) of the displacing fluid, μ_w is the water viscosity, θ is contact angle and σ_{ow} is the interfacial tension between oil and water. The correlation between N_c and residual oil saturation has been shown by Stegemeier (1976) [10], Chatzi and Morrow (1984) [11], Lake (1989) [6] and Mohanty and Salter [12]. This relationships can be visualized through the capillary desaturation curve, CDC. A plateau of S_{or} persists until capillary number reaches a critical value and oil saturation decreases. This happens when capillary forces become sufficiently reduced.

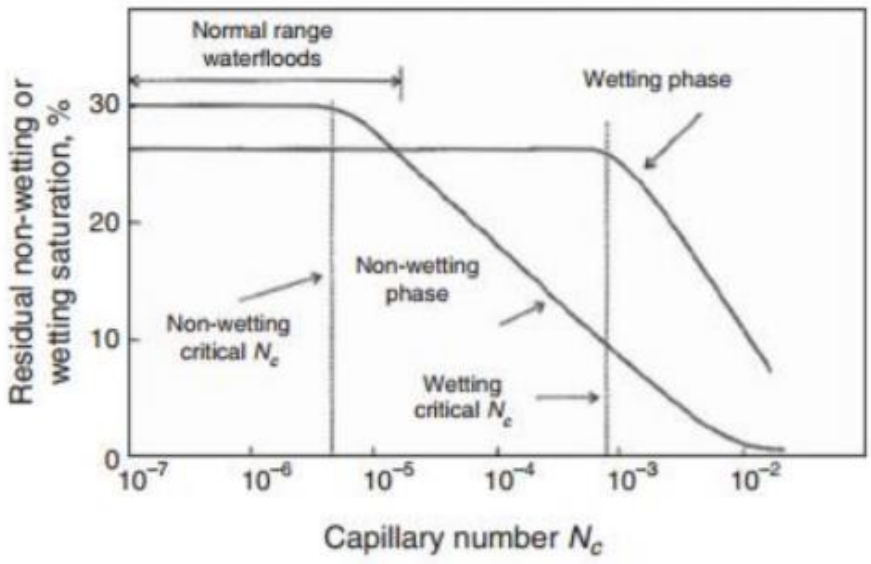

Figure 1.6: Capillary desaturation curve, from Lake (1989) [6].

As seen in figures 1.6 and 1.7 the capillary desaturation curve is affected by wettability preferences and pore size distribution [13].

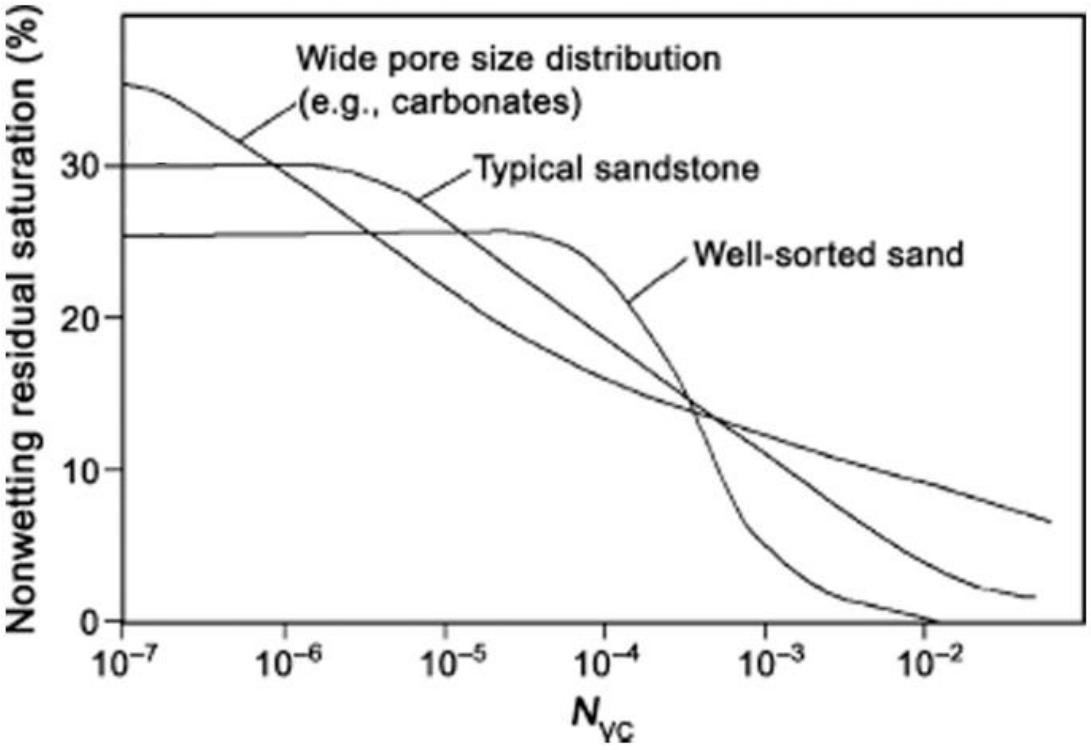

Figure 1.7: Effect of pore size distribution on CDCs, from Lake (1989) [6].

3. Enhanced Oil Recovery

Oil recovery can be defined through the oil recovery factor [8]:

$$E_R = E_D \cdot E_A \cdot E_V = E_D \cdot E_{vol} = \frac{Volume\ oil\ displaced}{Volume\ oil\ contacted} \cdot \frac{Volume\ oil\ contacted}{Volume\ oil\ in\ place} \quad (3,1)$$

Where E_D is the microscopic displacement efficiency and E_{vol} is the volumetric displacement efficiency. Vertical and areal displacement efficiency

Field scale oil recovery is divided into three categories: primary, secondary and tertiary recovery. During primary recovery, the natural drives of the reservoir are utilized to produce oil. As time progresses there will be a reduction in pressure and primary recovery is therefore often referred to as pressure depletion.

Injecting fluids to increase reservoir pressure and improve volumetric sweep efficiency is called secondary recovery. The injected fluids are usually gas, recovered from the reservoir, or sea water.

In Lake (1989), enhanced oil recovery, EOR, is defined as "oil recovery by the injection of materials not normally present in the reservoir" [6]. Even though enhanced oil recovery is usually initiated as a tertiary recovery method, it can potentially be utilized during all phases of production. EOR increases oil recovery by maintaining reservoir pressure, improving oil displacement and/or fluid flow in the reservoir.

In this thesis the focus will be on a hybrid EOR method.

3.1. Low Salinity Waterflooding

The impact of brine composition on oil recovery has been examined since 1942 [14]. Injection brine has historically been selected based on availability. For offshore reservoirs, sea water is abundant and widely used for injection. The salinity of sea water is in the range of 30 000 to 40 000 ppm total dissolved solids while low salinity is typically between 500 and 5000 ppm. The mechanisms leading to increased oil recovery are not fully understood, but the most acknowledged mechanisms are presented in the next chapter.

3.1.1. Previous Studies

In 1967 Bernard [15] observed that oil recovery could be increased by freshwater- flood. He proposed that the mechanism behind the increased production was swelling of clay in the rock, decreasing pore space available, and thereby increasing recovery. Another explanation he had was that freshwater allowed clay to disperse into fine particles. The particles would follow the established flow channels and partially or fully plug them. New flow channels would be established and additional oil recovered, as these channels were flooded.

In 1995 Jadhunandan and Morrow [16] proposed that brine composition can have a significant effect on oil recovery from waterfloods. This was shown by Yildiz and Morrow, in 1996 [17], to be true for their specific study. In 1995 [18] and 1999 [19], Yildiz, Morrow and Valat concluded that the effect of salinity on oil recovery is dependent on the specific crude oil.

Tang and Morrow (1999) [20], presented a study on the effect of salinity on oil recovery by displacement and spontaneous imbibition experiments. Characteristics of the crude oil, reservoir rock and the presence of connate water all had an influence on the impact of low salinity brine on oil recovery. Displacement tests were performed on Berea, Bentheimer, Clashach and CS reservoir cores. Tests were also performed in clean fired and acidized mode on the Berea sandstone to stabilize fines. These experiments showed that brine salinity had no effect on oil recovery when cores were fired and acidized. For the CS and Berea cores, oil recovery by waterflood increased significantly with decrease in salinity. The Clashach and Bentheimer sandstones, which contained less clay, showed that oil recovery was only marginally increased with lowered salinity.

In the experiments of Sharma and Filoco in 1998 [21], it was observed that oil recovery was improved with a reduction in connate water salinity. In 2000 Sharma and Filoco [22] concluded

that this effect could be attributed to wettability alteration from water- wet to mixed- wet conditions.

The effects of low salinity as a secondary and tertiary recovery method was investigated by Zhang and Morrow in 2006 [23]. Improved oil recovery with low salinity brine was observed in both secondary and tertiary mode. Three different crude oils on four Berea sandstone cores were tested. The effect of low salinity varied greatly between the cores suggesting that mineralogy potentially could be the most important factor of oil recovery.

Agbalaka et al. (2009) [24] investigated changes in oil recovery by altering wettability, brine salinity and temperature. It was found that low salinity brine, at both ambient and elevated temperature, resulted in more water- wet conditions. pH of the injected brine could be a decisive factor as high pH brine yielded more water- wet conditions while less water- wet conditions were observed for lower pH brine.

Lager et al. (2008) [25] studied the effects of brine pH on oil recovery. A rise in pH due to carbonate dissolution and cation exchange and subsequent IFT reduction or emulsification and fines migration was observed. The change in pH was found to be an effect rather than the cause of these changes. The primary mechanism of increased oil recovery was found to be cation exchange between the mineral surface and the invading brine. No effect of low salinity water injection on fired and acidized cores was observed as the clay minerals capacity for cation exchange was destroyed. It explained why low salinity had no effect on mineral oils, because there were no polar components present to interact with the clay minerals. And it might be an explanation to why no increased recovery had been observed in carbonate reservoirs during low salinity waterflooding. In addition, it was found that removing Ca^{2+} and Mg^{2+} from the rock surface before waterflooding led to higher recovery regardless of salinity. This confirmed the importance of multicomponent ionic exchange (MIE) as the mechanism behind increased oil recovery during low salinity injection.

Shiran and Skauge (2012) [26] showed that low salinity flooding had a limited increase on recovery from aged neutral- wet Berea cores(0.4% of OOIP) and weakly oil wet Bentheimer cores(2% of OOIP). And showed no increased recovery in strongly water wet Bentheimer cores. This indicated that wettability is more important than clay content for improved oil recovery by low salinity.

Webb et at. (2004) [27] performed a log- inject- log field tests. They demonstrated an increase in oil production after low salinity injection. The work was based on the experimental works of

Tang and Morrow [28] [29] [20], but was the first ever demonstration of low salinity applicability to the near well bore environment.

McGuire et al. (2005) [30] reported the results from four, single well tracer tests performed in Alaskas North slope. Secondary injection of low salinity brine resulted in an incremental oil recovery from 6 to 12 % OOIP.

Vledder et al. (2010) [31] demonstrated, on the Omar field in Syria, that injection of low salinity water altered wettability from oil- wet to a water- wet. This lead to incremental recovery of 10-15% of stock tank oil initially in place (STOIIP).

Secombe et al. (2010) [32] presented a field test trial to demonstrate that reduced- salinity waterlooding worked as well at inter- well distances as it did in corefloods and single well tests. The trial was performed at the Endicott field where a drop in watercut was experienced 3 months after reduced- salinity water injection. The timing of the drop coincided with the breakthrough of reduces- salinity water. An incremental oil recovery equal to 10% of the total pore volumes in the swept area was achieved after injection of 1.3 PV reduced salinity water.

3.1.2. Low Salinity Modeling

Modeling of low salinity waterflooding has been of increasing interest as its potential effect on oil recovery has been shown extensively through experimental work.

Jerauld et al (2006) [33] created a model to represent corefloods, single- well tests and field-scale simulations. The model was one- dimensional and utilized salinity dependent oil/water relative permeability functions to represent the change in wetting conditions.

Wu and Bai (2009) [34] presented a general numerical model for multi- dimensional, low salinity waterflooding in porous or fractured reservoirs. Salt was modelled through adsorption, relative permeability, capillary pressure and salinity dependent residual oil saturation.

Omekeh et al. (2012) [35] presented further development of a one- dimensional mathematical model for the study of waterflooding laboratory experiments. The model described the effects of dissolution and precipitation of various carbonate minerals and multiple ion exchange (MIE) on water-oil flow functions. Relative permeability changes were modeled through desorption

of divalent cations from the rock surfaces. The model successfully matched pH and ion composition of two phase corefloods.

Dang et al. (2013) [36] presented a comprehensive ion exchange model with geochemical processes coupled with multi- phase, multi- component flow equations in the equation- of- state compositional simulator, GEM from CMG. Wettability alterations were modeled through adsorption of divalent ions rather than desorption, as modeled by Omekeh et al. (2012) [35]. Results were shown to be highly compatible with an ion- exchange model of the geochemistry software PHREEQC for both low and high salinity. The model efficiently matched experimental effluent pH, ion concentrations, and oil recovery, rendering it as a powerful tool for low salinity waterflood simulations.

Korrani et al. (2014) [37] investigated the geochemical package IPhreeqc, with the compositional reservoir simulator UTCOMP, from The University of Texas at Austin. Their purpose was to make a robust, accurate and flexible integrated tool to mechanistically model low salinity waterflooding. Through the coupling of the simulators they were able to: "simulate homogeneous and heterogeneous (mineral dissolution/precipitation), irreversible, ion exchange reactions under non- isothermal, non- isobaric and both local- equilibrium (away from wellbore) and kinetic (near wellbore) conditions." The integrated tool was used to match and interpret a field trial done by BP at the Endicott field.

3.2. Surfactant

3.2.1. Phase Behavior

Surface active agents, from here on referred to as surfactants, are amphiphilic compounds, meaning they possess hydrophilic(water "loving") and hydrophobic(water "hating") properties [38]. These properties are bound to either side of the compound, making them soluble in both water and oil. This results in monomers (single surfactant molecules) being drawn towards interfaces of aqueous and organic phases, thereby reducing interfacial tension. The indicated quality makes surfactants able to remobilize capillary trapped oil, as illustrated by the CDC (figure 1.6), forming a producible oil bank.

Surfactants are divided into groups based on the polarity of the head group, as illustrated in figure 3.1. The polarity impacts the surfactants reaction to pH, salt, alcohol and charged surfaces [38].

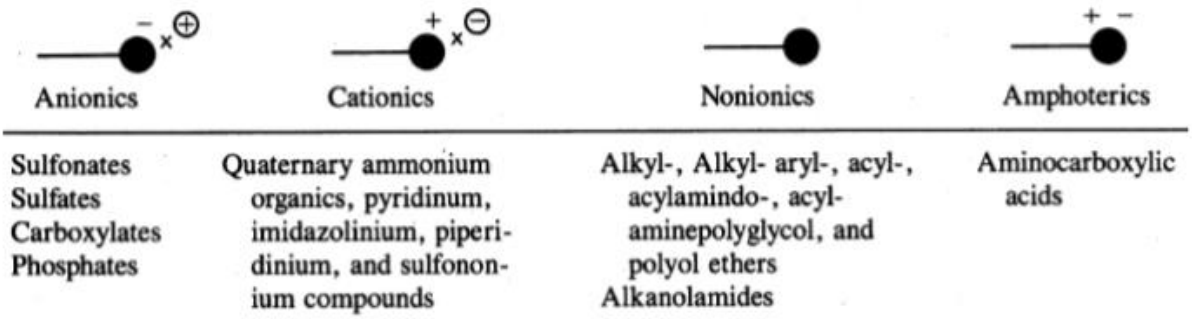

Figure 3.1: Surfactant classification as presented in Lake (1989) [6].

In this thesis, an anionic surfactant, the most commonly used surfactant in chemical flooding, is modelled. The other categories of surfactant will therefore not be discussed further. Anionic surfactants are preferred because of their resistance to retention, stability and low cost [6].

Anionics are ionized salts, usually a sodium ion connected to the anion head, with a long hydrophobic chain [38]. When the anionic surfactant is dissolved inn an aqueous solution it dissociates into a free cation (Na^+) and the anionic monomer. Because of the negatively charged head group, the anionic surfactant has low adsorption on negatively charged surfaces.

As surfactant concentration increases, monomers start to aggregate into micelles. Above a certain concentration, referred to as critical micelle concentration (CMC), adding surfactant

will no longer yield any significant decrease in interfacial tension. These changes are sudden and attributable to the formation of micelles as illustrated in figure 3.2.

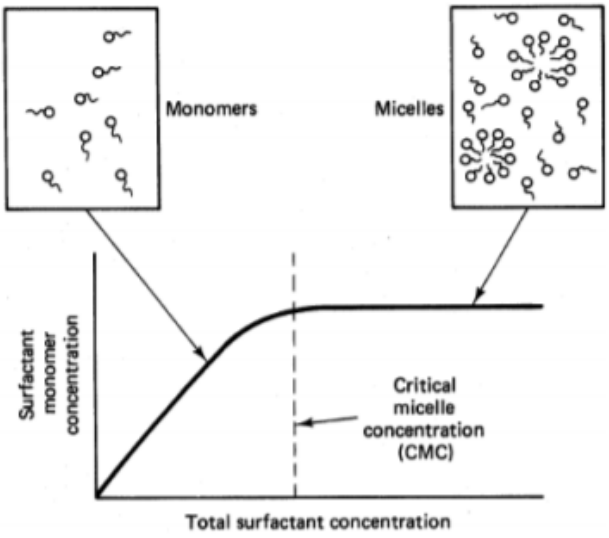

Figure 3.2: Critical micelle concentration as illustrated in Lake (1989) [6].

Classifications can also be made regarding surfactant-oil-brine phase behavior [39], as illustrated in figure 3.3. Behavior depends on surfactant structure, concentration, salinity, temperature and pressure [38].

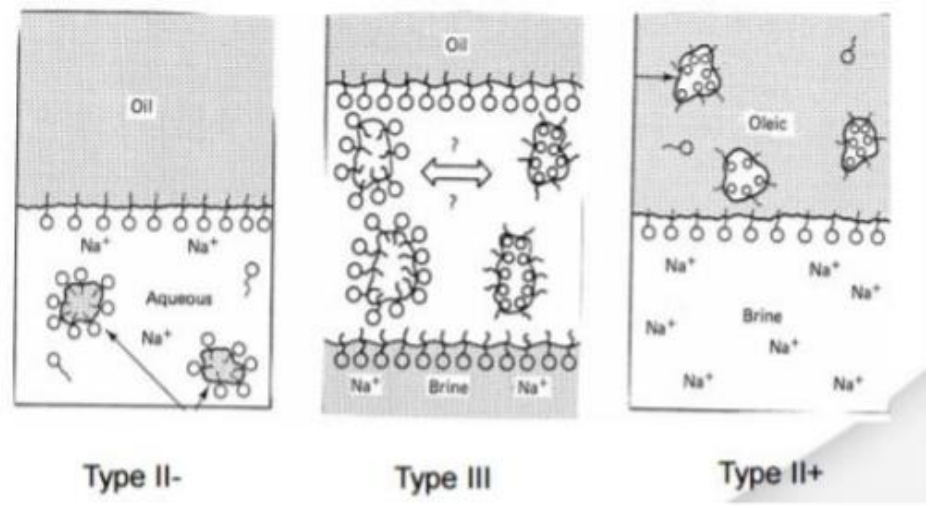

Figure 3.3: Classification of surfactant-oil-brine colloidal systems, modified from Lake (1989) [6].

At low brine salinities, an excess oil phase exists, while micro- emulsions inhabit the water phase consisting of brine, surfactant and solubilized oil. Because of the hydrophobic tail and hydrophilic head of surfactants, the solubilized oil is oil surrounded by monomers, thus creating swollen micelles in the water phase. This is called a type II(-) or Winsor type I system.

At high salinities, electrostatic forces reduce surfactant solubility in the aqueous phase. This leads to inverted micelles in the oil phase, while the excess brine phase is almost void of surfactants. A water in oil micro- emulsion system like this is called a type II(+) or Winsor type II system.

The aforementioned two phase systems exist at the extremes of salt concentration. A continuous transition system between the two, with a three phase region of brine, oil and micro- emulsion phases, also exists. The micro- emulsion phase can be either water or oil external depending on salinity and overall composition, but not both simultaneously. This is referred to as a type III or Winsor type III system.

Reed and Healy (1977) [40] proposed the relationship between surfactant flooding and interfacial tension. It was proven experimentally by Huh in 1979[41] and the relationship is shown in figure 3.4.

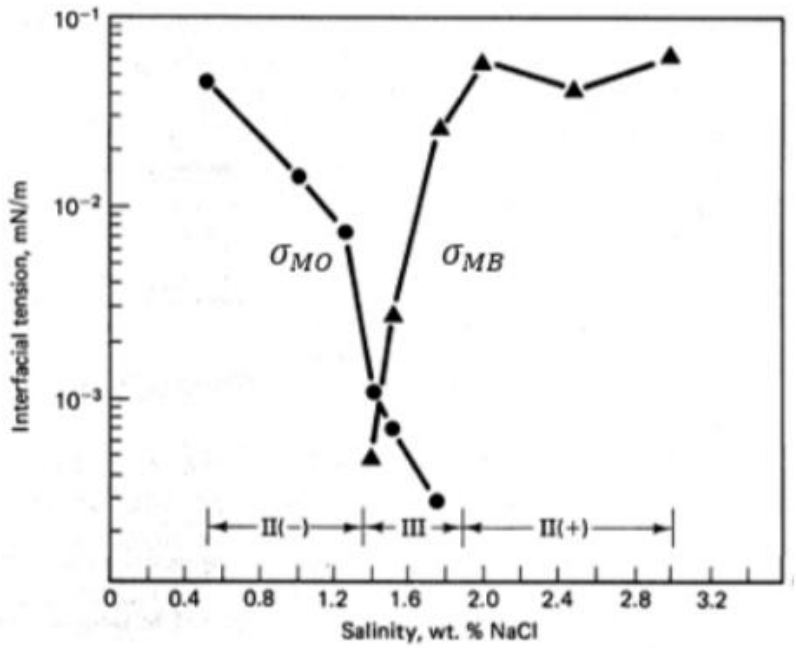

Figure 3.4: Interfacial tension as a function of brine salinity, with micro- emulsion classification. Modified from Lake (1989) [6].

Loss of surfactant to the formation is a major problem during surfactant flooding. Retention can occur due to adsorption, precipitation, ion exchange and phase trapping [8]. In this thesis, the main focus of retention is adsorption.

Because of the polarity of anionic surfactants, monomers adsorb to cationic surface sites. At concentrations lower than CMC, the adsorption increases with surfactant concentration [42]. Potentially, this means that only a fraction of the injected surfactant contributes to IFT-reduction.

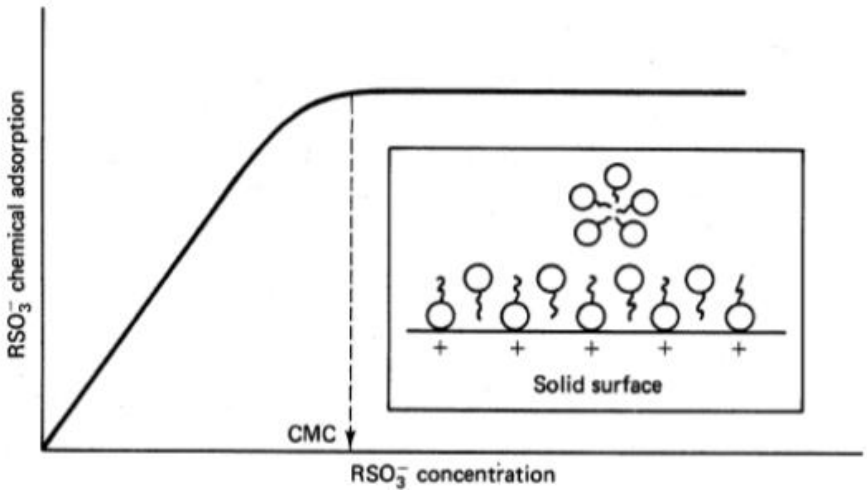

Figure 3.5: Surfactant adsorption as a function of concentration, from Lake (1989) [6].

3.3. Polymer Flooding

3.3.1. Phase Behavior

The addition of polymer into injection brine to increase viscosity is the most widespread chemical EOR technique [43]. The viscosity increase improves mobility ration between oil and water, which in turn can increases the volumetric sweep efficiency, accelerate oil production and stabilize fluid fronts. The most commonly used polymer in field operations is the synthetic polymer hydrolyzed polyacrylamide(HPAM) [4], which is modelled in this thesis.

Polymer molecules are long chains of repeating units (monomers) linked by covalent bonds. Synthetic polymers are often hydrolyzed to make them more soluble in water. Hydrolyzation makes polymers more sensitive to salinity, which can make them unstable. The degree of hydrolyzation is therefore important.

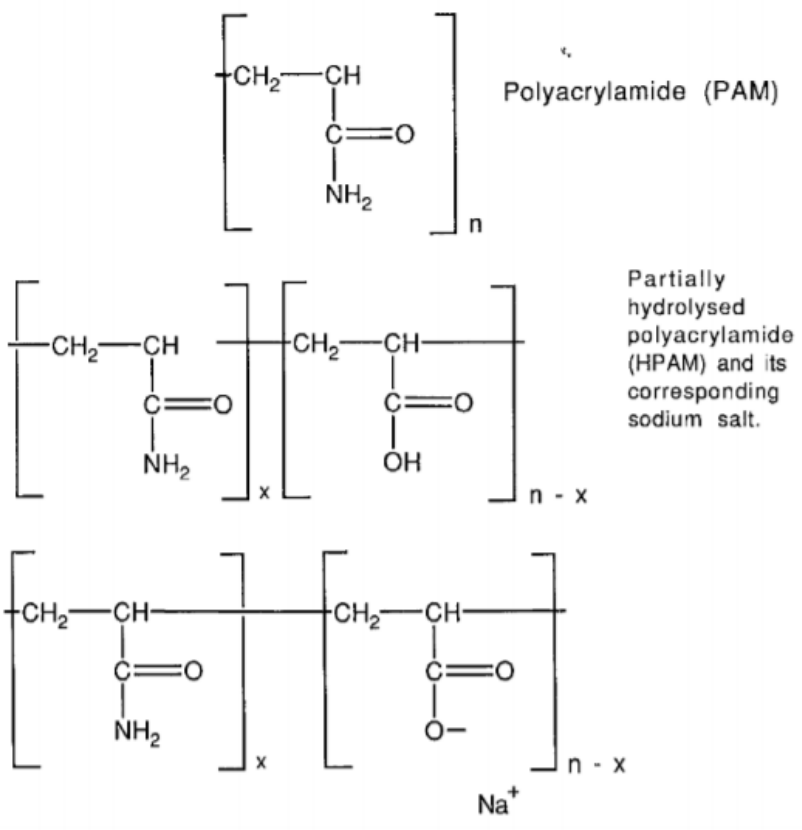

Figure 3.6: Primary chain structure of polyacrylamide (PAM) and partially hydrolyzed polyacrylamide (HPAM), from Sorbie (1991) [43].

HPAM has multiple anionic carboxyl groups distributed along its chain and is therefore a negatively charged polyelectrolyte. Large molecular weight and a flexible coil structure together with anionic repulsion is what leads to the viscosity increasing trait of HPAM [6] [43].

In general, polymers increase viscosity of water because of their molecular size and shape creating drag force around surrounding water molecules. The viscosity of a polymer solution is dependent on shear rate. They are so called non- Newtonian liquids (non- linear relationship between shear stress and shear rate) and may exhibit shear thinning or shear thickening behavior at low and high shear rates respectively [43].

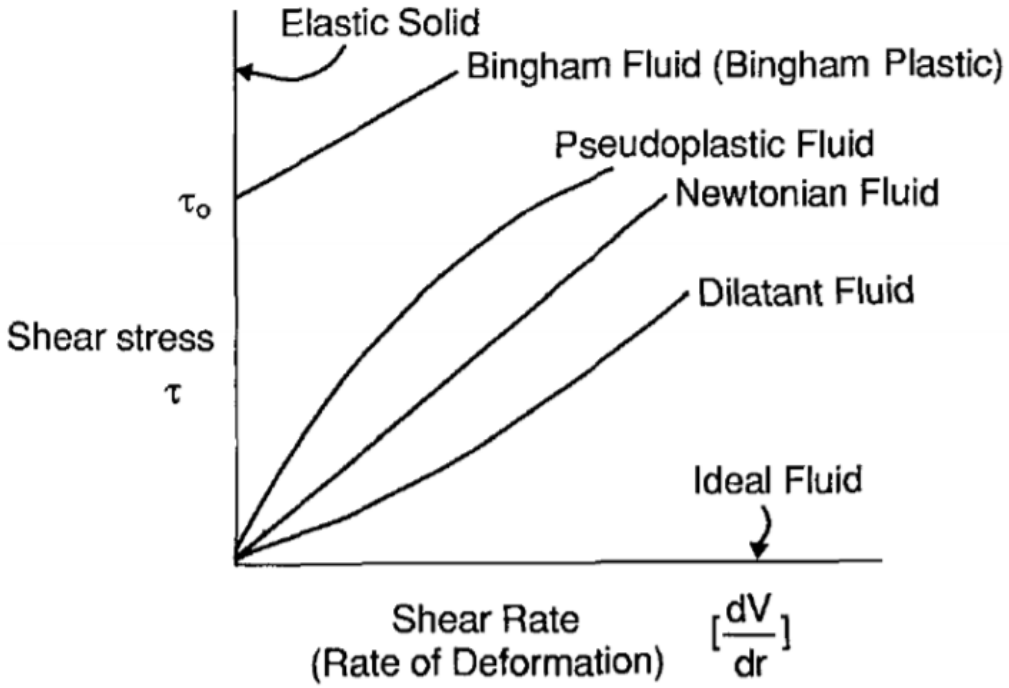

Figure 3.7: Various types of shear stress/shear rate behavior, from Sorbie (1991) [43].

The behavior of a polymer solution can be described by the Carreau model [44]:

$$\mu_p - \mu_\infty = (\mu_p^0 - \mu_\infty)[1 + (\lambda\dot{\gamma})^2]^{(n-1)/2} \quad (3.2)$$

where μ_p is polymer viscosity, μ_p^0 is zero shear rate viscosity, μ_∞ is infinite shear rate viscosity, λ is a relaxation constant, $\dot{\gamma}$ is shear rate, and n is the power law exponent

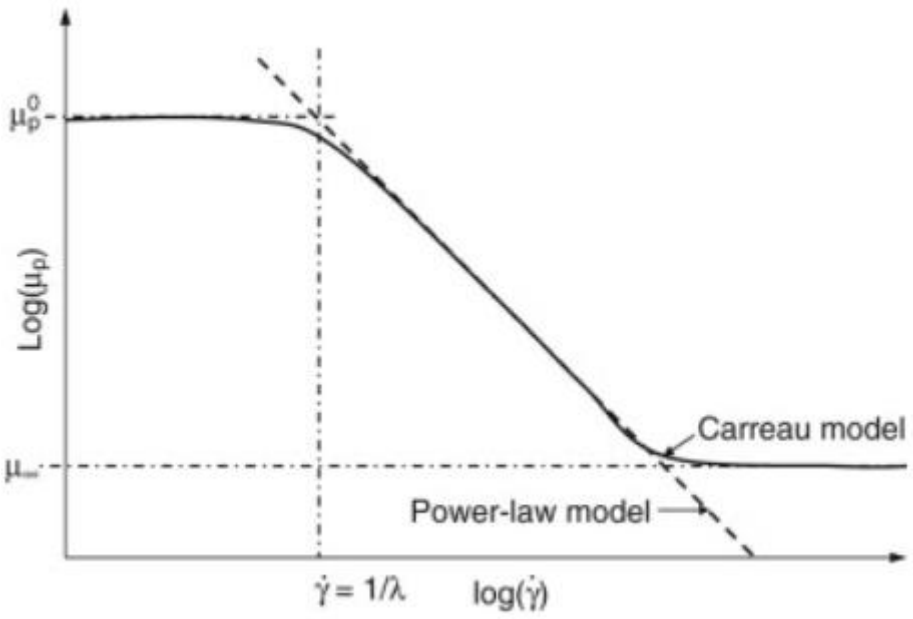

Figure 3.8: Carreau model for viscosity of polymers, from Sheng (2011) [44].

As a polyelectrolyte, HPAM will interact with ions in solution and with charged surfaces. High salt concentrations leads to contracted HPAM molecules, reducing its viscosity effect. Additionally, a relationship of increased adsorption of HPAM with increasing salinity was shown by Smith (1970) [45].

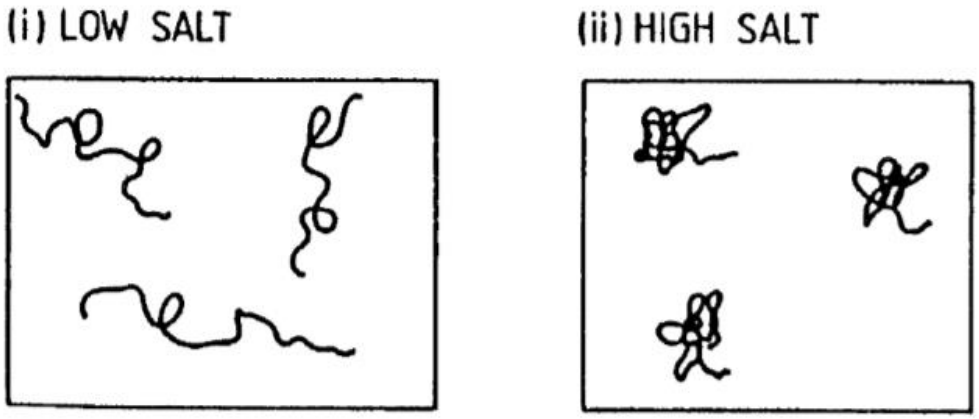

Figure 3.9: Schematic of the effect of increasing salt concentration on the conformation of flexible coil polyelectrolytes such as HPAM. Taken from Sorbie (1991) [43].

Polymer retention, like surfactant retention, is caused by adsorption, mechanical trapping and local accumulation of polymer molecules (precipitation). Where polymer is retained, lower permeability, lower front velocity and a decrease in polymer concentration, which in turn reduces the reach and mobility effects of polymer, is experienced[4] [8].

Due to the relatively large size of polymer molecules, smaller pore spaces will not be invaded by the polymer. This is called inaccessible pore volume (IPV). IPV has the opposite effect of retention as it causes an acceleration of the polymer solution [4].

3.4. Combined EOR Literature Study

In this chapter, a literature study of combined EOR methods, specifically low salinity surfactant and low salinity polymer injection, is presented.

3.4.1. Lab and field- scale

Alagic and Skauge (2010) [46] presented a hybrid EOR process combining low salinity brine injection with surfactant flooding. An anionic surfactant was selected to yield low IFT at 0.50 wt% NaCl. The surfactant formed a type II(-) micro emulsion system and showed improved solubility and reduced retention. Flooding experiments performed on Berea sandstone cores showed a recovery of more than 90% OOIP when surfactant is injected after a low salinity flood. Destabilization of oil layer caused by change in brine salinity and simultaneous mobilization of the residual oil at low IFT, was proposed as the underlying mechanism. Surfactant was injected to reduce capillary forces and avoid re- trapping of oil mobilized by the salinity change.

Alagic et al. 2011 [47] investigated the effects of low salinity water injection and combined low salinity surfactant injection on oil recovery from aged/unaged Berea sandstones. Results showed that oil recovery was highest for the aged cores. A qualitative investigation showed a decrease in water- wetness for the aged cores. This supported the theory of increased recovery for aged cores (more oil- wet) due to more unstable oil layers available for surfactant mobilization.

Spildo et al (2012) [48] investigated to which extent capillary forces needed to be reduced to take advantage of the incremental oil recovery during low salinity- and low salinity surfactant flooding. Experiments showed good recovery and low retention for type II(-) micro- emulsion systems. Additionally intermediate- wet conditions were found to be more favorable than water-wet conditions. Tests on both homogeneous and heterogeneous Berea cores showed an insignificant response to low salinity brine injection. Since capillarity was reduced and oil might have been redistributed due to changes in crude oil- brine- rock interactions, it was concluded that the increased recovery would be beyond the expected recovery by surfactant alone.

Ayirala et al. (2010) [49] investigated economic viability of offshore, low salinity polymer flooding. The results showed that when the reservoir fits the criteria the extra cost of desalination would be paid off within 1.6 – 4.0 years due to the large savings associated with chemical and polymer facility costs. As a result of lower salinity, the polymers viscofying effect was higher and the need for higher concentrations, storage and mixing facilities were reduced. The pay- out time therefore decreased favorably with salinity.

Shiran and Skauge (2013) [50] performed low salinity polymer, flooding experiments on Berea sandstone cores. The results showed an increased oil recovery of about 13% of OOIP in secondary- mode compared to tertiary- mode low salinity waterflooding. Additionally, oil recovery by polymer injection was significantly better when a low salinity environment was established at initial water saturation rather than residual oil saturation. For this case, recovery increased to 90% OOIP.

Vermolen et al (2014) [51] performed a study on the effect of low salinity injection water effect on polymer flooding. Even with no incremental oil recovery, economics of the project could improve due to wettability alteration and decrease in required polymer concentration by a factor of 2-4. Additional benefits were: increased visco- elasticity, reduced mechanical shear and potentially less production chemistry issues. Low salinity mixing with the already present high salinity brine was found to not affect polymer viscosity due to the fact that a low salinity slug (void of polymer) would form in between the fluids because of polymer adsorption. The high salinity brine would be stably displaced by the low salinity polymer. Even though polymer adsorption was found to have buffer effect against mixing, it would also delay oil recovery. In case of delayed recovery, the stability of the brine and/or the polymer concentration could be optimized to improve economic viability.

3.4.2. Modeling

In 2010 Kallevik [52] presented her master thesis "Implementations of Methods for Modeling Low Salinity Waterflood and Low Salinity Surfactant Flooding". She demonstrated that the simulator UTCHEM was able to modeled the effects of low salinity and low salinity surfactant flooding. This was achieved through salinity dependent oil/water capillary pressure and relative permeability curves, as a result of wettability alteration. In addition, the software Sendra was used to estimate relative permeability- and capillary pressure curves to be utilized in the reservoir simulator ECLIPSE. Results showed that the underlying mechanisms of low salinity were more complex than the proposed UTCHEM and ECLIPSE models.

Skauge et at. (2011) [53] presented a study using UTCHEM and ECLIPSE to model low salinity- and low salinity surfactant injection. In both models, the assumed mechanism of increased oil recovery was relative permeability alteration (to more water- wet) with lowering of brine ionic strength. ECLIPSE was found to possess a more flexible, salt mixing, interpolation scheme, while UTCHEM utilized a more predictive approach that was could be more easily upscaled. They concluded that the underlying mechanisms of low salinity are more complex than wettability alteration and that more and additional experimental information is needed to distinguish these mechanisms.

Mohammadi and Jerauld (2012) [54] presented a mechanistic model of low salinity waterflood and polymer flood using the VIP reservoir simulator. Key features of the low salinity model were based on Jerauld et al. (2008) [55]. Polymer was modeled through concentration, shear rate and salinity dependent viscosity. Transport parameters such as adsorption, permeability reduction, cation exchange and inaccessible pore volume were considered. 1- Dimensional simulations were conducted with VIP to study the effects of the combined EOR process on displacement efficiency. 3- Dimensional simulations using STARS were performed to provide independent assessments. Simulations showed effectiveness of both secondary and tertiary injection of low salinity polymer, but a greater synergistic effect during tertiary mode due to better timing of oil recovery.

Skauge (2015) [56] modeled a complex, multistage hybrid EOR process of high salinity, low salinity, surfactant, polymer and low salinity chasewater using the STARS simulator. It was shown that experimental data could be history matched within the frame of established low salinity models and flexibility of surfactant/polymer options.

Drønen (2015) [57] presented an investigation into modeling of hybrid EOR methods using the STARS simulator. Wettability alteration was modeled using salinity dependent oil/water relative permeability curves. Surfactant flooding was enabled by interpolation based on capillary number and polymer was added as a viscosity component. Experimental low salinity waterfloods and combined low salinity, surfactant and polymer floods were history matched. Matches showed STARS as an adequate simulator for this combined EOR method, but limitations on multiple interpolation parameters were experienced.

Tavassoli et al. (2016) [58] utilized UTCHEM- IPhreeqc to investigate low salinity- and low salinity surfactant flooding. A history match was performed on experimental data from Alagic and Skauge (2010) [46]. Additional simulations of higher salinity and lower IFT were compared. The high salinity surfactant flood recovered 100% of OOIP within 2PV of injection, compared to 92.3% of OOIP for the low salinity surfactant flood after 15PV. They concluded that proper surfactant selection and surfactant flood design might surpass the benefits of low salinity flooding with regards to both oil recovery and cost.

Khorsandi et. al (2017) [59] constructed an analytical solution for low salinity polymer flooding in sandstones. The solution was based on mechanistic modeling of wettability alteration through cation exchange and was validated with numerical simulation and experimental data. Matching of experimental data indicated cation exchange as the likely mechanism. Wettability alteration only happened along the wettability front, and recoveries were therefore matched through front retarding parameters alone. Small slugs of low salinity water were found to be potentially ineffective. This was due to the high- salinity shock front moving faster than the wettability front. Most oil was recovered after the wettability front broke through in the producer.

Pettersen and Skauge (2016) modelled complex composite EOR processes at lab and field scale using a black oil simulator and a compositional based simulator. History matching was used to validate experiments. Both simulators successfully rendered lab and upscaling(unchanged model size while grid cell size is increase) experiments. Extension (changing the size of the simulation model without changing grid size) was handled better by the compositional simulator than the black oil simulator. The black oil model found to be sensitive to the smoothness of relative permeability curves. The authors recommended the component model simulator when detail accuracy is needed. The black oil model can be used for qualitative screening studies with awareness of its limitations.

4. STARS Reservoir Simulator

4.1.1. Relative permeability interpolation

Low salinity waterflooding was modelled by assigning a dedicated relative permeability set. This was done to render the effects of wettability alteration of the reservoir rock. In the model, sodium, Na^+, and chloride, Cl^-, were modelled individually, but whit the same attributes. To model the concentration changes of Sodium chloride(NaCl), Na^+ was chosen to be the component used for interpolation. This was done using keyword INTCOMP. Two sets of relative permeability curves, representing high salinity and low salinity waterfloods, were added and interpolation between them was based on Na^+ concentration in the water phase. The keyword DTRAPW/N enables interpolation based on the mole fraction of a component in a the oil or the water phase, both defined through keyword INTCOMP. DTRAPW/N can also interpolate based on capillary number, as is the case when modeling surfactant flooding. Interpolation between relative permeabilities, in STARS, is based on the following equations [60]:

$$k_{rw} = k_{rwA} \cdot (1 - wtr) + k_{rwB} \cdot wtr \tag{4,1}$$

$$k_{ro} = k_{roA} \cdot (1 - oil) + k_{roB} \cdot oil \tag{4,2}$$

where A and B refers to rock fluid sets A and B. wtr and oil are described as:

$$wtr = ratw^{WCRV} \tag{4,3}$$

$$oil = ratn^{OCRV} \tag{4,4}$$

where ratw and ratn, varying from 1 to 0, are defined as:

$$\text{ratw} = \frac{\log_{10}(N_c) - \text{DTRAPWA}}{\text{DTRAPWB} - \text{DTRAPWA}} \tag{4,5}$$

$$\text{ratn} = \frac{\log_{10}(N_c) - \text{DTRAPNA}}{\text{DTRAPNB} - \text{DTRAPNA}} \tag{4,6}$$

For concentration based interpolation, ratw and ratn are set to 1. When IFT- tables are present, eg. during surfactant flooding, relative permeability must be interpolated based on capillary number (N_c), which is dependent on interfacial tension. STARS calculates capillary number by substituting Darcy velocity [60]:

$$N_c = \frac{K \cdot \Delta P}{\sigma \cdot \Delta x} \tag{4.7}$$

4.1.2. Dispersion

Total dispersion is defined by keywords DISPI/J/K, representing the total dispersion coefficients in directions I, J and K. The coefficients are based on effective molecular diffusion and mechanical dispersion. The former being a property of the defined component and phase while the latter a property of the reservoir rock. The total dispersive flux J_{ijk} of component I in phase j in direction k is given by [60]:

$$J_{ijk} = -\mathbf{D}_{ijk} \nabla_k (\rho_j x_{i,j}) \tag{4,8}$$

where $\mathbf{D}_{ijk}$ is the total dispersion coefficient of component I in phase j in direction k and ∇_k is the concentration gradient of component I in phase j in direction k.

4.1.3. Adsorption

In this thesis, component adsorption to the rock matrix is included by using STARS keywords: ADSCOMP, ADSLANG, ADMAXT, and ADRT. ADSCOMP is used to define the component and phase from which adsorbing components composition dependence will be taken from. ADSLANG relates the Langmuir adsorption isotherm to the parameters tad1, tad2 and tad3, given in the equation [60]:

$$\text{ads} = \frac{(\text{tad1}+\text{tad2}\cdot\text{xnacl})\cdot\text{ca}}{(1+\text{tad3}\cdot\text{ca})} \tag{4,9}$$

which relates adsorption, ads (mol/cm^3) to xnacl, the salinity of the brine and ca, the mole fraction of the component defined by ADSCOMP. Langmuir coefficient tad1 has units mol/cm^3, tad2 is associated with salt effects, but is currently not used in STARS and thus equals 0, while tad3 is dimensionless. tad3 controls the curvature while the relation between tad1 and tad3 controls the adsorption plateau of the Langmuir adsorption isotherm.

ADSMAXT defines the maximum adsorption capacity, in mol/cm^3 and ADRT specifies the residual adsorption level. If ADRT is 0 then adsorption is completely reversible, while a value equaling ADMAXT implies completely irreversible adsorption.

4.2. Wettability Study – High Salinity

In this chapter, an investigation into the effects of wettability on oil production is studied. The observed trends were taken into account during history matching later on. An arbitrary core of dimensions 100cm x 1cm x 1cm, in i, j and k direction respectively, was modeled. An oil viscosity of 13.80cP and water viscosity of 1.07cP was entered into the model. To adjust wettability, relative permeability curves were altered by changing the Corey parameters n_o, n_w, $k_{rw}(S_{orw})$ and S_{or}. The complete model can be viewed in the appendix.

To create the relative permeability curves the equations defined by Corey in 1954 [61] were used:

$$k_{rw} = k_{rw}^{\circ}(S_w^*)^{n_w} \tag{4,10}$$

$$k_{ro} = k_{ro}^{\circ}(1 - S_w^*)^{n_o} \tag{4,11}$$

Where k_{rw}° and k_{ro}° are end- point relative permeability of water and oil respectively and S_w^* is the normalized water saturation given by:

$$S_w^* = \frac{S_w - S_{wi}}{1 - S_{wi} - S_{or}} \tag{4,12}$$

Table 4.1: Corey parameters used in calculation of base case relative permeability:

S_{wi}	S_{or}	n_w	$k_{rw}(S_{orw})$	n_o	$k_{ro}(S_{wi})$
0.2	0.3	2	0.3	2	1

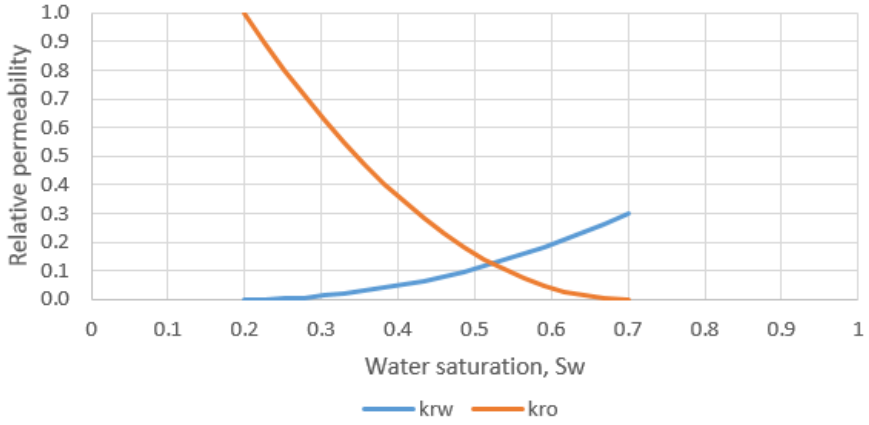

Figure 4.1: High salinity, base case, relative permeability curves.

The effects of wettability on oil recovery have been investigated extensively [62] [63] [64]. Wettability affects waterflooding by determining fluid flow and fluid distribution in porous media. Since relative permeability is a function of wettability, so too is the fractional flow of water. This relation can be observed in equation (2.18).

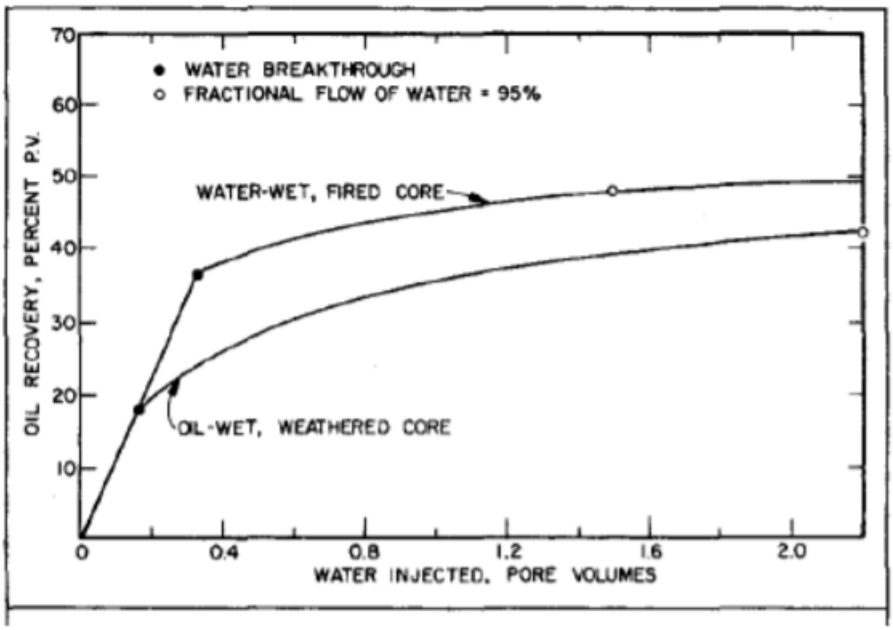

Figure 4.2: Oil recovery for an oil- wet core compared to the same core made- water wet. From Anderson (1987) [64].

In a water- wet system, a waterflood with favorable mobility ratio will move uniformly through the porous medium [3]. In such a system, water lies as a continuous thin film against the pore walls. Initially, water displaces oil in the smallest pores before entering larger and larger pores. Oil, occupying the center of the pores, will be mobile as long as it acts as a continuous phase. Since flow resistance is relatively low in the center of the pores, propagate quickly through larger and larger pores ahead of the displacement front. Narrow pore throats lead to snap- off and a disconnected oil phase. The fast propagation together with snap- off implies a high initial production until water breakthrough and minimal production thereafter.

In an oil- wet reservoir, the opposite trends are present. Oil first displaces water in the smallest pores before propagating into larger and larger pores. In the center of the pores water flows with relatively low resistance. This implies that most oil is bypassed during a waterflood, but since it is continuous, production will continue past water breakthrough. These trends can be observed in figure 4.2.

Salathiel (1973) [65] observed that reservoirs with a mixed- or intermediate- wet rock generally showed a greater oil recovery during waterflooding. This was attributed to strongly oil- wet pores, forming continuous, oil- wet paths through the porous medium, which allowed for oil permeability to persist for low oil saturations.

4.2.1. Relative permeability - n_o variation

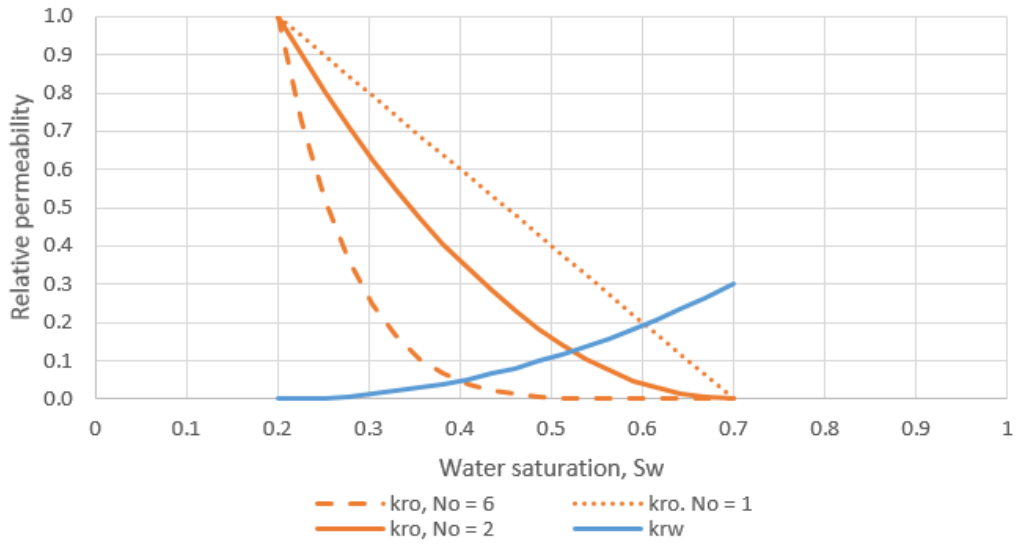

Figure 4.3: Trends of relative permeability curves as a function of Corey parameter n_o.

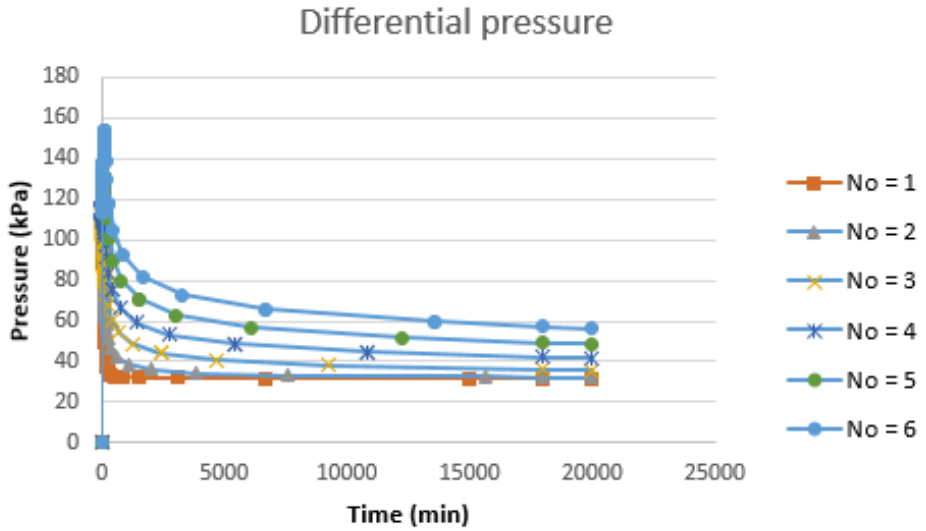

Figure 4.4: Differential pressure as a function of Corey parameter n_o.

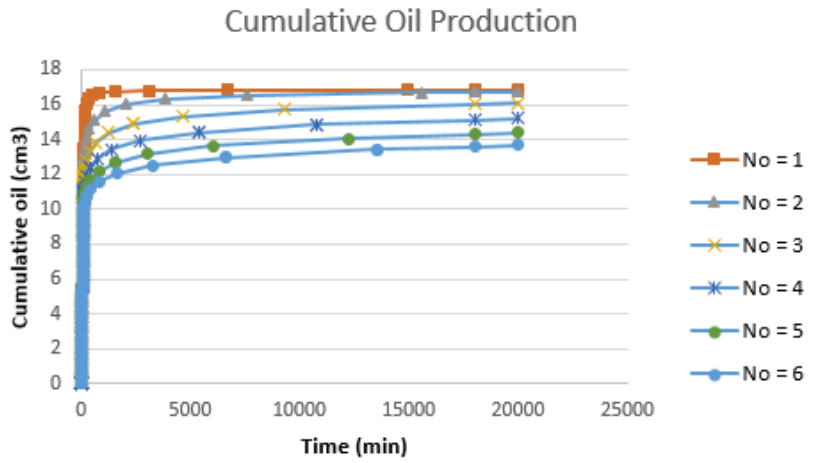

Figure 4.5: Cumulative oil production as a function of Corey parameter no.

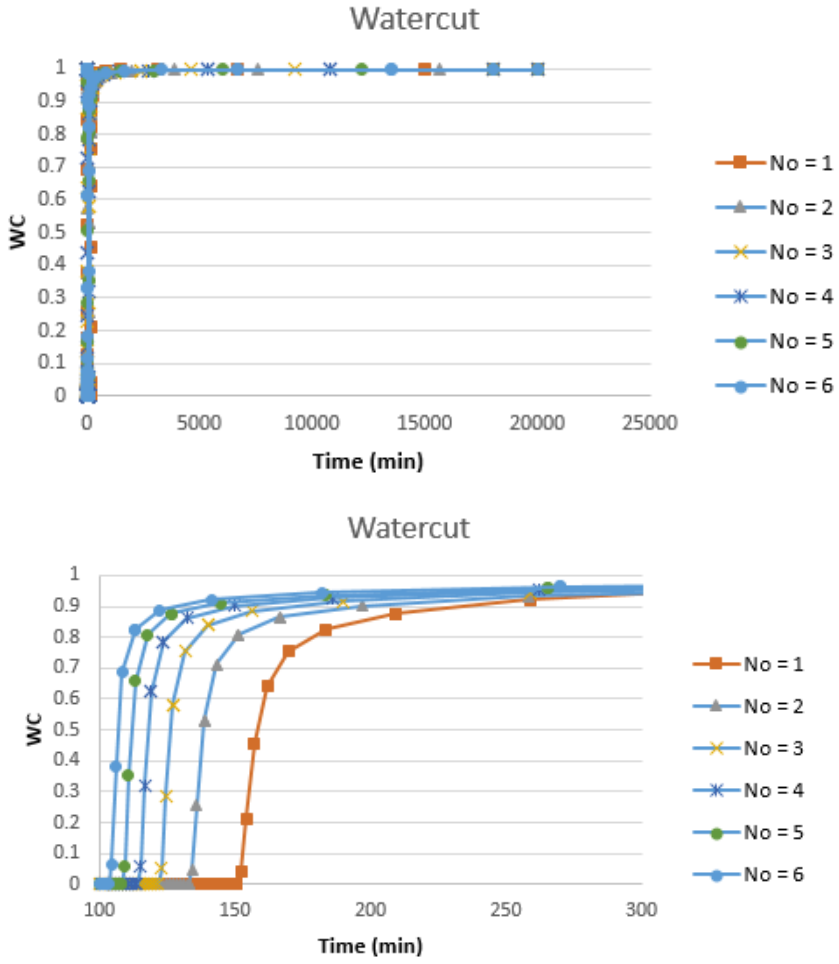

Figure 4.6: Watercut (WC) as a function of Corey parameter n_o. Lower graph x- axis is altered.

Increasing n_o from 1 - 6 implies a reduction in oil, relative permeability outside end point values. This corresponds to a more oil- wet state leading to earlier water breakthrough and subsequent lower cumulative oil production. Higher differential pressure results from the lowered k_{ro} increasing resistance of flow.

4.2.2. Relative permeability – n_w variation

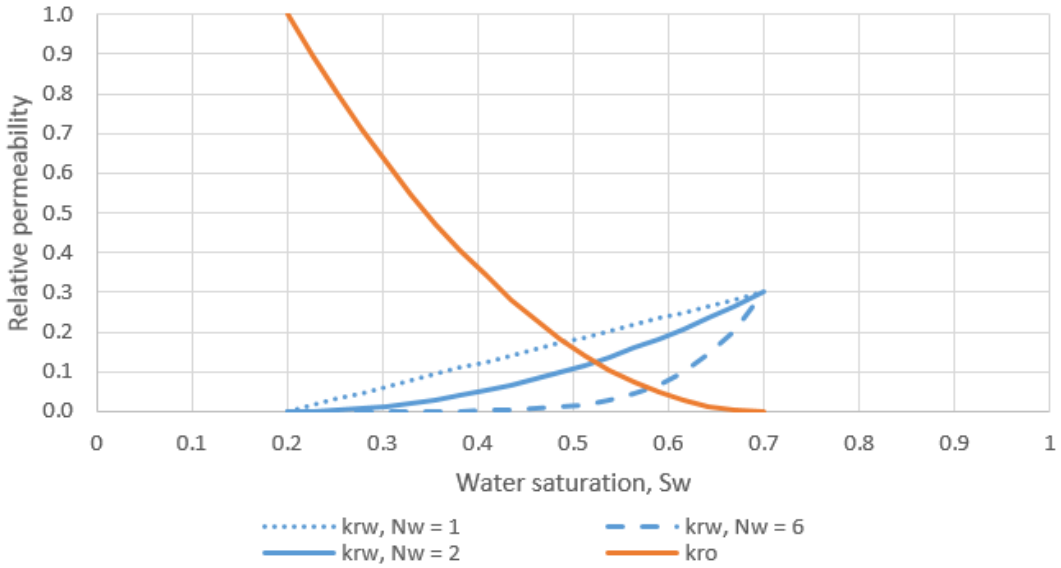

Figure 4.7: Trend of relative permeability curves as a function of Corey parameter n_w.

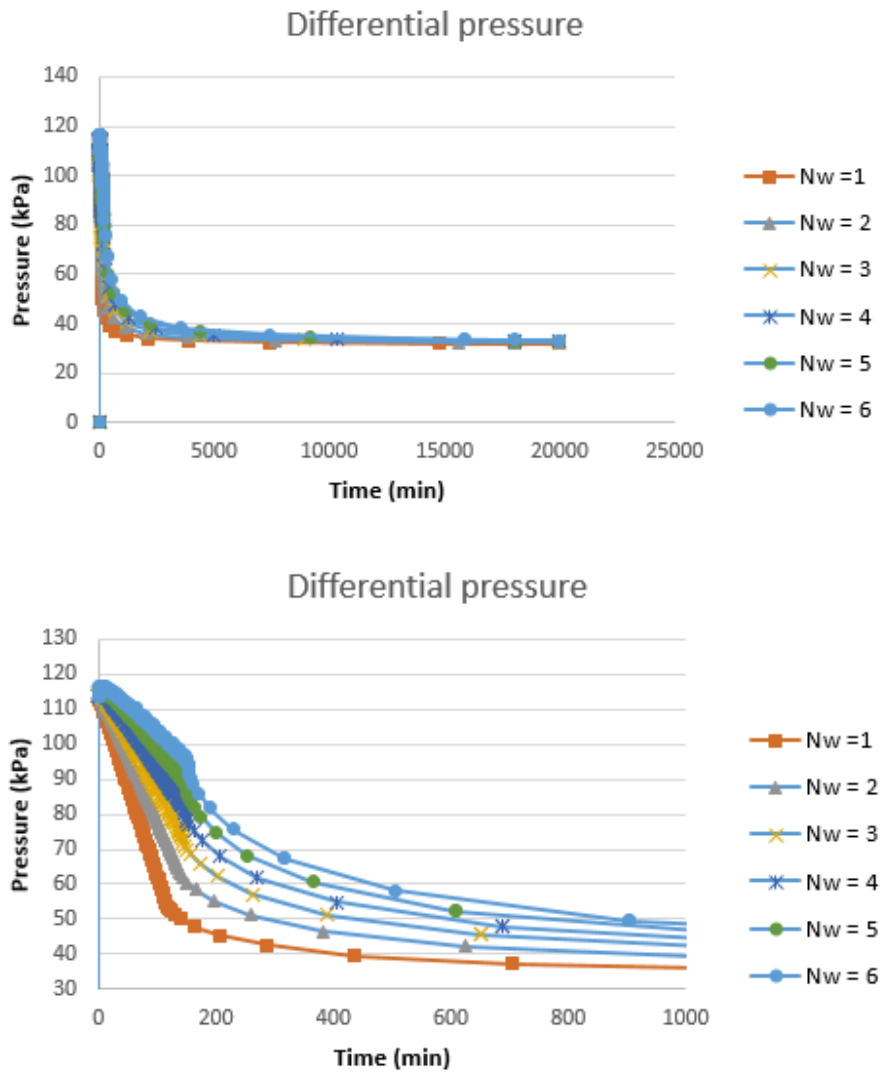

Figure 4.8: Differential pressure as a function of Corey parameter n_w. Lower graph has been zoomed in.

Increasing n_w from 1-6 implies a general reduction in water, relative permeability outside end point values. The core becomes more water- wet, breakthrough happens later and more oil is cumulatively produced. The decrease in k_{rw} results in higher differential pressure, but the response is weaker compared to variations in n_o. Since, in this model, oil viscosity is more than ten times higher than water viscosity, changes in oil relative permeability will have a greater impact on mobility ratio and subsequently differential pressure.

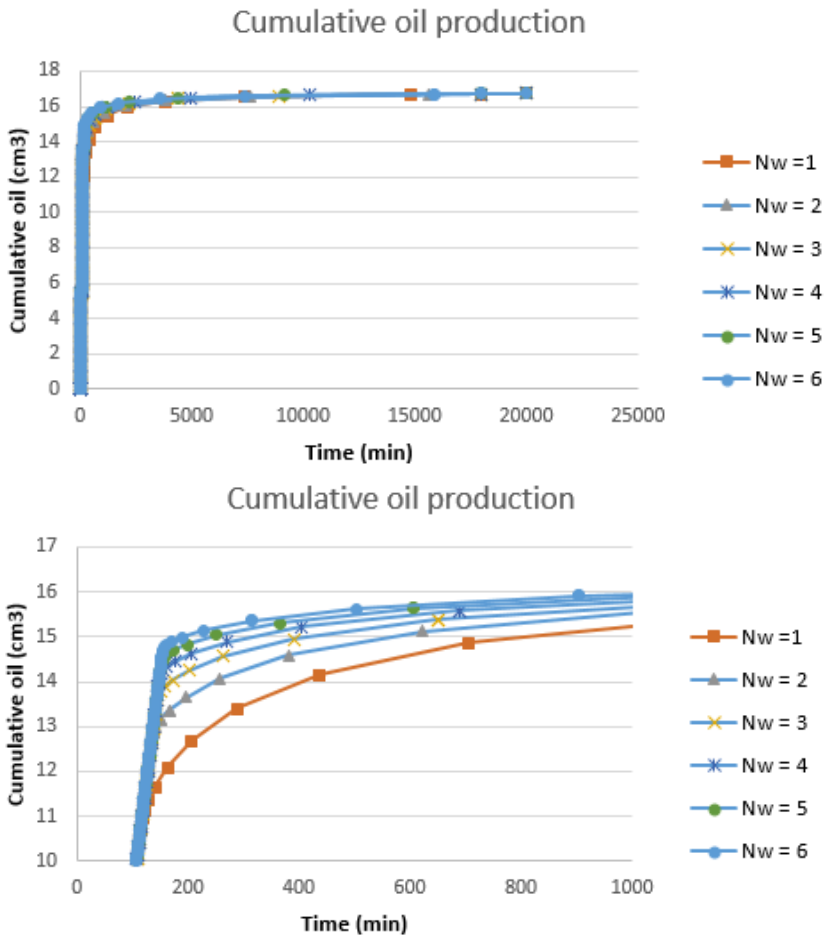

Figure 4.9: Cumulative oil production as a function of Corey parameter n_w. Lower graph is a zoomed in version.

Table 4.2: Total oil production of Corey parameter n_w.

n_w	1	2	3	4	5	6
Oil production [m^3]	16.7323	16.7374	16.7273	16.7319	16.7406	16.7391

Looking at table 4.2., the trend of uniformly increased/decreased oil production with increasing Corey exponent is not observed. Instead, the more in intermediate wetting conditions for n_w equaling 1 and 2 come close to the oil- wet conditions of n_w equal 5 and 6. Still the most oil-wet conditions yielded the greatest oil recovery. In order of highest oil production to lowest: $n_w = 5$, $n_w = 6$, $n_w = 2$, $n_w = 1$, $n_w = 4$, $n_w = 3$

Breakthrough times correspond with what is explained in the theory as water wetness is decreased.

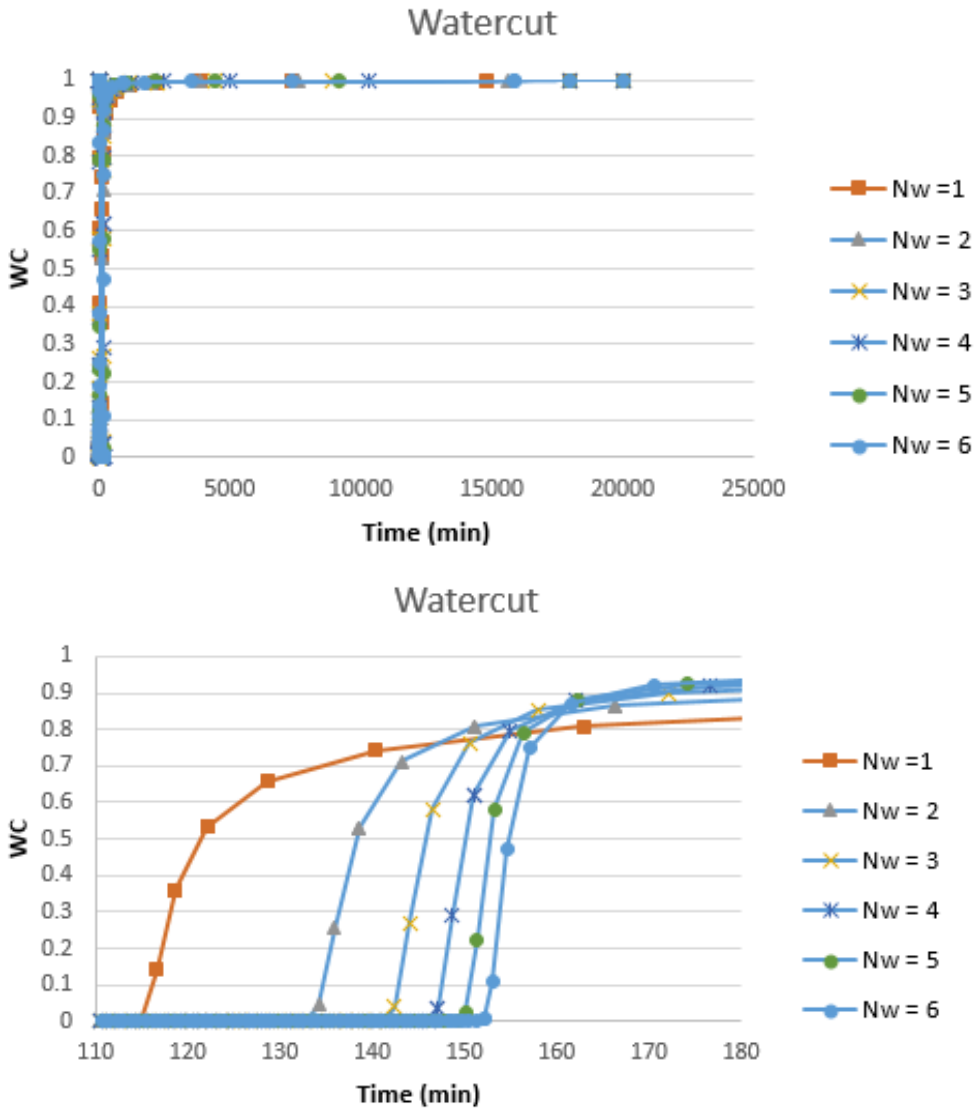

Figure 4.10 Watercut as a function of Corey parameter n_w. The bottom graph has been zoomed in.

4.2.3. Relative permeability – $k_{rw}(S_{orw})$ variation

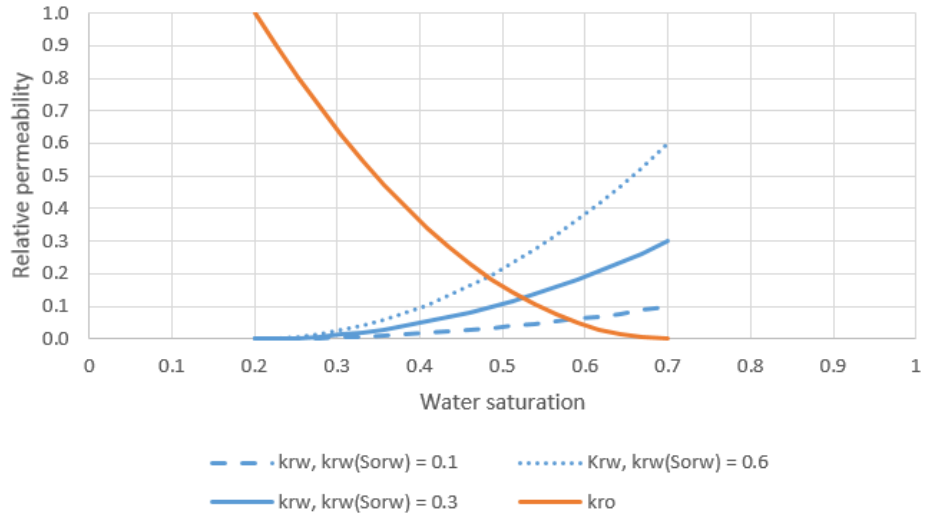

Figure: 4.11: Trends of relative permeability curves as a function of Corey parameter $k_{rw}(S_{orw})$.

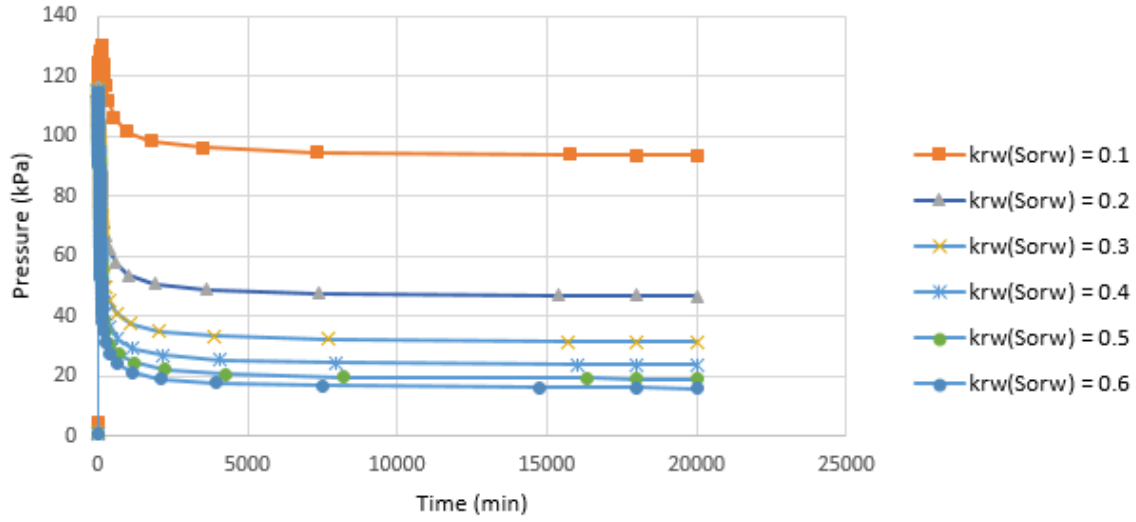

Figure 4.12: Differential pressure as a function of Corey parameter $k_{rw}(S_{orw})$.

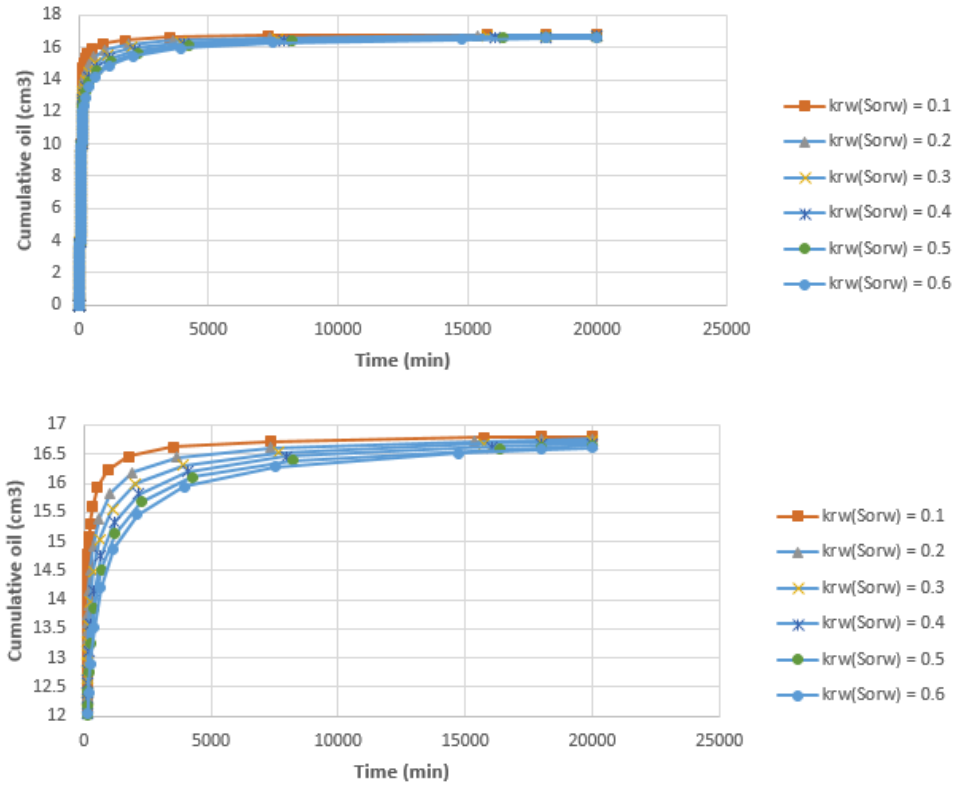

Figure 4.13: Cumulative oil production as a funciton of Corey parameter $k_{rw}(S_{orw})$. Bottom graph has been zoomed in.

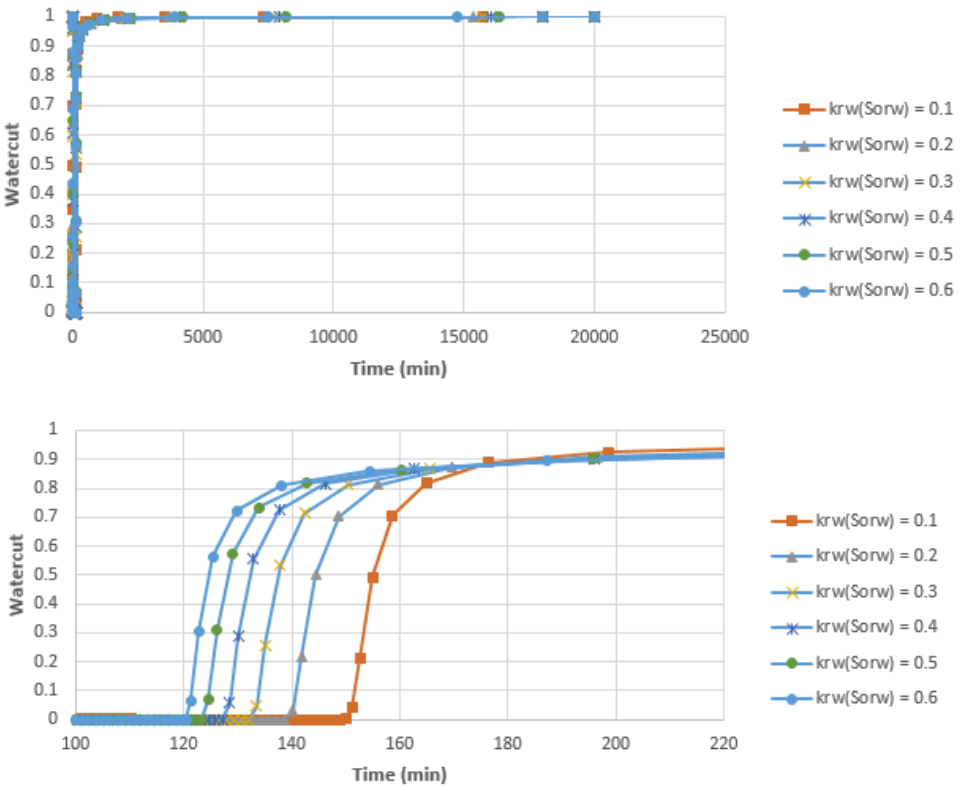

Figure 4.14: Water cut as a function of Corey parameter $k_{rw}(S_{orw})$. Bottom graphs x- axis has been zoomed in.

Increasing end point, water relative permeability, $k_{rw}(S_{orw})$, from 0.1 - 0.6 implies an increase in water, relative permeability outside initial water relperm, $k_{rw}(S_{wi})$. The change, to a more oil-wet state, results in earlier water breakthrough and lower oil production. As for the n_w curves, the effect on production and watercut is less pronounced when changing relative permeability of water, because of the relative impact on mobility ratio and fractional flow.

4.2.4. Relative Permeability – S_{or} variation

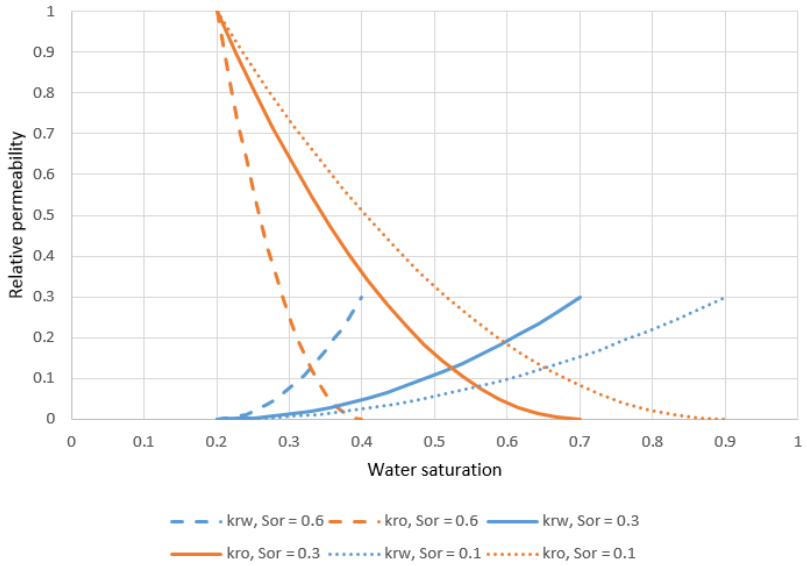

Figure 4.15: Relative permeability as curves as a function of Corey parameter S_{or}.

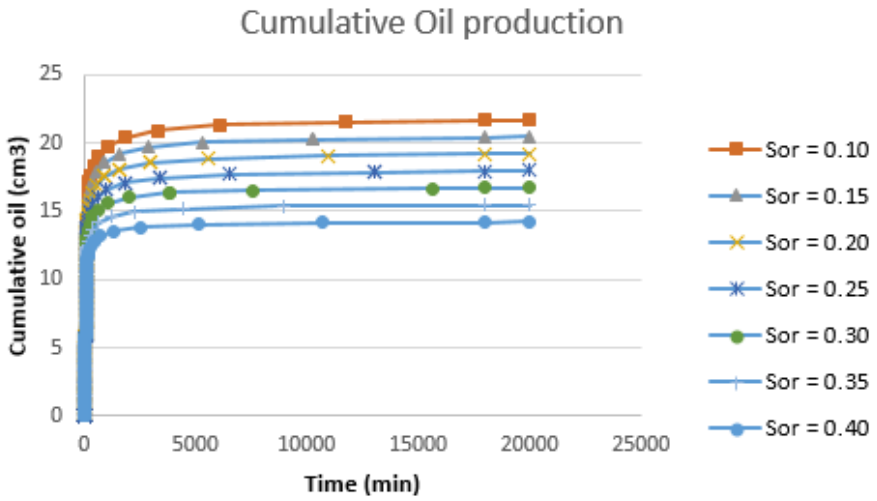

Figure 4.16: Cumulative oil production as a function of Corey parameter S_{or}.

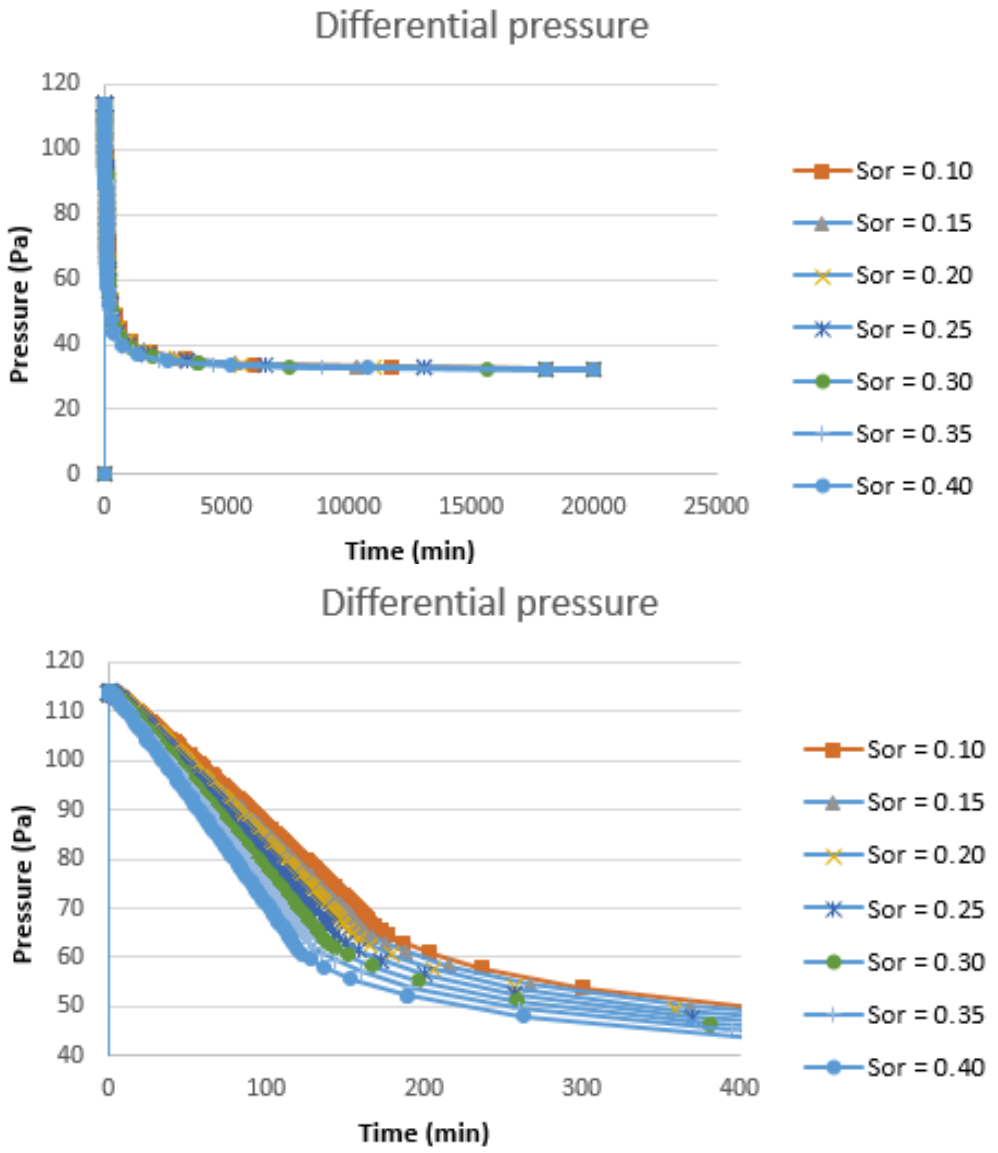

Figure 4.17: Differential pressure as a function of Corey parameter S_{or}. Bottom graph has been zoomed in.

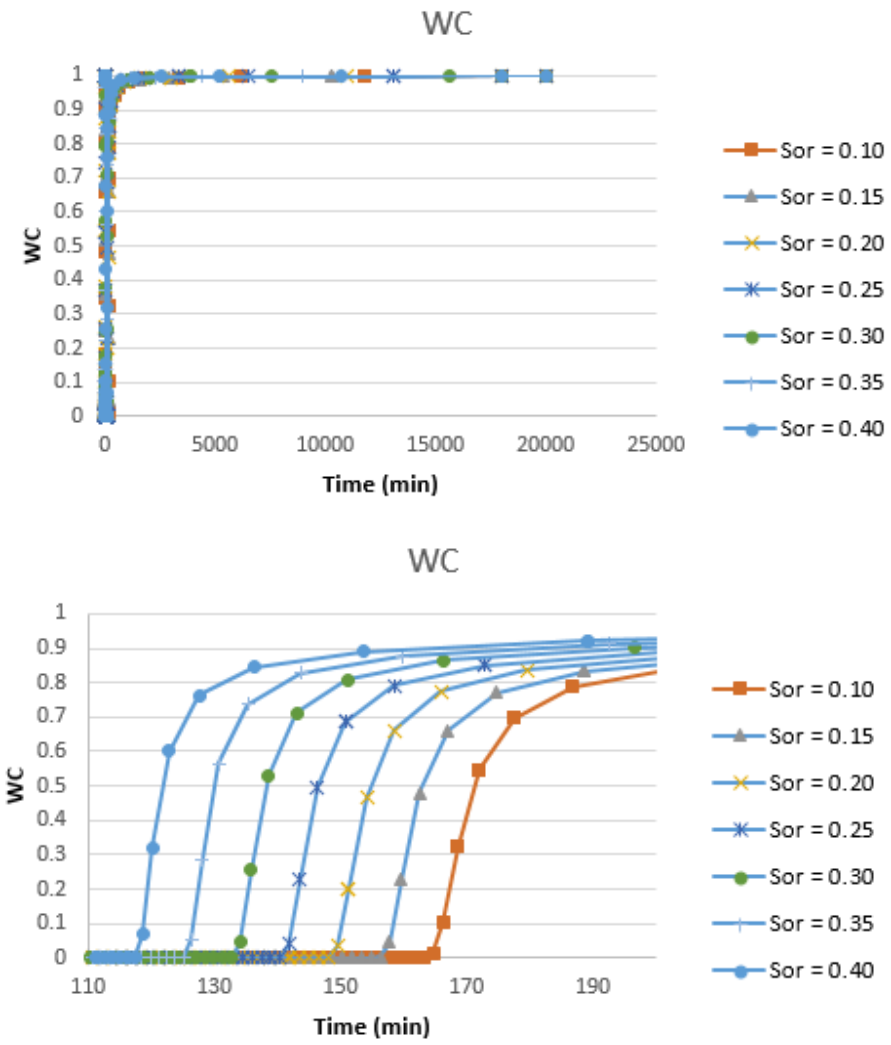

Figure 4.18: Watercut as a function of Corey parameter S_{or}. Bottom graph has been zoomed in.

Increasing residual oil saturation, S_{or}, from 0.10 - 0.40 implies an increase in k_{rw} and a decrease in k_{ro}, outside of $k_{rel}(S_{wi})$. Both influence wettability towards more oil- wet conditions. As expected, water reaches the producer at an earlier time and cumulative oil production decreases. The relative permeability changes for water and oil have opposing effects on differential pressure. In the current model, the variation in oil mobility has the greatest influence, thus resulting in a slight pressure decrease with increasing residual oil saturation. When it comes to cumulative oil production, it is affected more by the value of residual oil saturation, in itself, than the corresponding change in curvature of relative permeability graphs.

4.2.5. High Salinity – Summary

The trends observed during water- and oil- wet conditions correspond well with the theory. Mixed- wet conditions show some of the expected trends, but not to the extent observed in Salathiel (1973) [65].

At first glance, changing $k_{rw}(S_{orw})$ seems to generally have a larger impact than changing n_w. This is because the two variables, and corresponding changes, are not equal in size and do not affect wettability equally. There will also be some variation from case to case, with regards to viscosity and mobility ratio. As a result, the variable alterations cannot be directly compared. The important observations are the trends that accompany these variations.

4.3. Low salinity

Defined in the code is relative permeability curves for low salinity water. When the simulator goes from injecting SSW to LS, relative permeability is interpolated between the respective relative permeability curves. The interpolation happens on the basis of mole fraction Na^+ in water. If salinity equals that of LS the associated relative permeability is in effect. When salinity is between the defined curves of SSW and LS an interpolated value is calculated, as described in chapter 4.1.1.

Table 4.3: Variables used in calculation of base case relative permeability:

S_{wi}	S_{or}	N_w	$K_{rw}(S_{orw})$	N_o	$K_{ro}(S_{wi})$
0.2	0.25	2	0.3	2	1

S_{or} is the only difference between HS/LS base case.

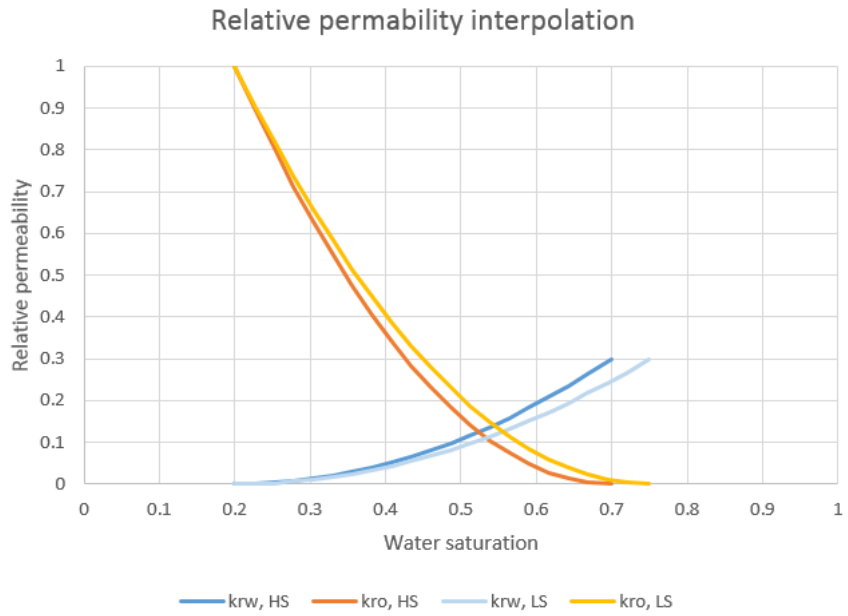

Figure 4.19: Relative permeability curves for high- and low salinity, as defined in the code

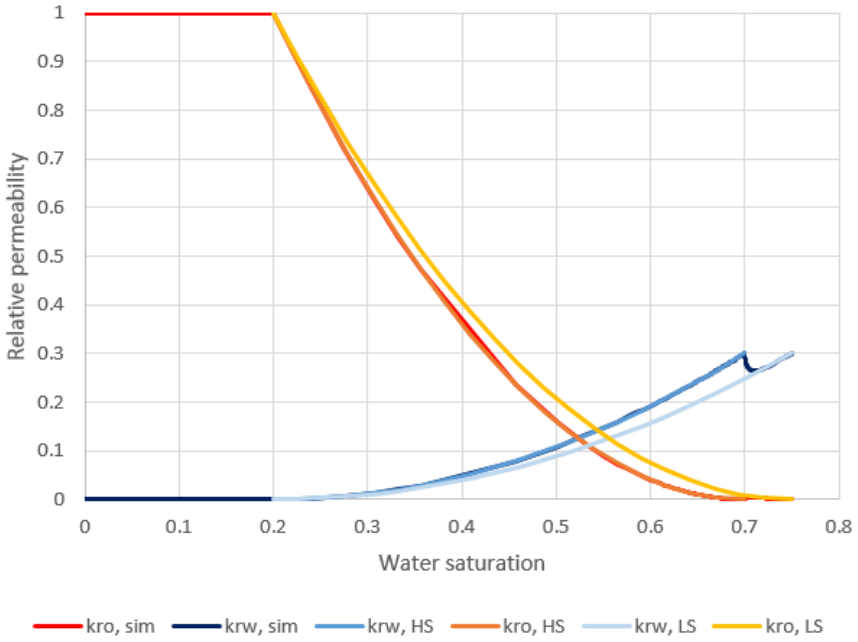

Figure 4.20: Comparison of simulated relative permeability with input curves in cell 1,1,1:

Salt concentration drops from high salinity to low salinity values. Figure 4.20 shows that relative permeability does the same and interpolates towards low salinity curves.

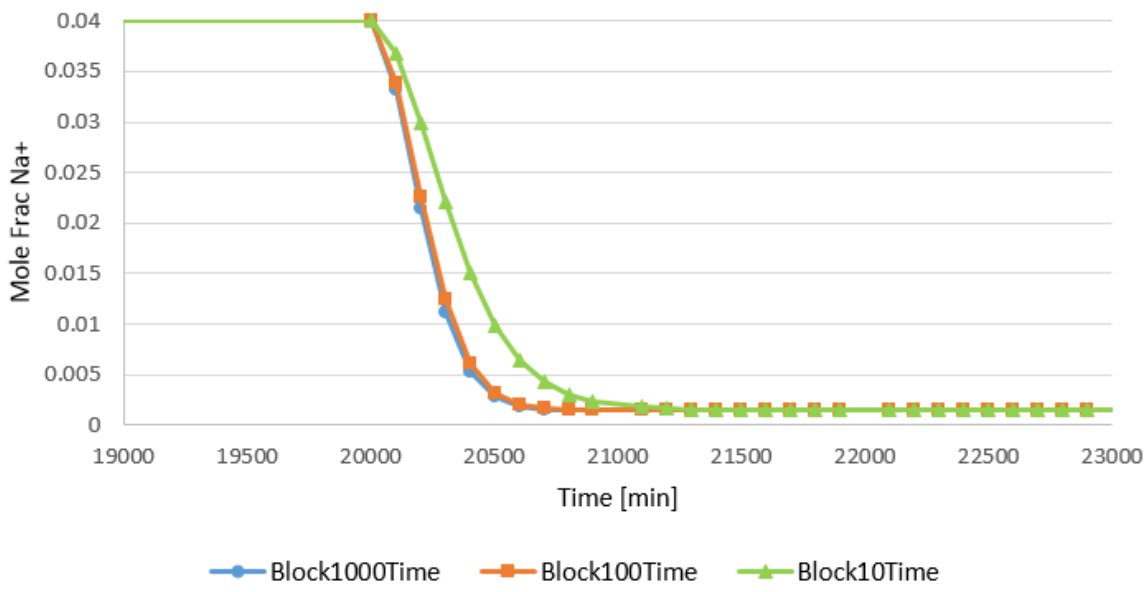

Figure 4.21: Dispersion of Na+ as a function of blocks in i- direction.

As observed in figure 4.21, the amount of blocks used to model the core has an impact on salt dispersion. The current amount of 100 blocks seems to be sufficient to decrease what is called numerical dispersion. This is further explanation in chapter 6. A physical dispersion equal to 0.01 cm^2/min was used in the model presented in this chapter. The effect of gradually decreasing salinity can be observed in the simulated relative permeability curves as the interpolation happens based on salt concentration.

5. Multiple Interpolation of Low Salinity, Surfactant and Polymer flooding, LSSP

The research group at the Centre for Integrated Petroleum Research (CIPR) encountered problems with multiple interpolation and CMG presented a possible solution for solving this problem. In this chapter, the presented solution has been evaluated.

The approach was inspected to determine viability of multi- dimensional relative permeability interpolation of low salinity, surfactant and polymer flooding. Two files were presented. One with code defining micro- emulsion viscosity in oil and one without. These will be referred to as MEVisc- and original- file respectively. Because of their similarities, only the MEVisc file has been added to the appendix.

STARS is able to handle interpolation between rock types and this is used as a tool for component based interpolation. The recommendation from CMG is that this tool is sufficient to handle component based interpolation.

5.2. Combined Processes

To model relative permeability of LSSP two rock types, RPT 1 and RPT 2, are defined. Within each rock type, relative permeability sets for high salinity, low salinity and surfactant are characterized. Interpolation parameters for these sets are $\log_{10}$ of the capillary number, N_c. Relative permeability curves for polymer are defined as an interpolation between RPT 2 and RPT 1 when polymer concentration goes from zero to max. The three sets in RPT 1 and RPT 2 are equal, except for a change in S_{or} between interpolation set 2 in the two rock types.

In the code KRTYPE CON 2 is entered to assign rock- fluid rock type, RPT, 2 to each grid block. This implies that RPT 1 is used for interpolation purposes only.

Polymer viscosity is greater at lower salinities (see chapter 3,1,1). This effect is modeled by utilizing keyword VSSALTCMP making the polymer viscosity a function of salinity. Also, polymer viscosity's shear rate dependence is modeled using keyword SHEARTAB. The increased viscosity should yield an increased capillary number, defined in equation (2.19), which leads to an increased oil recovery, as observed in the capillary desaturation curve. The

increased oil production is, as a result, a function of relative permeability interpolation for LS-LSP injection and salinity dependent viscosity for polymer.

As is discussed in chapter 3.2.1, surfactant efficiency reaches a maximum at some optimum salinity. This effect is captured in the model by defining IFT tables as a function of surfactant and salt concentrations. In addition, surfactant can create a micro- emulsion phase and thereby increase corresponding viscosity. In the MEVisc code, this is modeled as an increase in oil viscosity when surfactant is present in the oil phase and adding a viscosity mixing function for surfactant. In both files, surfactant partitioning is included as a function of salinity using liquid-liquid k value- tables.

```
OILPHASE
**ME viscosity increase to 15 cp when surfactant is in the oil phase
AVISC
.8177 10.8 15.0 .8177 10.94
BVISC
0 0 0 0 0
VSMIXCOMP 'Surfact'
VSMIXENDP 0 0.001
VSMIXFUNC 0 0.1 0.2 0.3 0.4 0.5 0.6 0.7 0.8 0.9 1
```

Figure 5.1: Additional code, found in MEVisc file, modeling micro emulsions viscosity in the oil phase.

```
DATE 2012 1  2.14449
INJECTOR MOBWEIGHT IMPLICIT 'INJTR'
INCOMP  WATER  0.995278703  1.25713011e-006  4.65169671e-005  0.00467352271  0.0
OPERATE  MAX  STW  0.00024  CONT REPEAT

DATE 2012 1  2.88266

INJECTOR MOBWEIGHT IMPLICIT 'INJTR'
INCOMP  WATER  1.0  0.0  0.0  0.0  0.0
OPERATE  MAX  STW  0.00024  CONT REPEAT

DATE 2012 1  6.91699
STOP
```

LSSP injection

NS injection

Figure 5.2: Code of injection sequence and dates. Day 1 starts off with freshwater injection.

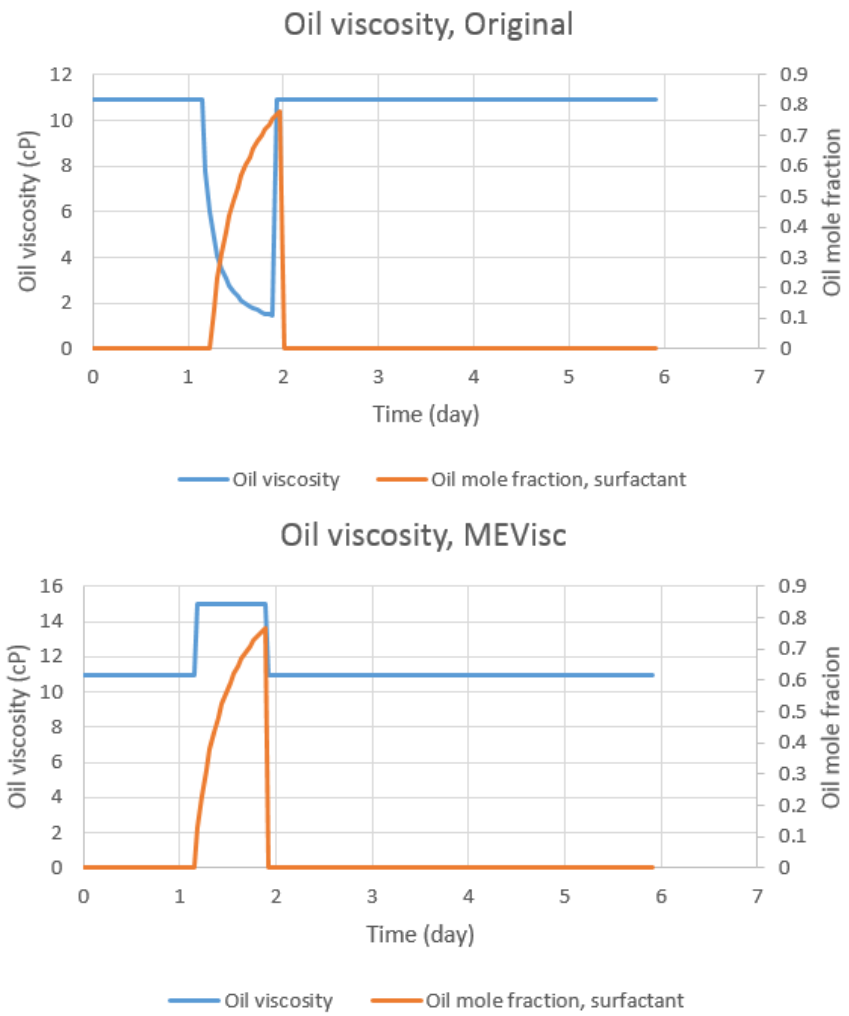

Fig 5.3: Effect of surfactant concentration on oil viscosity in block 1,1,1. Left: original file. Upper graph: Original file. Lower graph: MEVisc file.

As can be observed in fig. 5.3 the effect of MEVisc is obvious. For both cases, oil mole fraction surfactant reaches above 0.76, but the viscosity effect is dissimilar. For the original file, oil viscosity linearly decreases with surfactant concentration and approaches surfactant viscosity (equal to water viscosity). In the MEVisc run, viscosity rises to 15cP, as defined. The viscosity increase is almost instant because of viscosity mixing keyword having an end point value, mole fraction, of 0.001.

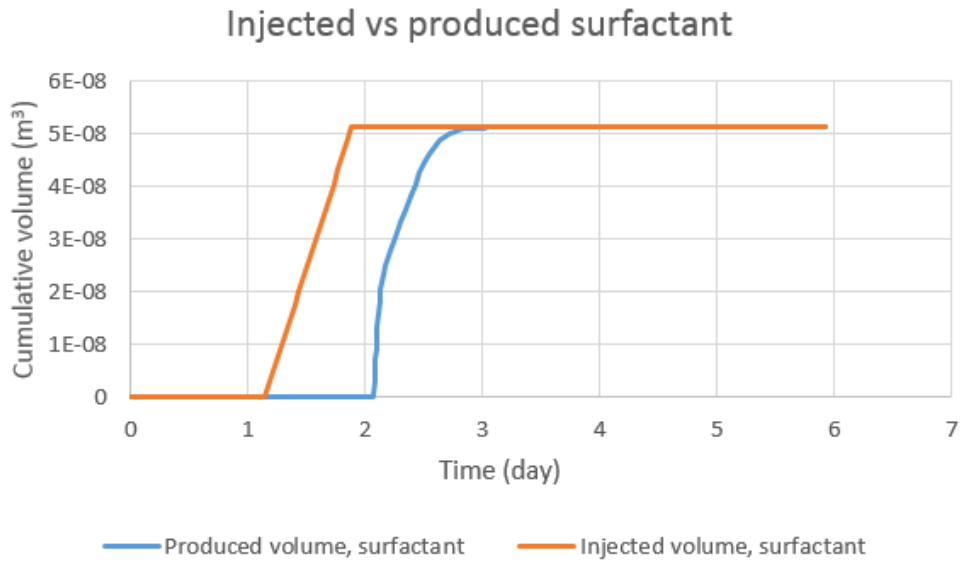

Figure 5.4: Cumulative- injected and produced volumes of surfactant.

Production curves reveal that surfactant does not reach the producer before the end of LSSP injection. During this time 3.4 pore volumes of combined LSSP was injected. Surfactant breakthrough, coincidently, takes place 3 hours after the initiation of freshwater injection. In contrast, polymer reaches the producer within an hour after LSSP starts.

Comparing Original and MEVisc files show similar production curves, but different concentrations in cell 1,1,1(injector cell). Both show the same trends, but differ greatly in water mole fraction peak value. This is due to increased pressure, from micro- emulsion viscosity, leading to different k values and thereby different surfactant partitioning.

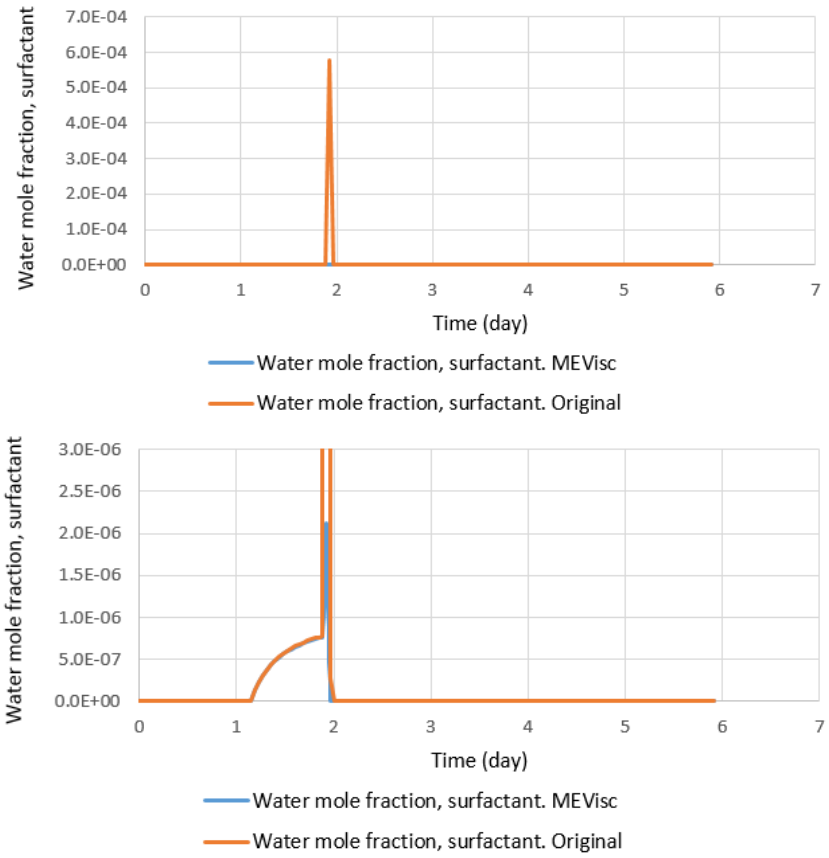

Figure 5.5: Comparison of surfactant concentration in water for cell 1,1,1. Lower graphs y-axis is zoomed in to enable visualization of the initial concentration profile.

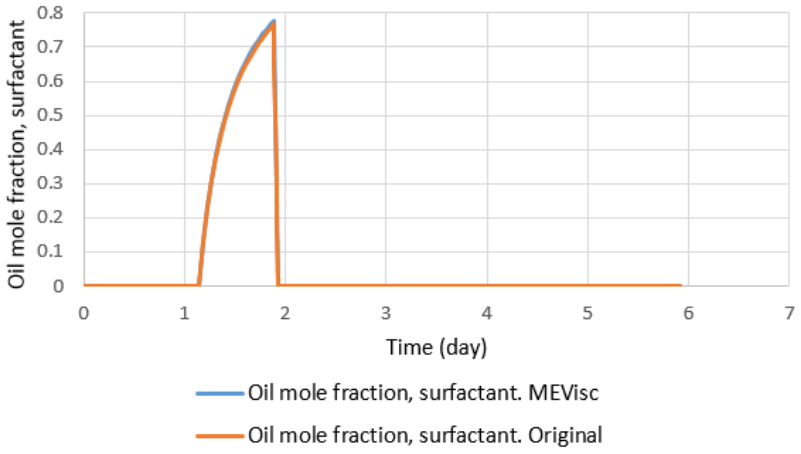

Figure 5.6: Comparison of surfactant concentration in oil for cell 1,1,1.

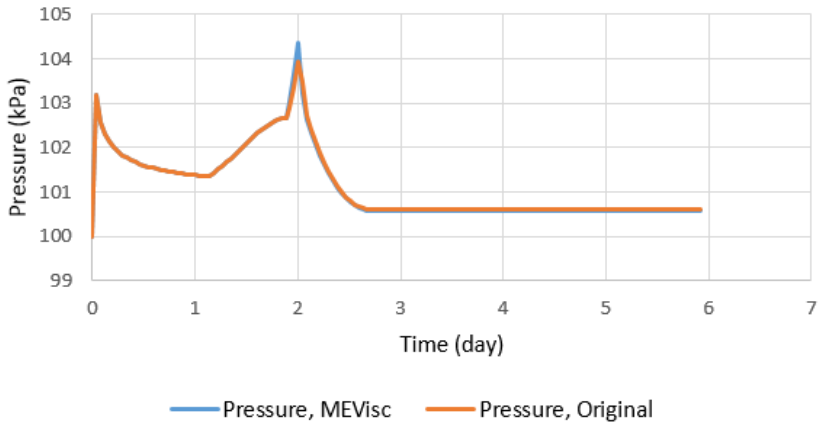

Figure 5.7: Pressure comparison of MEVisc and Original file in cell 1,1,1.

Table 5.1: Comparison of peak surfactant concentrations in cell 1,1,1.

	MEVisc	**Original**
Water mole fraction, surfactant	$2.1225 \cdot 10^{-6}$	$5.7913 \cdot 10^{-4}$
Oil mole fraction, surfactant	0.7670	0.7776

From table 5.1, and previous graphs, it becomes apparent that surfactant concentration in oil is unrealistically high compared to input values in the code. A consequence of this is that relative small changes in oil mole fraction surfactant cause significant concentration differences of surfactant in water.

When freshwater is injected salt concentration reaches zero, thereby yielding tables of zero k values. This implies no surfactant in oil, which can be observed as all surfactant moves into the water phase, causing the concentration spike observed in figure 5.8. Afterwards, surfactant concentration quickly approaches 0 as the chaseflood propagates surfactant through the core.

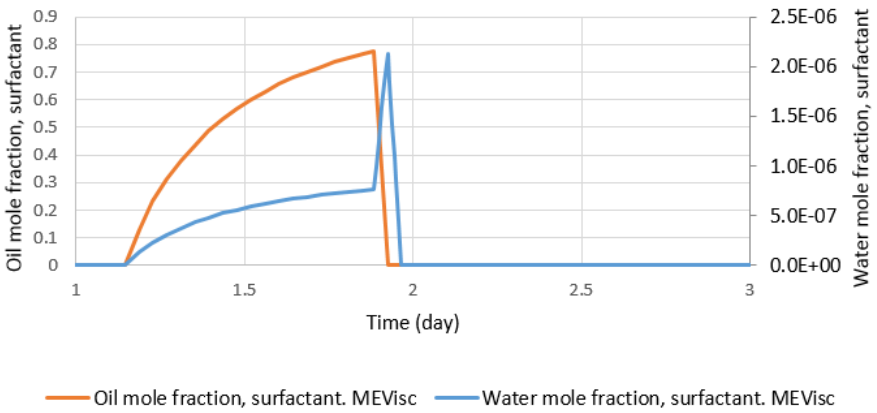

Figure 5.8: Surfactant concentration in oil and water in cell 1,1,1 for the MEVisc file.

As observed in fig. 5.9, $\log_{10}$ of capillary number, during LSSP injection, is not high enough to initiate any significant relative permeability interpolation of relative permeability sets 2 and 3. The spike in surfactant concentration coincides with an increase in capillary number, thus triggering interpolation of sets 2 and 3. This mobilizes surfactant and subsequently some trapped oil.

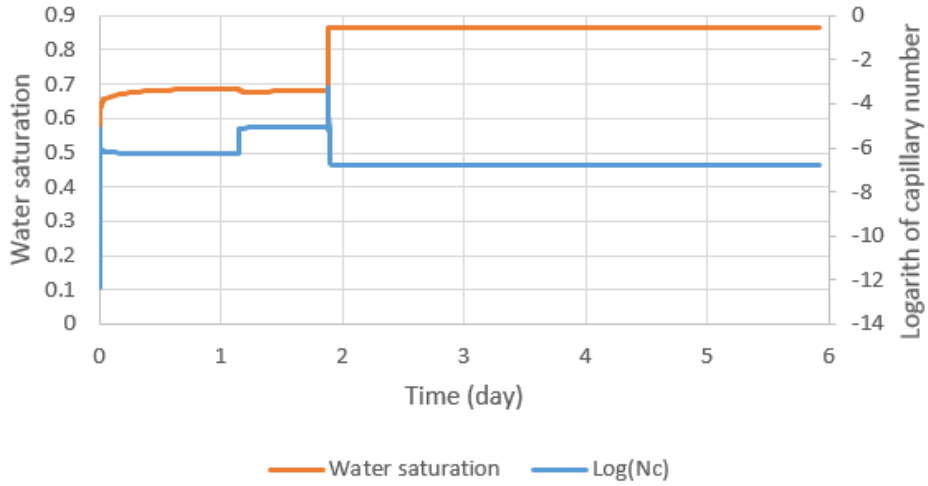

Figure 5.9: Capillary number and its effect on saturation in cell 1,1,1. Results from Original file.

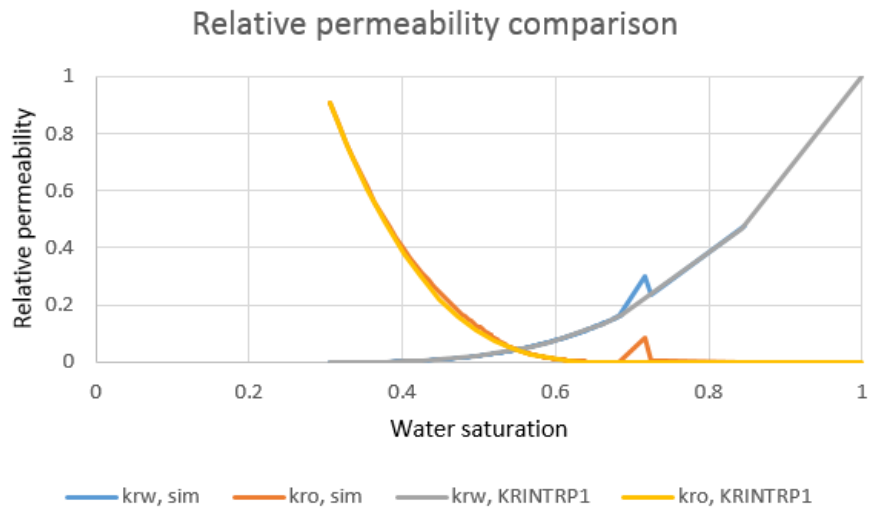

Figure 5.10: Simulated relative permeability in cell 1,1,1, compared to relative permeability set 1. Results from original file.

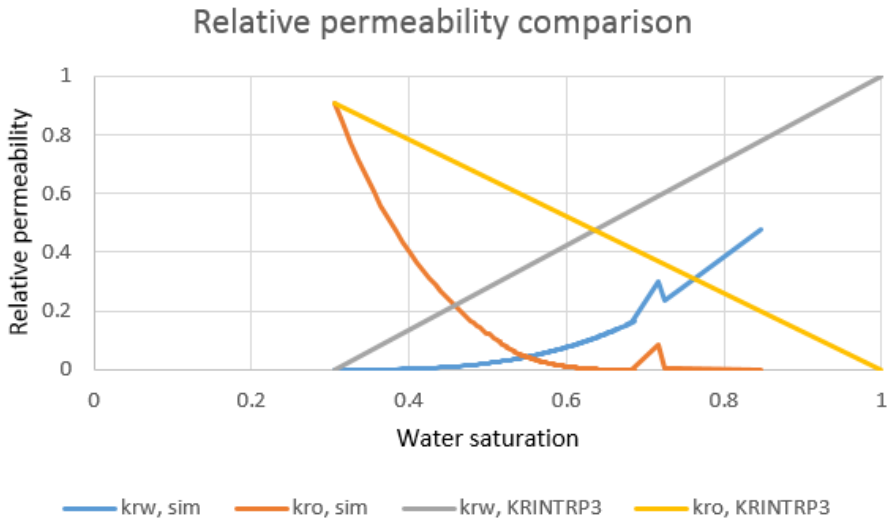

Figure 5.11: Simulated relative permeability in cell 1,1,1, compared to relative permeability set 3. Results from original file.

Comparing water saturation from figure 5.9 and relative permeabilities from figures 5.10-11, relative permeability interpolation towards set 3 is initiated at the time of freshwater injection.

5.2. Separated Processes

The injected sequence of components in LSSP were separated to investigate the cause of previously observed results. Injection durations were increased from 9 to 10 days for each process. Since it was unclear whether the mobilization of surfactant happened because of reaching a critical saturation or because of some effect of freshwater chaseflood, the LSP injection process, specifically, was extended an additional 10 days to see if surfactant stopped partitioning and/or mobilized during this time. Modeling micro emulsion viscosity in the oil phase was shown to work, but is of less interest when modeling low salinity flooding, since it generally implies a type II(-) micro emulsion system. The following runs are based on the Original file.

IFT- tables in the code were defined such that interfacial tension could potentially decrease from 23.400cP to 2.953cP, with increasing salinity alone. Since the current file was to be used in history matching the table was changed to make interfacial tension, realistically, less sensitive to salinity. This to better model the separate process of low salinity water injection. IFT- tables that were both salinity and surfactant dependent were left untouched.

```
INTCOMP 'NaCl' WATER
IFTTABLE
** Weight percent Surfact = 0
2CMPW 1e-007
**  Composition of component/phase  Interfacial tension
                    0.001547029274                23.4  ** Salinity(NaCl), ppm = 5000
                     0.00310483332               5.163  ** Salinity(NaCl), ppm = 10000
                    0.003887811122               4.356  ** Salinity(NaCl), ppm = 12500
                    0.004673525099               3.715  ** Salinity(NaCl), ppm = 15000
                     0.00546198962               4.102  ** Salinity(NaCl), ppm = 17500
                    0.006253219154               3.805  ** Salinity(NaCl), ppm = 20000
                    0.007047228271               3.521  ** Salinity(NaCl), ppm = 22500
                    0.007844031643               2.953  ** Salinity(NaCl), ppm = 25000

INTCOMP 'NaCl' WATER
IFTTABLE
** Weight percent Surfact = 0
2CMPW 1e-007
**  Composition of component/phase  Interfacial tension
                    0.001547029274                23.4  ** Salinity(NaCl), ppm = 5000
                     0.00310483332                23.4  ** Salinity(NaCl), ppm = 10000
                    0.003887811122                23.3  ** Salinity(NaCl), ppm = 12500
                    0.004673525099                23.2  ** Salinity(NaCl), ppm = 15000
                     0.00546198962                23.1  ** Salinity(NaCl), ppm = 17500
                    0.006253219154                23.0  ** Salinity(NaCl), ppm = 20000
                    0.007047228271                23.0  ** Salinity(NaCl), ppm = 22500
                    0.007844031643                23.0  ** Salinity(NaCl), ppm = 25000
```

Figure 5.12: Salinity dependent IFT tables before(top) and after(bottom).

A comparison was made on runs of the two component injection case, explained further in the next chapter.

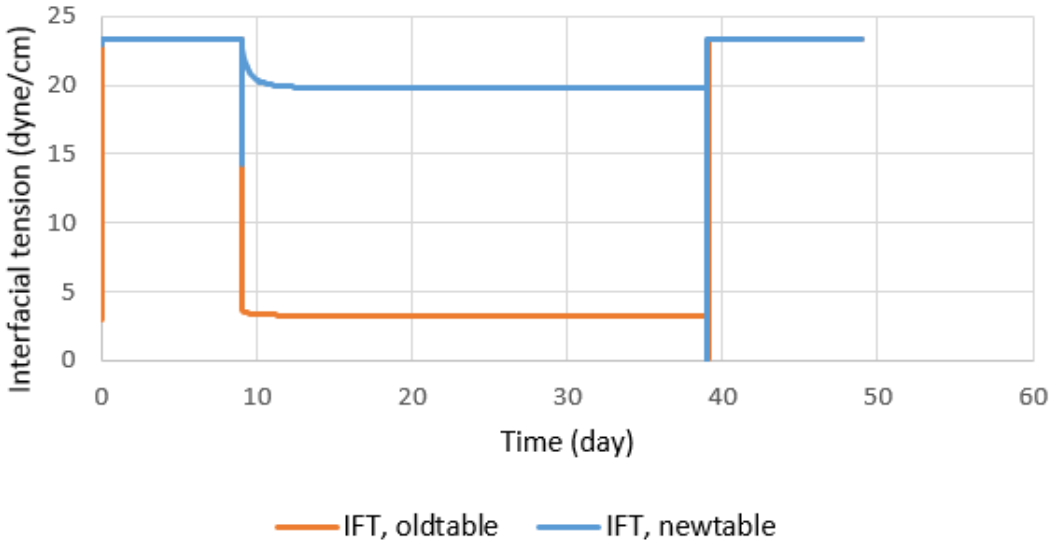

Fig. 5.13: Simulated interfacial tension before and after changing table values. Spike in values are caused by sharp increase and decrease in surfactant concentration. Spike trends are equal for the two runs.

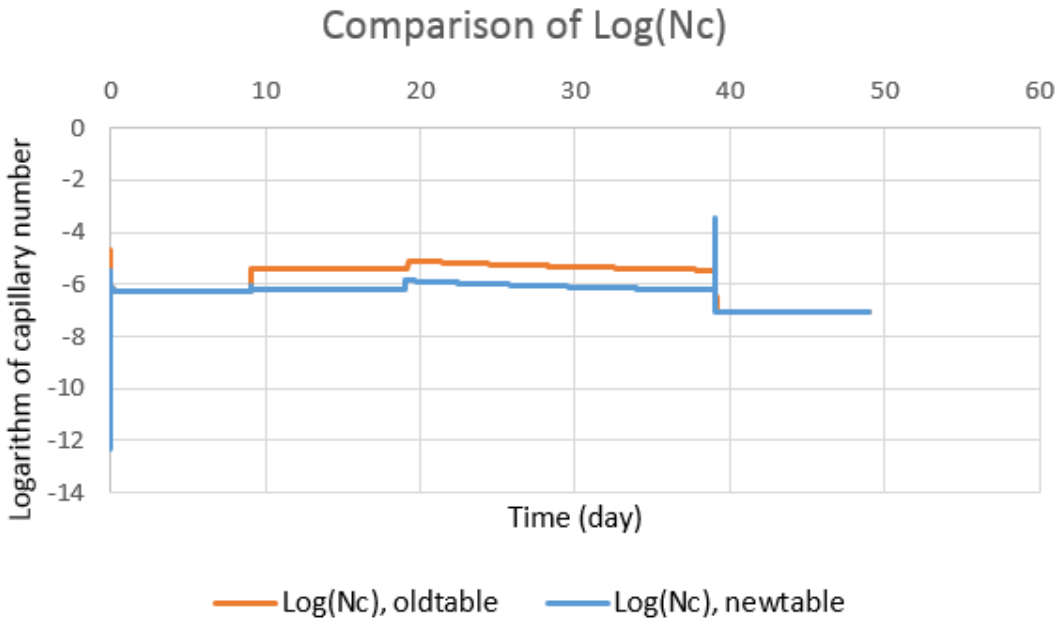

Figure 5.14: Simulated $\log_{10}$(Nc) values before and after changing IFT- tables. The spike trend is equal for the two runs.

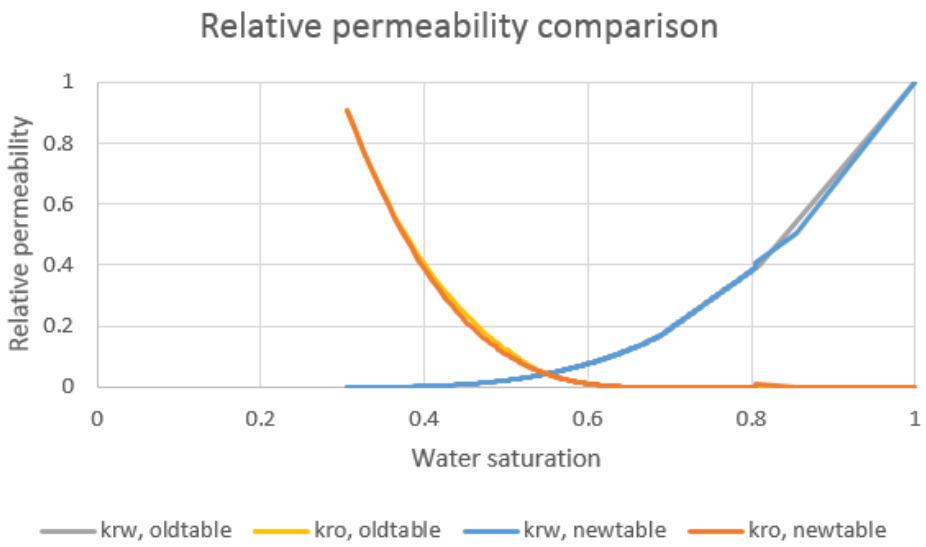

Figure 5.15: Simulated relative permeability before and after changing IFT- tables.

From figures 5.13 and 5.14 one can observe some of the direct effects of changing IFT- tabels. Even though the tables are more realistic, it does nothing to improve the relative permeability interpolation. Surfactant behaviour is still problematic. Observe from fig. 5.13 the importance of changing the tables as salinity, previously, had a comparable effect on interfacial tension as a surfactant.

Further simulations are run with the new IFT- tables.

5.2.1. Separated Processes – Dual Component Injection

Previous studies like Drønen (2017) [57] have shown that STARS handles the introduction of more than two rock types poorly. One theory was that this might also be true for more than two relative permeability interpolation sets. To investigate this, no more than two components were injected, together with water, at a time. This run will be referred to as 2comp.

```
DATE     2012     1   10.00000
INJECTOR MOBWEIGHT IMPLICIT 'INJTR'
**           'Water'      'Polymer'       'Surfact'       'NaCl'      'Dead_Oil'
INCOMP   WATER  0.9952799603229  0.0  4.65169671e-005  0.00467352271  0.0
OPERATE  MAX  STW  0.00024  CONT REPEAT

DATE     2012     1   20.00000

INJECTOR MOBWEIGHT IMPLICIT 'INJTR'
INCOMP   WATER  0.99532522015989  1.25713011e-006  0.0  0.00467352271  0.0
OPERATE  MAX  STW  0.00024  CONT REPEAT

DATE     2012     2   9.00000

INJECTOR MOBWEIGHT IMPLICIT 'INJTR'
INCOMP   WATER  1.0  0.0  0.0  0.0  0.0
OPERATE  MAX  STW  0.00024  CONT REPEAT

DATE     2012     2   19.00000
STOP
```

LSS injection

LSP injection

NS injection

Figure 5.16: Code of injection sequence and dates. Day 1 starts off with freshwater injection.

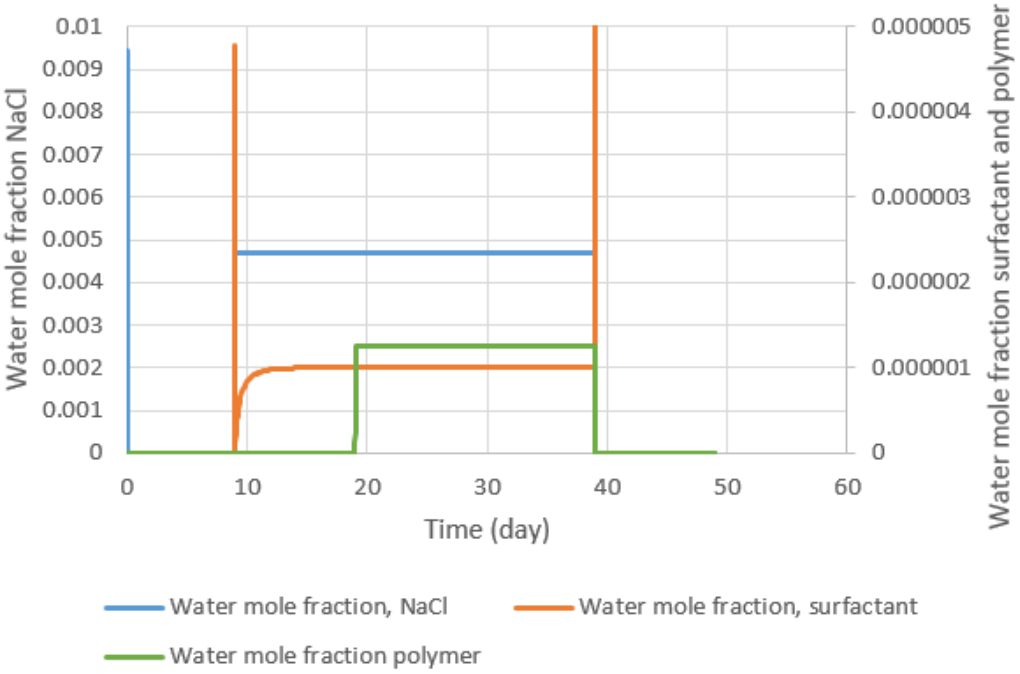

Figure 5.17: Component concentrations in water of cell 1,1,1. Note that the y2- axis does not include max concentration of surfactant.

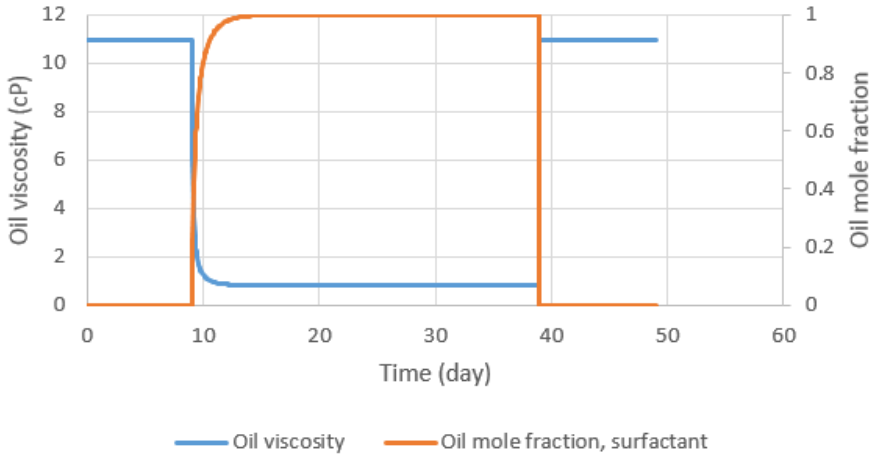

Figure 5.18: Oil viscosity and surfactant in oil concentration of cell 1,1,1.

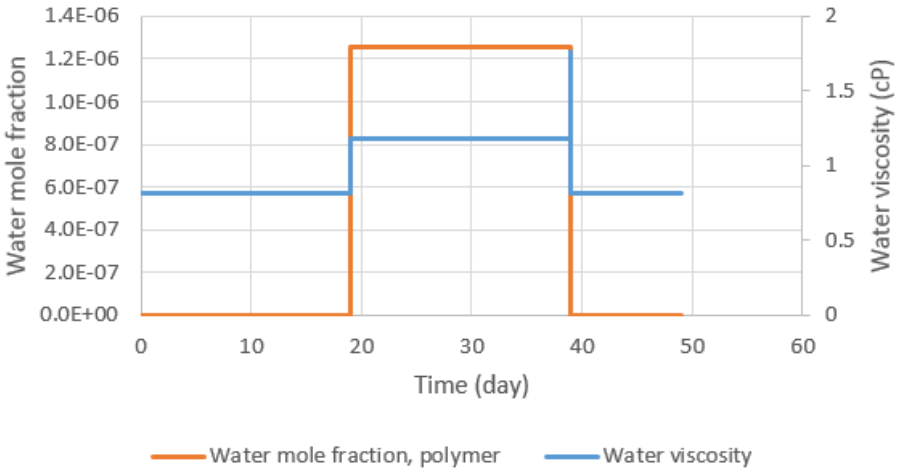

Figure 5.19: Water viscosity and polymer in water concentration of cell 1,1,1.

When comparing mole fractions of surfactant in water and oil, in cell 1,1,1, a few things can be observed. Surfactant is injected into the water phase and quickly partitions into the oil phase. Concentration in water stabilizes at a very low mole fraction and does not decrease during subsequent 20 days of LSP injection. It then spikes right as freshwater flood is initiated before quickly being reduced to zero. Oil mole fraction surfactant approaches one asymptotically, which is an unrealistically high concentration. This explains why surfactant in water concentration does not increase further and why oil viscosity approaches surfactant viscosity.

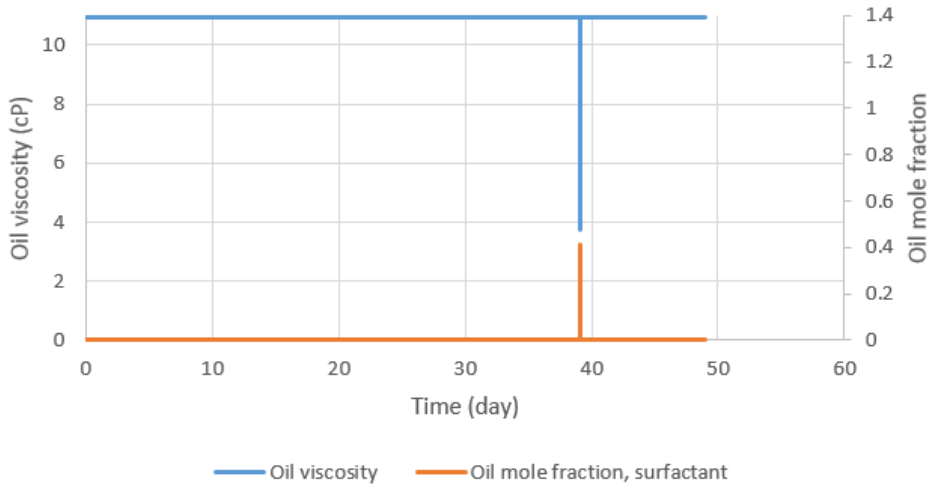

Figure 5.20: Oil viscosity and surfactant concentration in oil of cell 50,1,1.

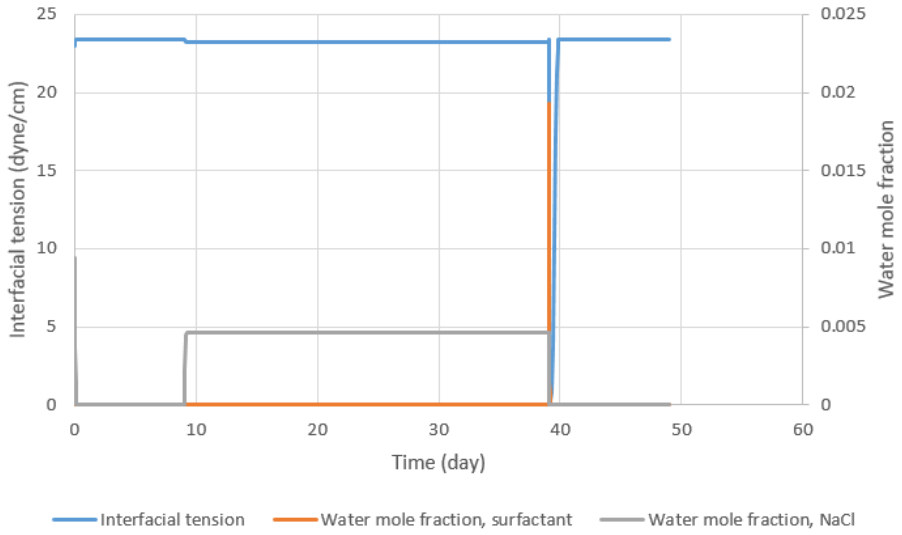

Figure 5.21: Interfacial tension and salt and surfactant concentration in water of cell 50,1,1.

Comparing cell 1,1,1 with 50,1,1, surfactant is still not moving through the core as it should. Because of surfactant partitioning, mole fraction in water is zero until freshwater chaseflood. The same goes for concentration of surfactant in oil. Oil viscosity is constant until concentration spike. Note that the duration of this spike is shorter as oil mole fraction is dependent on salinity, which is also reduced during the chaseflood.

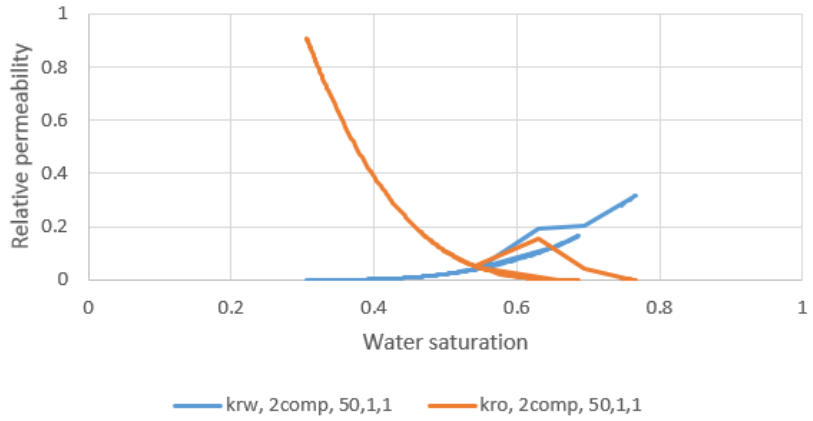

Figure 5.22: Relative permeability of cell 50,1,1.

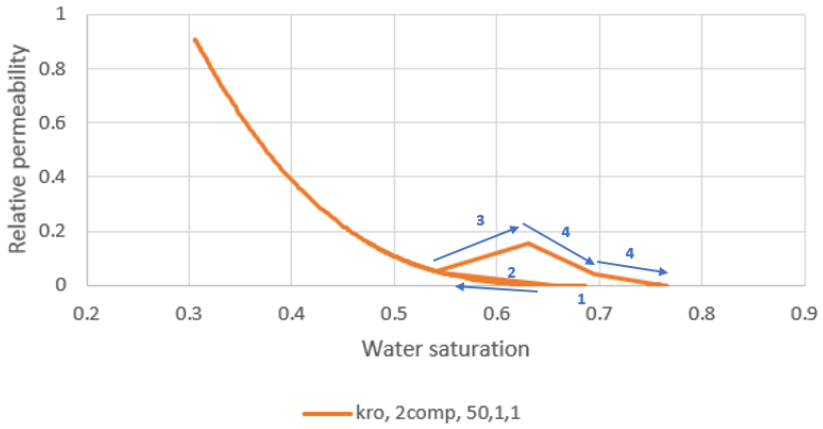

Figure 5.23: Oil relative permeability of cell 50,1,1

Due to the sharp saturation changes and subsequent relative permeability interpolation, cell 50,1,1 is interpolated through all 3 sets over a short period of time. This can be observed in figure 5.23 as:

1. Water saturation, about 0.68, at the time of freshwater injection and subsequent surfactant concentration increase.
2. Water saturation decreases accompanied by relperm change along previous path.
3. S_w increases again with interpolations toward relperm set 3.
4. Interpolation renders curves approaching relative permeability set 1 and its associated S_{or}.

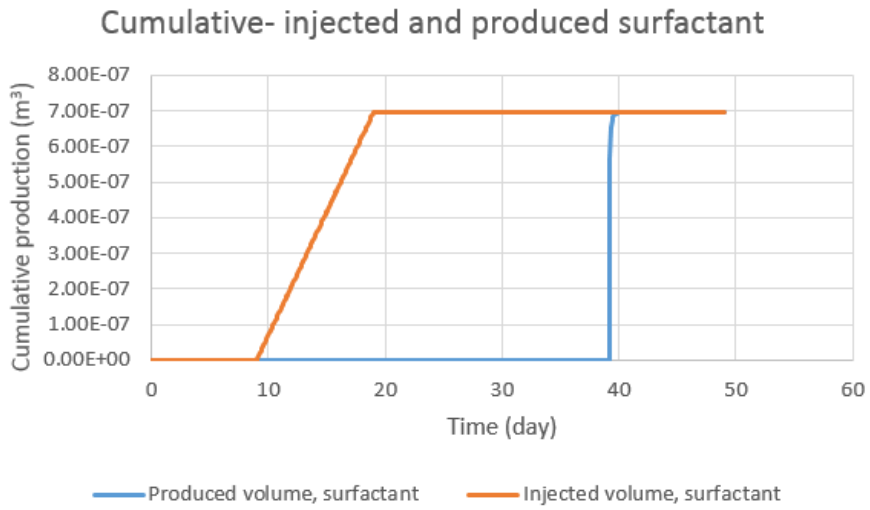

Figure 5.24: Injected- and produced volumes of surfactant.

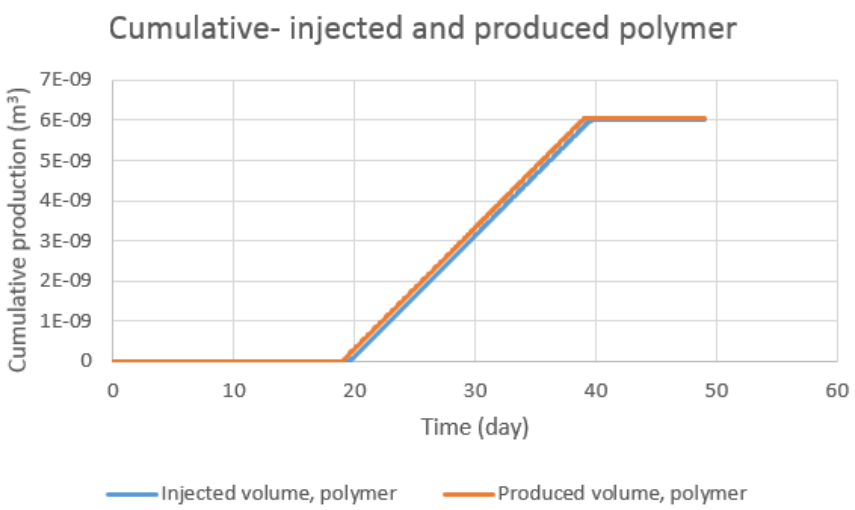

Figure 5.25: Injected- and produced volumes of polymer.

From figures 5.24 and 5.25 the pre- freshwater flood, immobility of surfactant becomes clear when compared with polymer behaviour.

5.2.2. Separated Processes – Single Component Injection

Due to the persistence of surfactant immobility, a maximum number of 1 component was injected at a time, together with water. Concentrations and variables controlling the interpolation of relative permeability were assesed. The only changes from the original file were IFT-tables, injection sequences and injection times. This simulation will be referred to as 1comp.

```
DATE    2012    1   10.00000
INJECTOR MOBWEIGHT IMPLICIT 'INJTR'
INCOMP  WATER  0.995326477  0.0  0.0  0.00467352271  0.0
OPERATE  MAX  STW  0.00024  CONT REPEAT

DATE    2012    1   20.00000
DTMAX 0.0001
INJECTOR MOBWEIGHT IMPLICIT 'INJTR'
INCOMP  WATER  0.999953483  0.0  4.65169671e-005  0.0  0.0
OPERATE  MAX  STW  0.00024  CONT REPEAT

DATE    2012    1   30.00000

INJECTOR MOBWEIGHT IMPLICIT 'INJTR'
INCOMP  WATER  0.999998743  1.25713011e-006  0.0  0.0  0.0
OPERATE  MAX  STW  0.00024  CONT REPEAT

DATE    2012    2   9.00000

INJECTOR MOBWEIGHT IMPLICIT 'INJTR'
INCOMP  WATER  1.0  0.0  0.0  0.0  0.0
OPERATE  MAX  STW  0.00024  CONT REPEAT

DATE    2012    2   19.00000
STOP
```

LS injection

S injection

P injection

NS injection

Figure 5.26: Code of injection sequence and dates. Day 1 starts off with freshwater injection.

All component concentrations quickly reach their corresponding injection input values. When a new component is injected the concentration of previously injected components approach 0. Component immobility, seemingly, is no longer an issue.

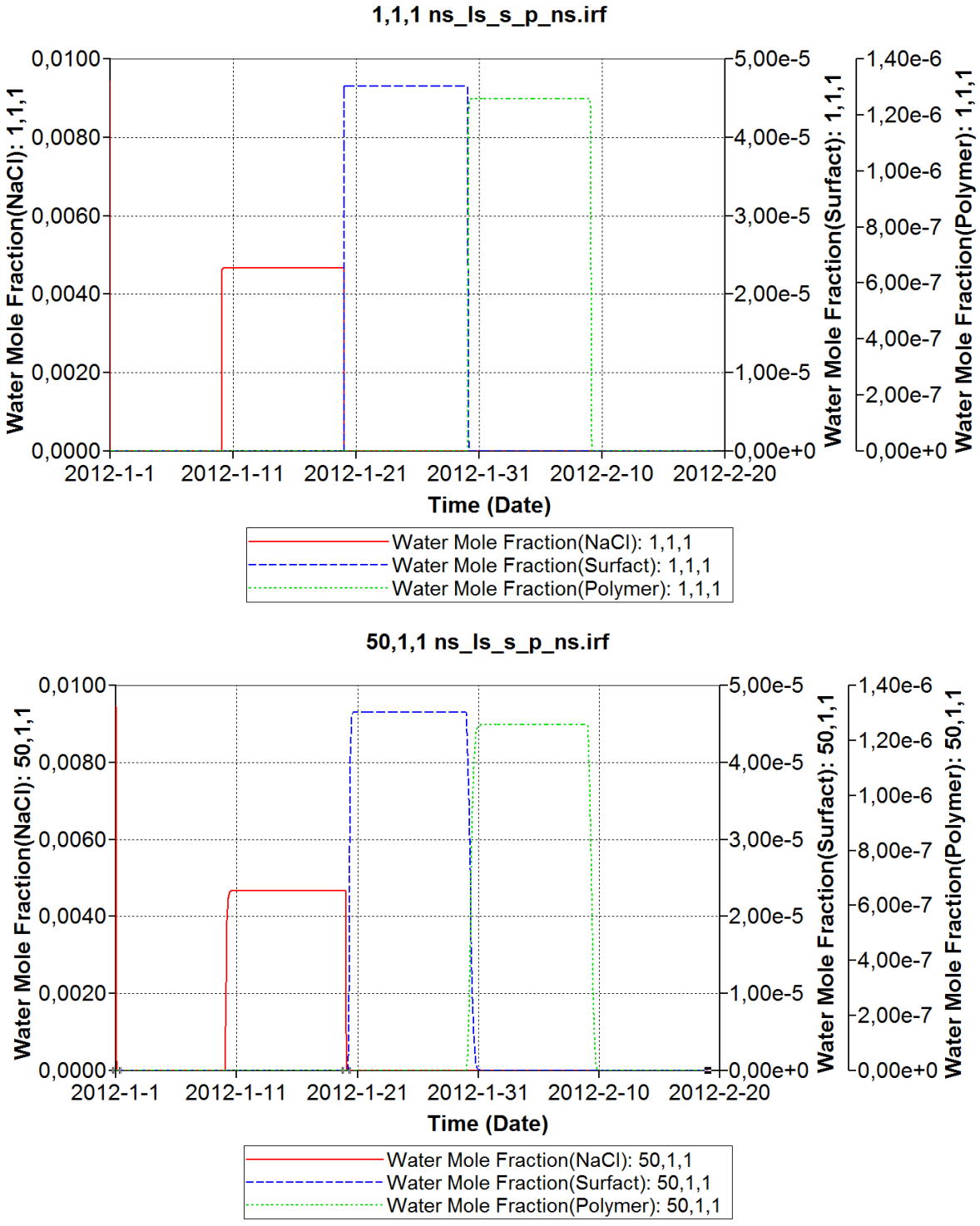

Figure 5.27: Component concentrations in cell 1,1,1 and 50,1,1.

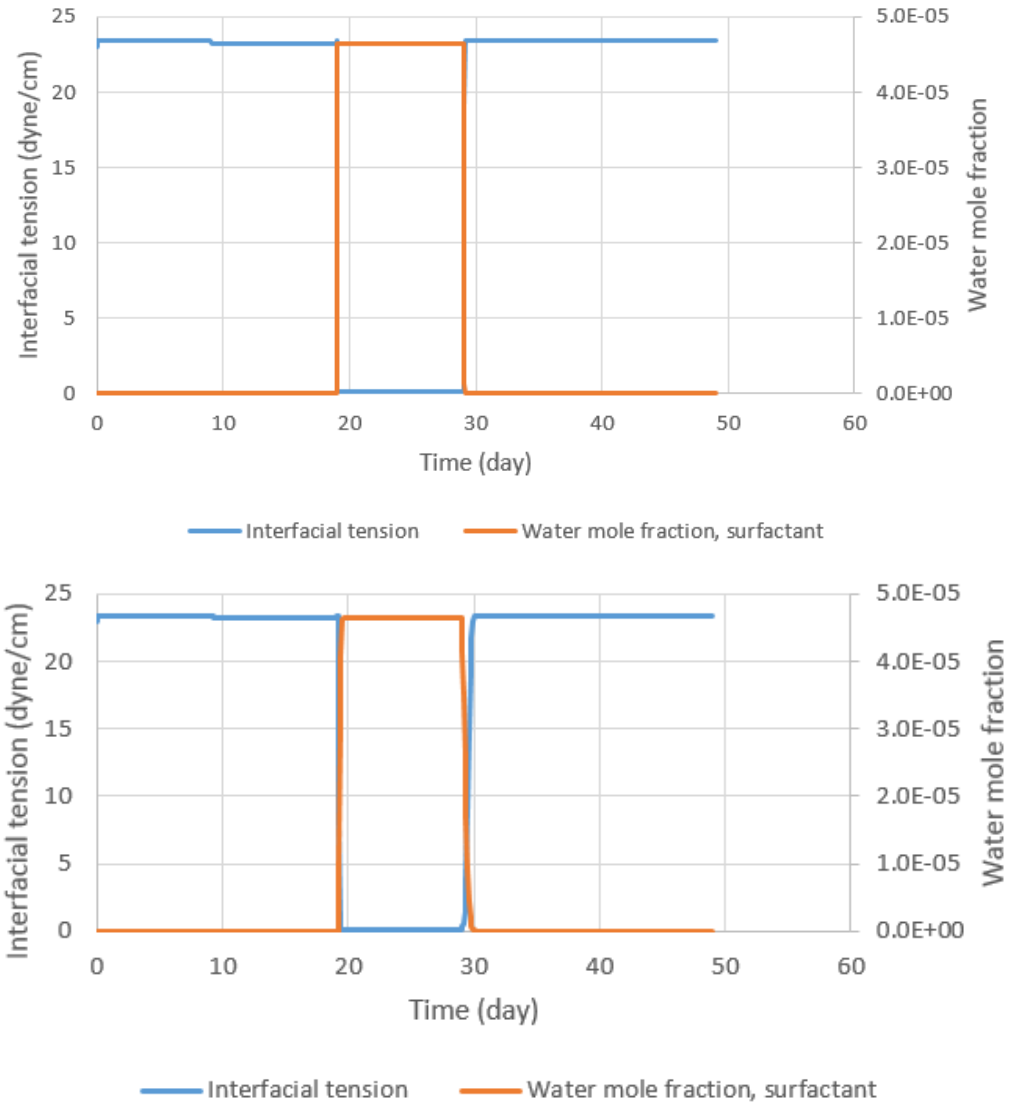

Figure 2.28: Interfacial tension and surfactant concentration in water for cells 1,1,1(Top) and 50,1,1(Bottom)

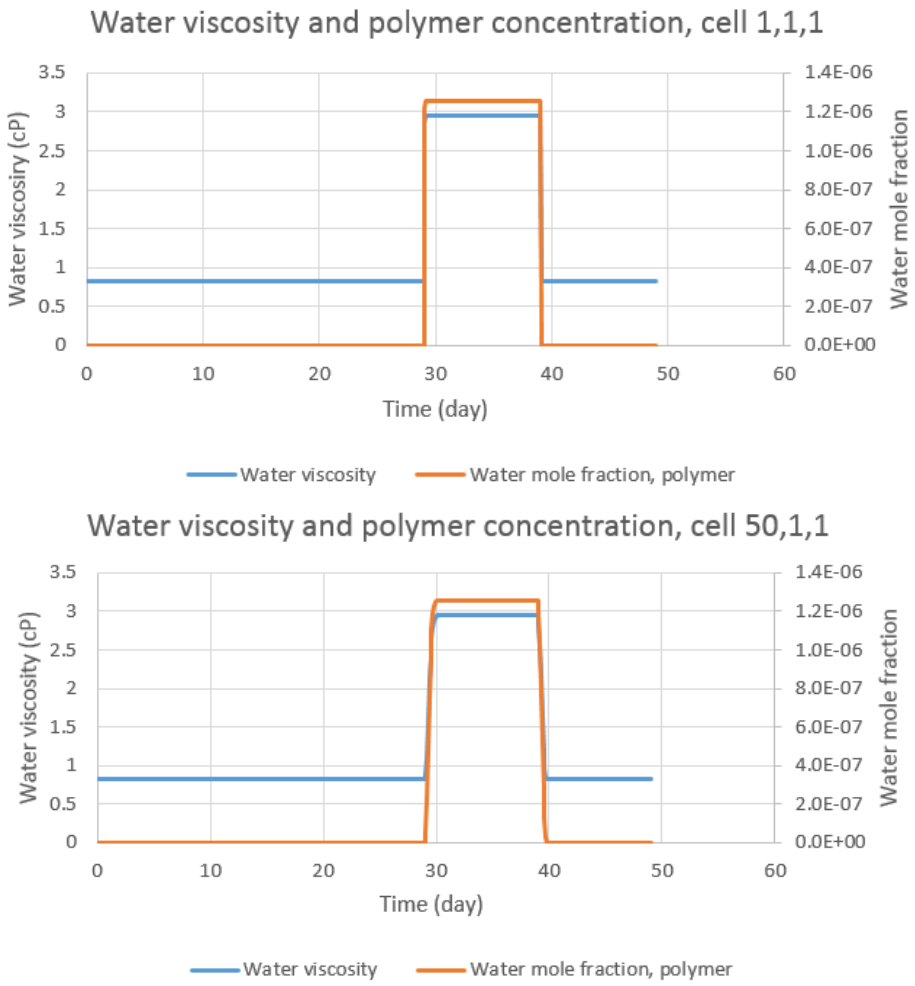

Figure 5.29: Water viscosity and polymer concentration for cells 1,1,1 and 50,1,1.

From the graphs in figure5.27 it becomes apparent that components are mobile since concentration trends are the same throughout the core. Observed in figures (IFT) the interfacial tension has a small dip, arround day 10, due to salt concentration, before being reduced significantly by the pressence of surfactant. The graphs show good corespondence with tables and input values in the file. The same goes for figure 5.29 where water viscosity is changed by polymer alone, since surfactant viscosity equals water viscosity. Water viscosity is still dependent on surfactant viscosity, in this case, reducing the viscosity increase polymer would otherwise have.

Another observation to make from figures 5.28 and 5.29 is that concentration changes are not as sharp, but more smeared, as distance from the injector increases. This will, in turn, have a slight effect on corresponding, concentration dependent variables. The smearing is caused by dispersion, which will be covered in chapter 6.

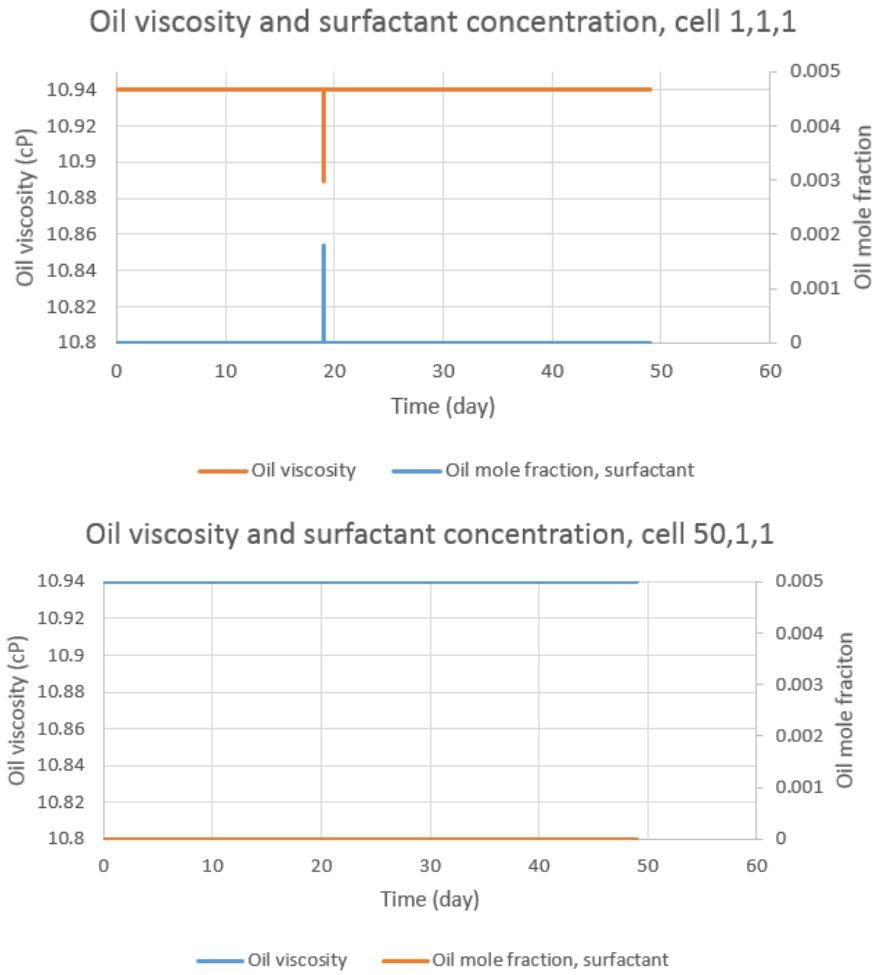

Figure 5.30: Oil viscosity and surfactant concentration in oil of cells 1,1,1 and 50,1,1

Since surfactant partitioning is dependent on the pressence of salt there is no change in oil viscosity. Only in cell 1,1,1 where a slight overlap in salt and surfactant concentrations exists, can there be found an increase in oil mole fraction surfactant. This overlap only exists for 1min and 17sec which can be observed in figure 5.30 as rapid changes in viscosity and conenctration. In cell 50,1,1 there is no concentration overlap and therefore no surfactant in oil nor any viscosity change.

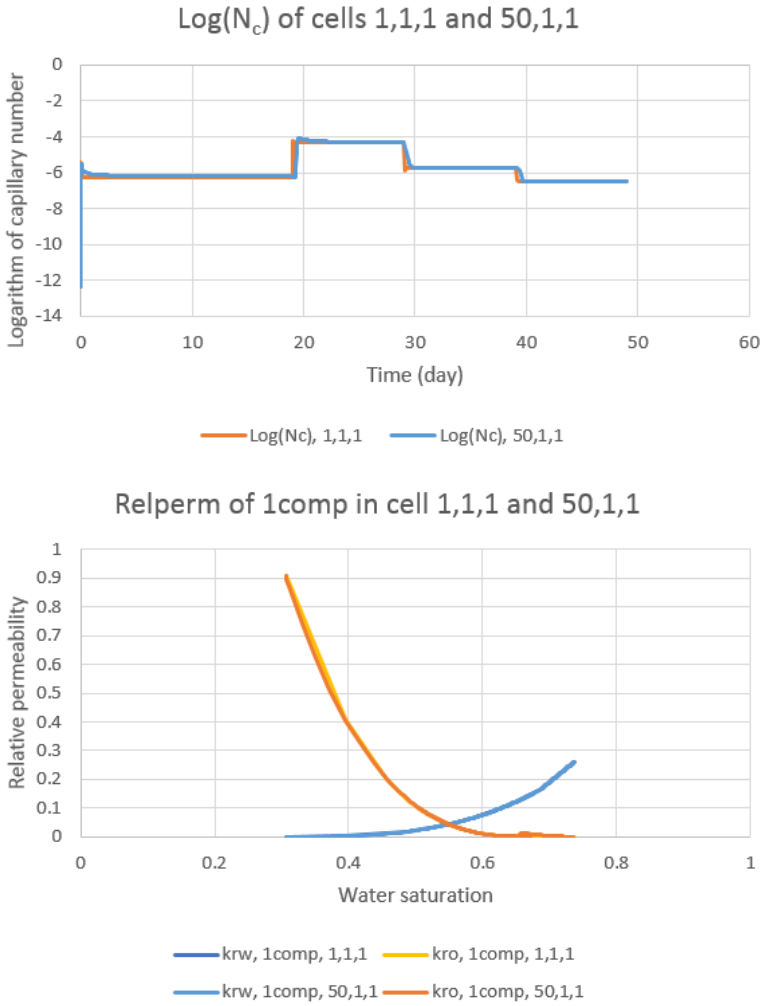

Figure 5.31: Log10(Nc) and corresponding relative permeability of cells 1,1,1 and 50,1,1

Since variables controlling capillary number are almost identical when moving through the core, so too are the relative permeability curves. Because interfacial tension is lowest when surfactant and salt concentrations are high in combination, capillary number is insufficiently high to trigger interpolation of relative permeability set 3. This can be observed as residual oil saturation is higher, as defined in set 2, and that there is no change in relative permeabilities caused by injection of surfactant. The slight increase in oil relative permeability is an effect of the increased S_{or}.

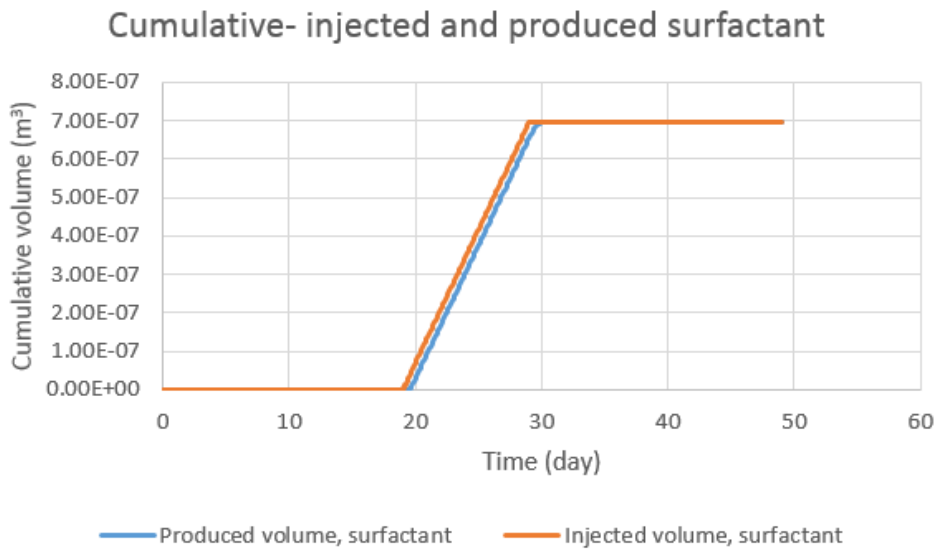

Figure 5.32: Cumulative- injected and produced volumes of surfactant

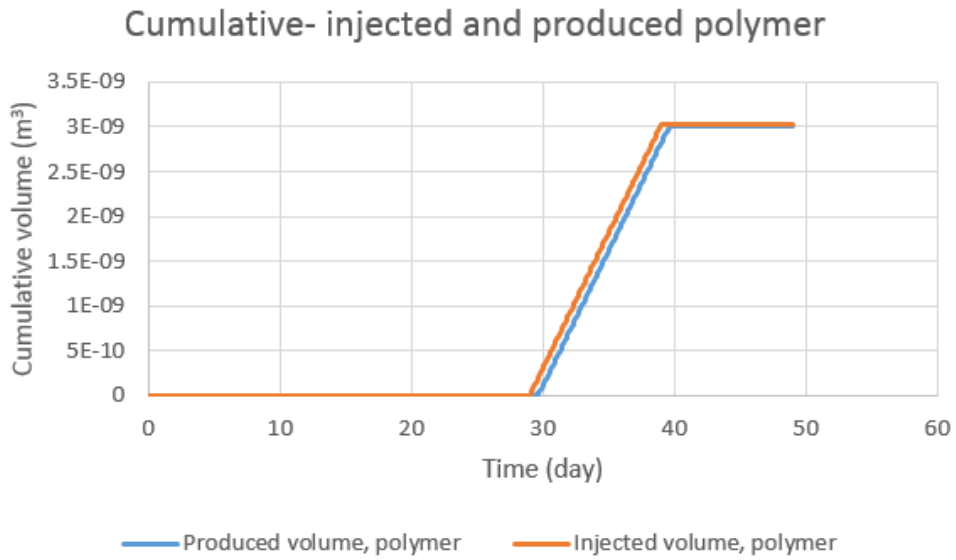

Figure 5.32: Cumulative- injected and produced volumes of polymer.

Figures 5.31 and 5.32 confirm that surfactant and polymer have good mobility in the model. A slight retention due to adsorption, defined in the code, was observed as produced volumes were smaller than produced volumes.

5.2.3. Separated Processes - Summary

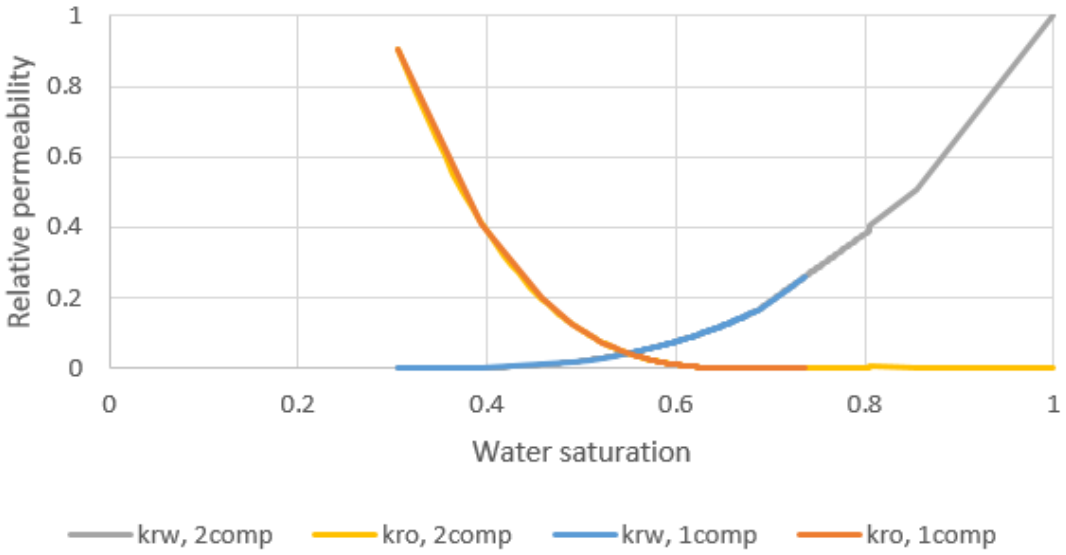

Figure 5.34: Relative permeability comparison of 2comp and 1comp runs in cell 1,1,1.

Relative permeability is almost equal for 1comp and 2comp injection except 2comp has lower residual oil saturation. A slight effect of surfactant injection can be viewed just after 0.8 water saturation. The minimal effects surfactant has on relative permeability makes it difficult to render the potential pressure change a surfactant flood could entail. This also affects production, but can to a greater degree be controlled by residual oil saturation, IFT- tables and interpolation set designator, DTRAPW/N($\log_{10}(N_c)$).

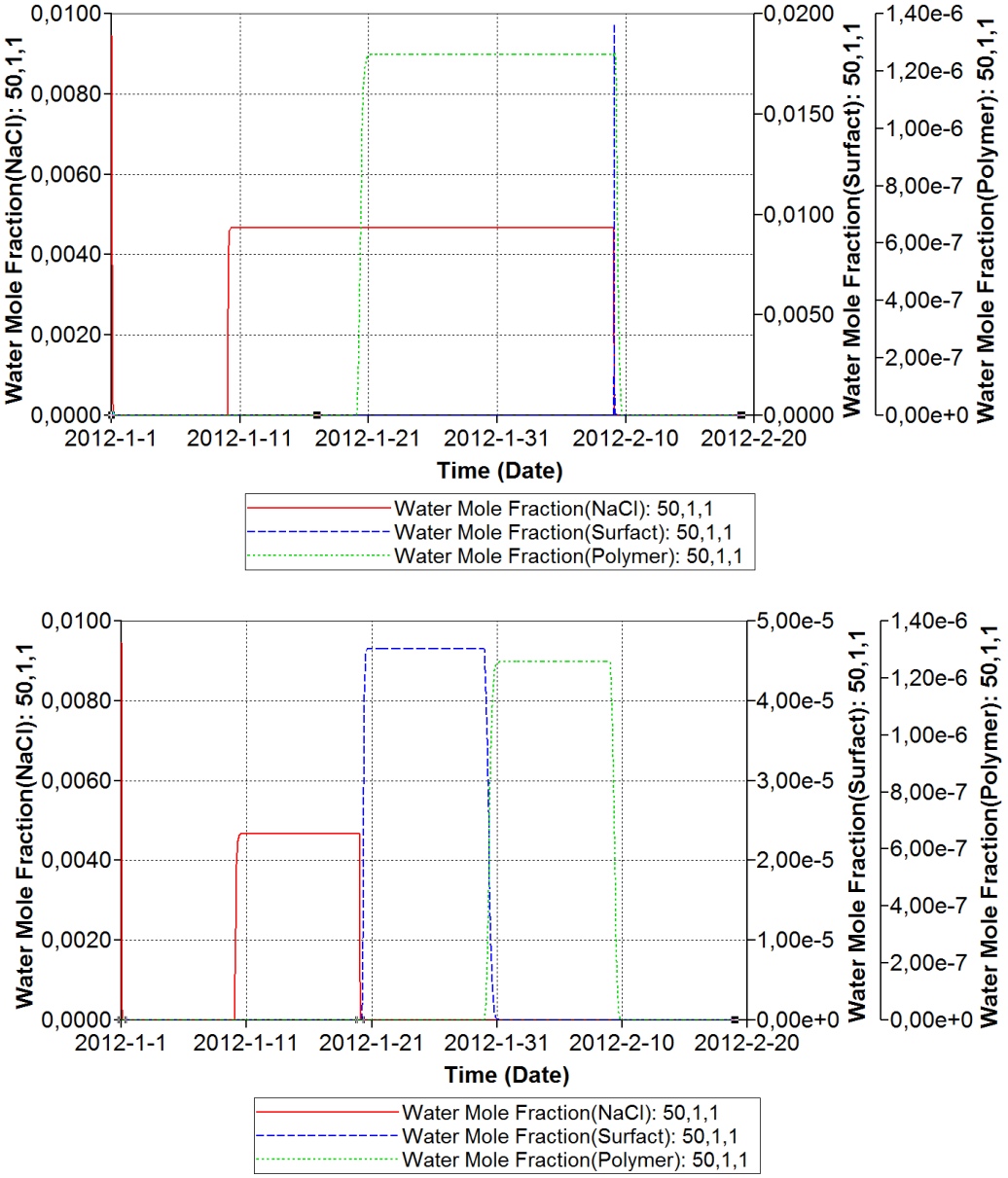

Figure 5.35: Component concentrations in cell 50,1,1 of 2comp(Top) and 1comp(bottom).

For the 2comp simulation, surfactant concentration is zero, in cell 50,1,1, up until chaseflood, unlike 1comp where concentrations curves directly follow the injection sequence and injected amounts. This is also reflected in relative permeability curves of cell 50,1,1 observable in figure 5.36.

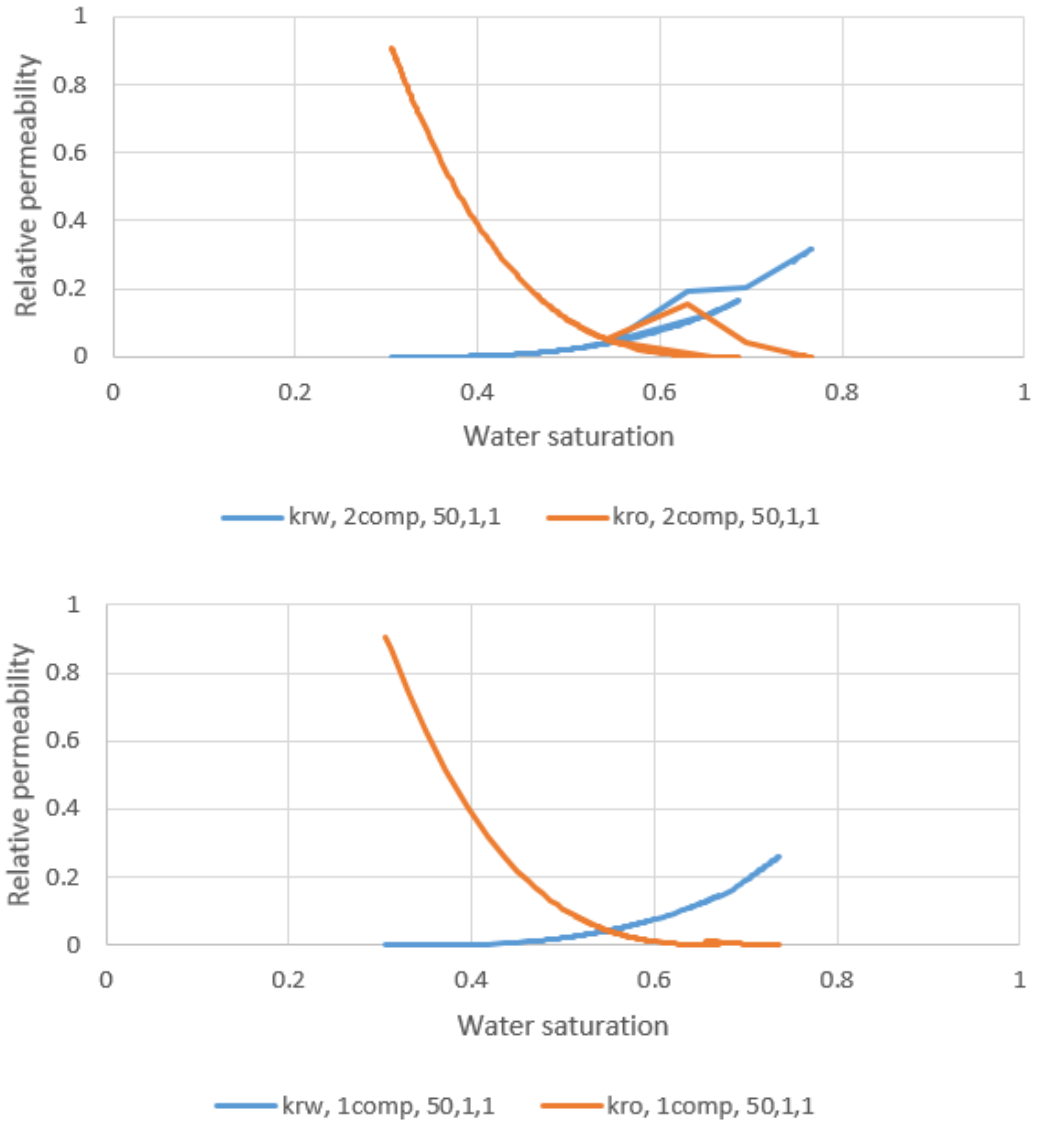

Figure 5.35: Relative permeability curves in cell 50,1,1 of 2comp(top) and 1comp(bottom).

5.2. Summary and Conclusion

1comp:

Since surfactant and salt generally are not present together, in the water phase, there is no surfactant mixing with oil. This keeps surfactant concentration in water sufficiently high for interpolation of relative permeability set 2. STARS then interprets this as surfactant relative permeability granting it the mobility it lacked during previous simulations.

The effects of k value- tables are practically not present in this run and can therefore be removed without consequences.

Micro emulsion viscosity can be modelled by assigning this feature directly to the surfactant. For a type II(+) system this can be done using the additional code present in the MEVisc file. In the original- and current file, surfactant viscosity equals water viscosity. Effect of micro emulsions, hence, are not modelled, but could easily be altered to feature ME- viscosity.

To make this code more viable, a revision of relative permeability interpolators DTRAPW/N ($Log_{10}(N_c)$) and/or IFT- tables should be made for better modeling of the individual processes.

2comp:

Low salinity, polymer flood does not propagate surfactant, even after 30 days. When freshwater injection starts, reducing salinity and making surfactant immiscible with oil, capillary number reaches the prerequisite for interpolation of relative permeability sets 2 and 3. Surfactant is then assigned to a relative permeability set granting it mobility.

The k value- tables defined in the initial files are reasonable when trying to model a type II(+) system. The problem is that IFT tables are defined through surfactant concentration in the water phase, thus making $\log_{10}(N_c)$ dependent relative permeability interpolation incorrect.

When modeling type II(+) systems, IFT- tables should be defined through surfactant concentration in oil as well. This could be managed with keyword 2CMPX, but might remove the possibility of modeling surfactant and salinity dependent interfacial tension, since there is no salt concentration in oil. New IFT- tables could possibly solve the problem of high oil mole fraction surfactant, as surfactant would become mobile and not accumulate in a single cell. Another challenge with a type II(+) system, especially when transitioning between micro

emulsion systems, is modeling adsorption, as it is currently defined through water phase concentration only.

Redefining k value- tables, or removing them altogether, is a solution if type II(-) systems are to be modelled. This, however, removes any modelling of micro emulsions systems transitioning from one type to another when salinity is altered. To model micro emulsion-viscosity, one can assign this characteristic directly to the surfactant phase. This would, in reality, only be viable if surfactant was in constant contact with oil. For simulation of small cores this might be a valid assumption/ approximation of micro emulsion behavior, but for large scale simulations, the resulting flow pattern and pressure change could potentially deviate heavily from reality.

The process of history matching each injection process, by defining the individual relative permeability curves one at a time, would not be viable for the currently applied approach. Considering relative permeability of polymer as an interpolation between two rock types is very complex in a history match. Matching of relative permeability would have to be made for the complete process, and would then only be true for the specific conditions and sequence of events in that simulation. Assuming parameters like viscosity and adsorption are not to be manipulated freely, but lie in some range of experimental values, this approach would either be narrow in its applicability or extremely complex.

6. R10 Coreflood Simulations

In this chapter, modelling of hybrid EOR, using established- and some of the previously investigated methods, was performed. The model was based on flooding experiments conducted at the Centre for Integrated Petroleum Research on a core named "R10". The complete model can be viewed in the appendix.

R10 is a cutout of a Berea sandstone outcrop. Experiments were conducted to investigate the effects of low salinity- (LS), low salinity surfactant- (LSS), and low salinity surfactant polymer slug injection (LSSP) on oil recovery. The model is one –dimensional meaning a grid block distribution of 100, 1, 1 in i, j and k directions respectively. Number of grid blocks in i-direction was subject of a sensitivity study presented in chapter x.x.x. Linear flow between injector and producer, defined through keyword TUBE-END, was deemed suitable for inflow and outflow simulations.

Table 6.1: Properties of core R10.

Length (cm)	Diameter (cm)	Rock density (g/cm^3)	Porosity	Absolute permeability (mD)	Pore volume (mL)
13.440	3.800	2.031	22.045	362	33.60

The core was initially saturated with synthetic seawater (SSW) under a vacuum of 1.12mbar. Absolute permeability was measured before the core was drained with Peregrino crude oil at 55°C and the back pressure regulator was set to 12b bar. Drainage was performed under gravity stable conditions. Before aging, the temperature of the core holder and Peregrino crude oil were measured at 51.2°C. Aging was performed at 70°C back pressure regulator set to 12 bar for 30 days. The core was then placed in an oven at 70°C where Peregrino crude oil was exchanged with Brage stock tank oil, measured at 25°C. The injection rate was 0.04 cm^3/min and the total injected volume equaled 180mL. Effective oil permeability was measured at 70°C after aging. Subsequent flooding experiments are summarized in figure 6.1. All experiments were performed under 70°C with the back pressure regulator 12bar with an injection rate of 0.1cm^3/min.

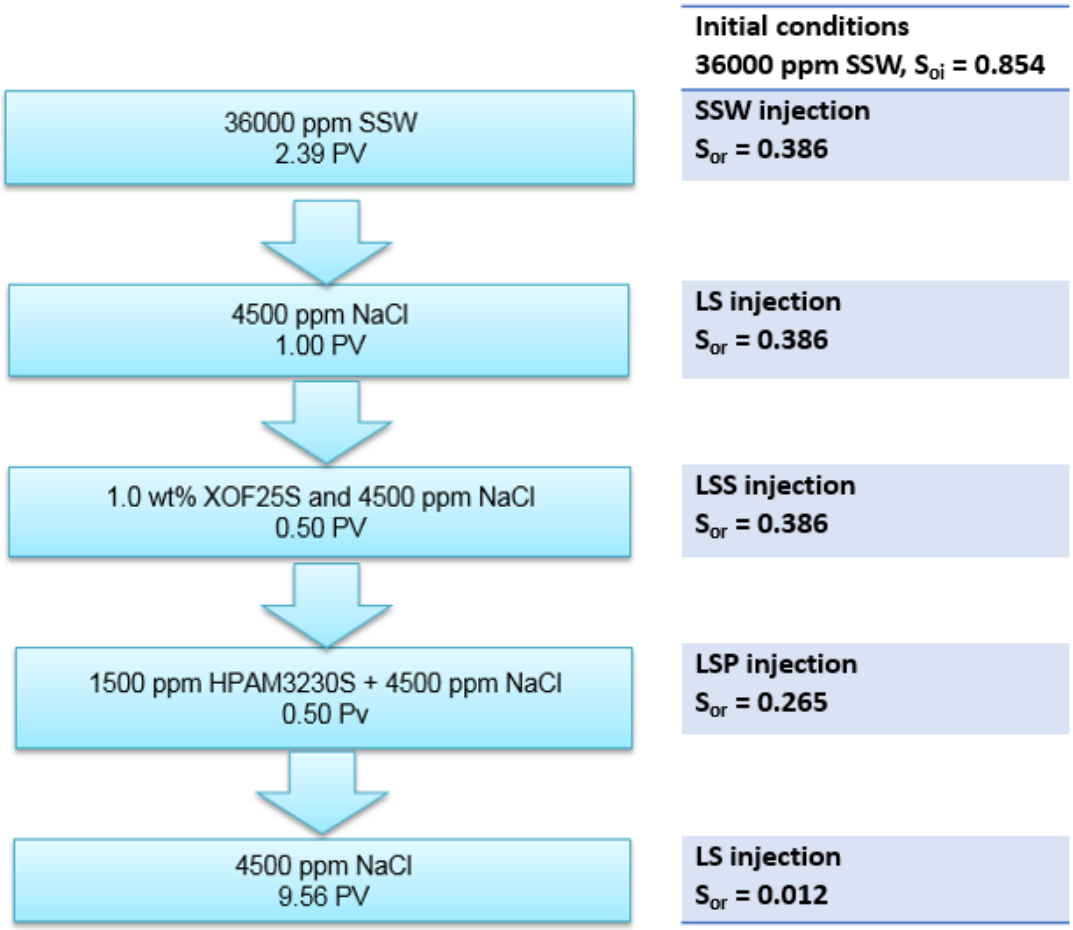

Figure 6.1: Summary of R10 experimental core flood.

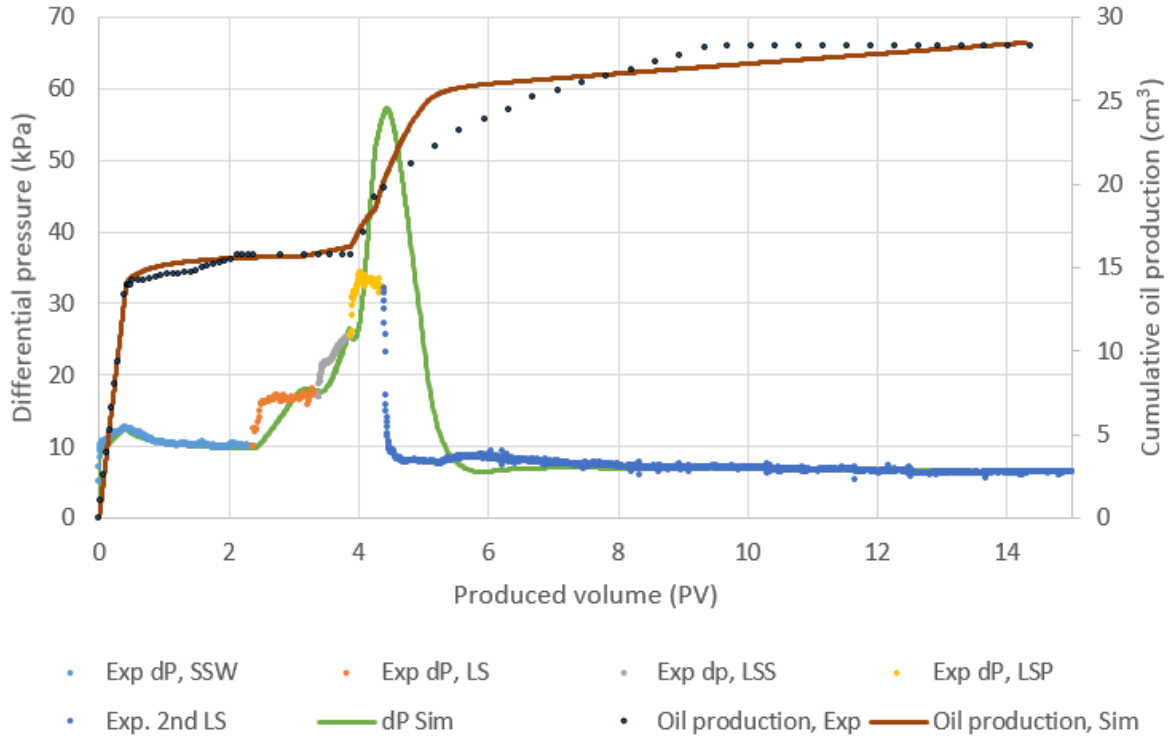

Figure 6.2: History match of differential pressure and oil production for the total flooding process.

6.1. R10 – Synthetic Seawater Injection, SSW

To model the synthetic seawater injection, relative permeability curves and salt composition was added to the model. Parameters, like viscosity were defined to mirror the pure water phase at 70°C.

The synthetic sea water had a more complex composition than was modeled. Salt was defined through Na^+ and Cl^- ions only. The complete composition can be viewed in table 6.2.

Table 6.2: Chemical composition of synthetic seawater

Ion	Na^+	Ca^{2+}	Mg^{2+}	Cl^-	HCO_3^-	SO_4^{2-}	K^+
C (ppm)	11 159	471	1 329	20 130	142	2 740	349

Table 6.3: Experimental permeability values.

Absolute permeability (mD)	Effective oil permeability (mD)	Effective water permeability after SSW (mD)	Effective water permeability after 2^{nd} LS (mD)
362.4	47.6	11.1	12.9

From experimental data the end- point relative permeabilities of SSW should be as follows: Oil relative permeability at initial water saturation, $k_{ro}(S_{wi}) = 0.130$ and water relative permeability at residual oil saturation, $k_{rw}(S_{orw}) = 0.031$. These values were used initially, but had to be adjusted to obtain matching pressures at the start and end of SSW injection. The experimental value of residual oil saturation was altered to match oil production.

Table 6.4: Corey parameters used in matching of SSW.

	S_{wi}	S_{or}	n_w	$k_{rw}(S_{orw})$	n_o	$k_{ro}(S_{wi})$
HS	0.15	0.49	2.8	0.023	1.7	0.150

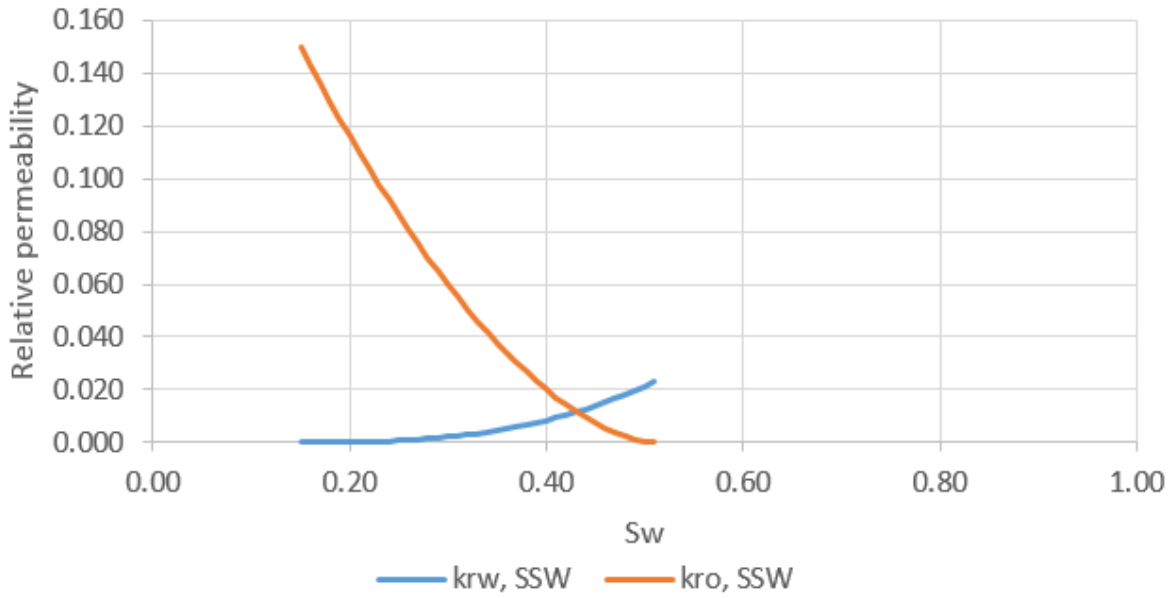

Figure 6.3: Relative permeability curves representing SSW flood.

The crossover point and relative oil permeability shown in figure 6.3 would imply an oil- wet rock [3]. This corresponds with the fact that the core has been aged. However, the water relative permeability is low and would indicate a water- wet system. The low end- point relative permeability was used to match the pressure at the end of SSW injection.

6.2. R10 – Low salinity Injection, LS

At the start of low salinity injection, a sharp pressure increase was observed. To match this, several attempts of altering relative permeability were made. Dispersion (discussed in chapter 6.2.3) was changed to force a close to instantaneous interpolation from HS relative permeability to low salinity permeability. The sharp transition between curves was still insufficient to yield an adequate pressure match without mismatching oil production.

Pressure increase during low salinity flooding has been observed in several experiments [15] [20] [23] [66]. Zhang et al. [66] proposed that resistance to flow was caused by pore plugging from complex crude oil/brine/rock interactions leading to changes in location and mobility of crude oil.

Table 6.5: Corey parameters used in match of the first low salinity injection.

S_{wi}	S_{or}	n_w	$k_{rw}(S_{orw})$	n_o	$k_{ro}(S_{wi})$
0.15	0.49	6.0	0.0135	3.0	0.15

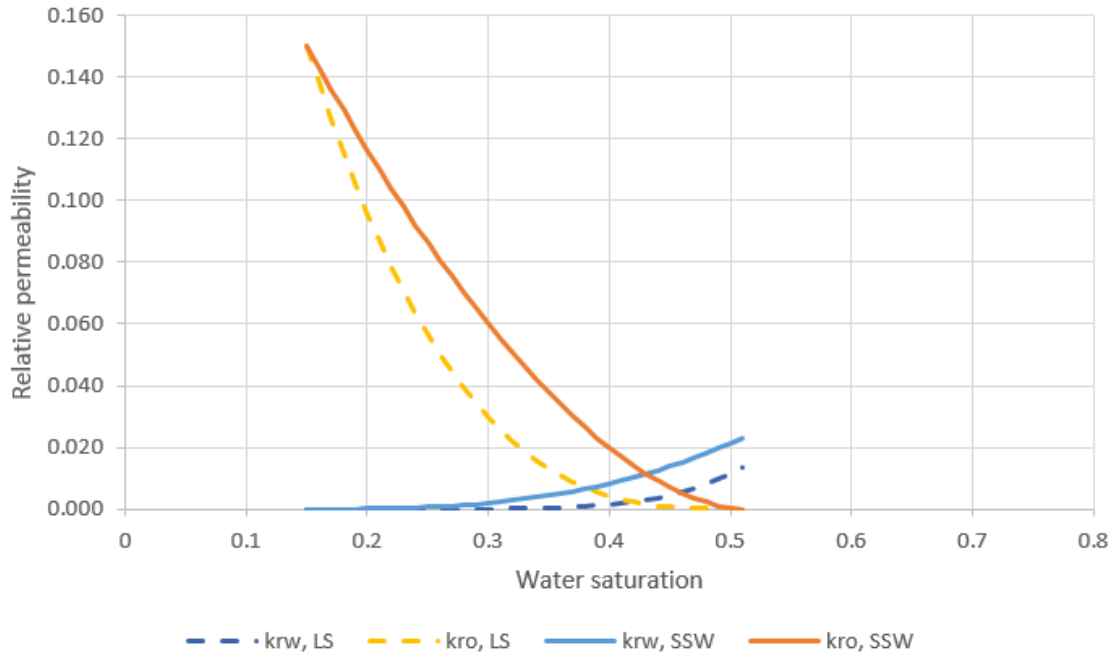

Figure 6.4: Relative permeability curves used in matching synthetic seawater- and the first low salinity flood.

The transition from high salinity to low salinity relative permeability curves seen in figure 6.4 is ambiguous with regards to wettability alteration. The decreased oil relative permeability implies oil- wet conditions. The reason for the low relative permeability of oil was to hinder/postpone the oil production response. Water relative permeability curve of LS imply more water- wet conditions.

6.2.3. LS – Dispersivity

Techniques used in numerical flow calculations can lead to approximation errors, manifesting as artificial diffusion in the simulation, termed numerical dispersion. To determine the degree of numerical dispersion of the simulated model, a sensitivity analysis was performed. Numerical dispersion can result in earlier water breakthrough [67] as sharp salinity profiles become smeared out [68]. In the code, salt is modeled by both Na^+ and Cl^- and are assigned the same attributes. Na^+ was chosen to be the studied component. Initially, high salinity (HS), synthetic seawater was injected for 802minutes before injection of low salinity (LS) brine was initiated. The time interval of low salinity injection was extended to be able to visualize the complete processes. In this investigation, max timestep size and number of grid blocks needed to minimize numerical dispersion is presented.

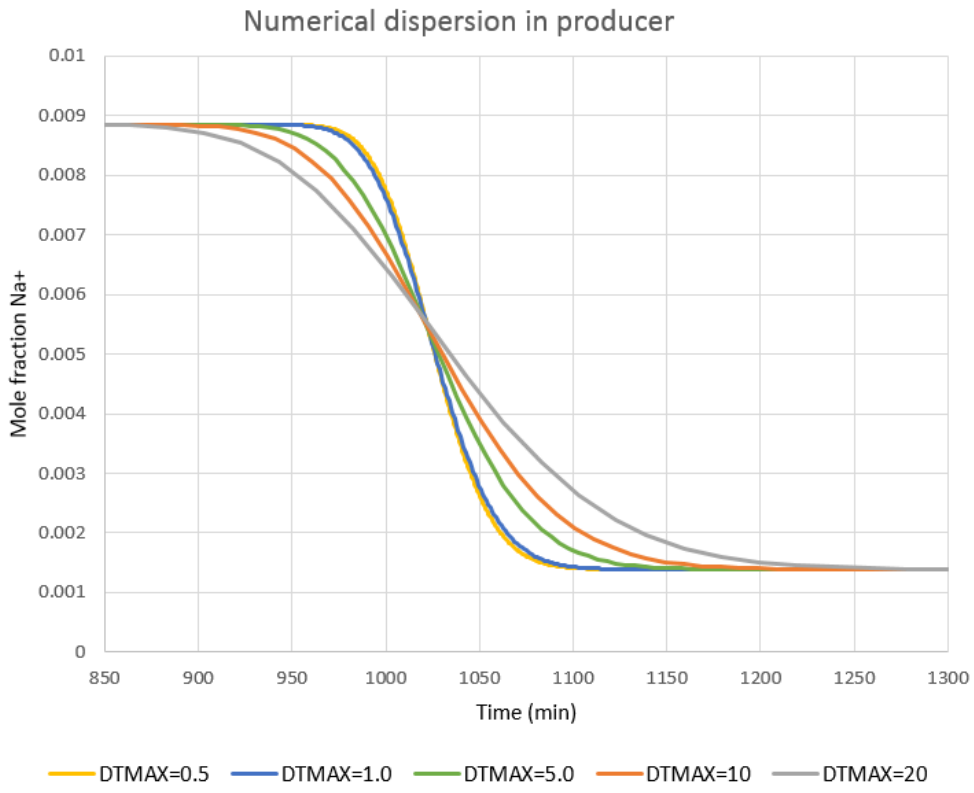

Figure 6.5: The effect of timestep size on numerical dispersion.

To properly evaluate numerical dispersion, numerical- and physical dispersion must not be present together. Their effects would become indistinguishable making evaluation of optimal grid- and time resolutions unnecessarily complex. Physical dispersion was therefore removed during this investigation.

Figure 6.5 shows that when time resolution is low, salt fronts become smeared. Reducing max timestep size from 1.0 to 0.5 minutes has little effect on numerical dispersion. A DTMAX of 1.0 therefore adequately minimizes numerical dispersion.

From previous experience, the core was modelled using 100 grid blocks. The number of grid blocks used was still investigated to reaffirm previous assumptions and to observe the effect it has on numerical dispersion.

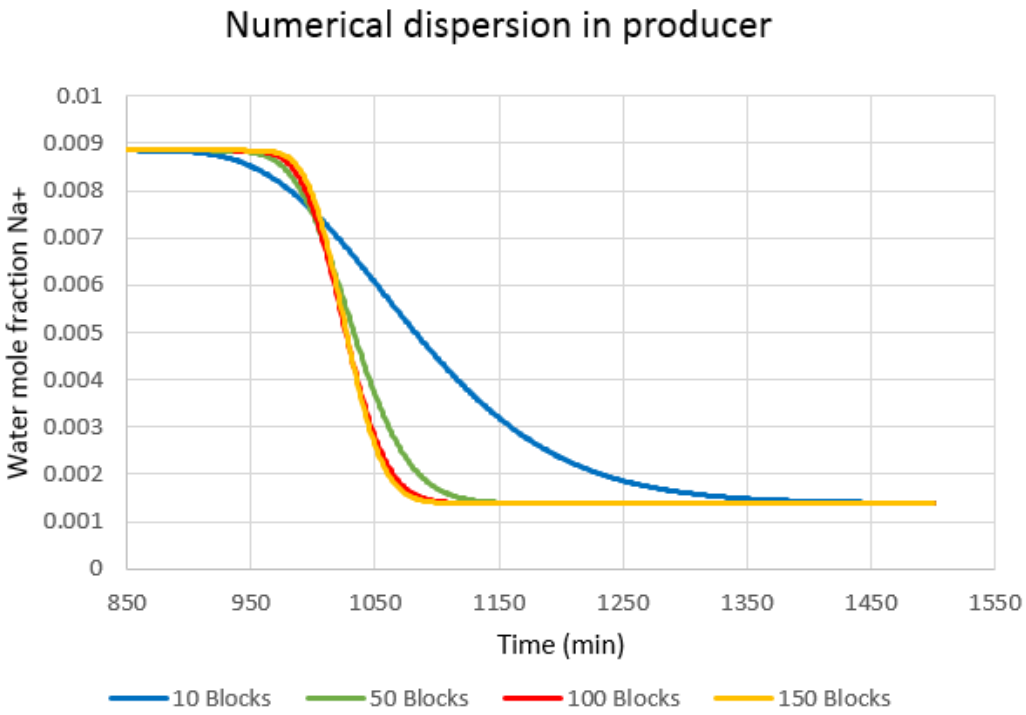

Figure 6.6: The effect of number of grid blocks modelled on numerical dispersion.

Even when no physical dispersion is defined, numerical dispersion can still be observed. As the number of grid blocks increases, the numerical dispersion is reduced and the salt front becomes less smeared. When the number of grid blocks is altered, so too must the size of each block. This is to honor the original size of the core. Since the model has thickness and width of 1 block, cells will, for simplicity's sake, be referred to as its i- direction value (i.e. block 50 rather than 50,1,1). 100 blocks seem to sufficiently reduce numerical dispersion in a model of this size.

Mahadevan (2002) [69] reports that dispersivity increases with length. Figure 6.7 shows that this phenomenon is also present in the current model. The graph show the salt fronts of blocks 1, 50 and 100, and how the fronts smear with length.

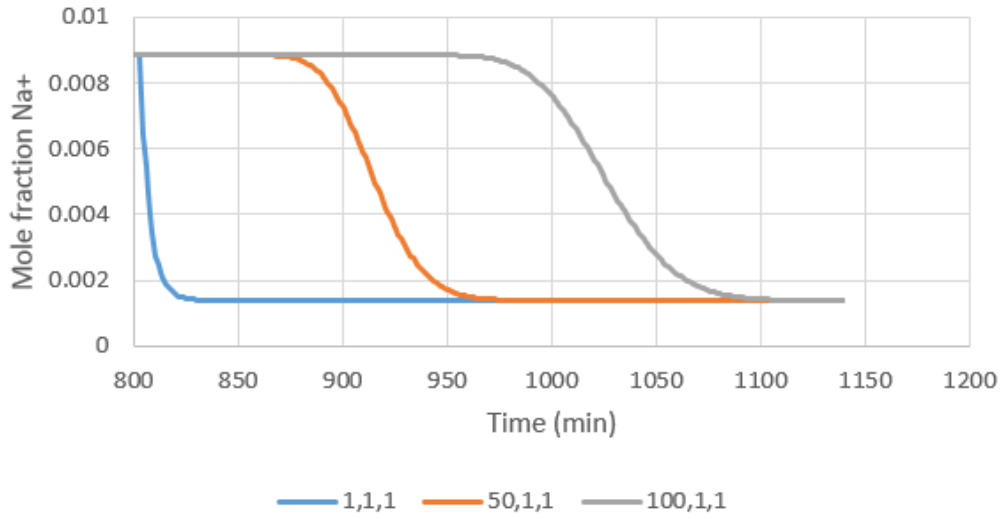

Figure 6.7: Salt fronts of blocks 1,1,1, 50,1,1 and 100,1,1.

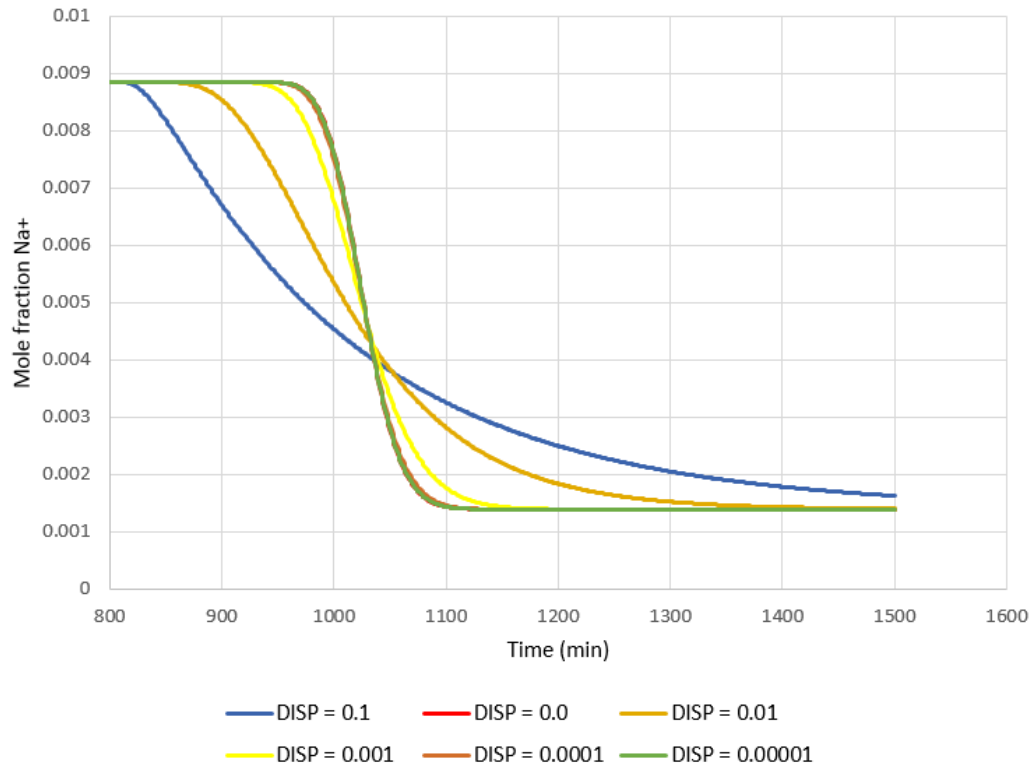

Figure 6.8: Salt fronts of block 100,1,1, at different values of physical dispersion.

After minimizing numerical dispersion, true physical dispersion was evaluated. Observable in Figure 6.8, decreasing the dispersion coefficient yields a less smeared salinity profile. Physical dispersion below $1x10^{-4}$ cm^2/min yields no significant change and comes close to having zero physical dispersion.

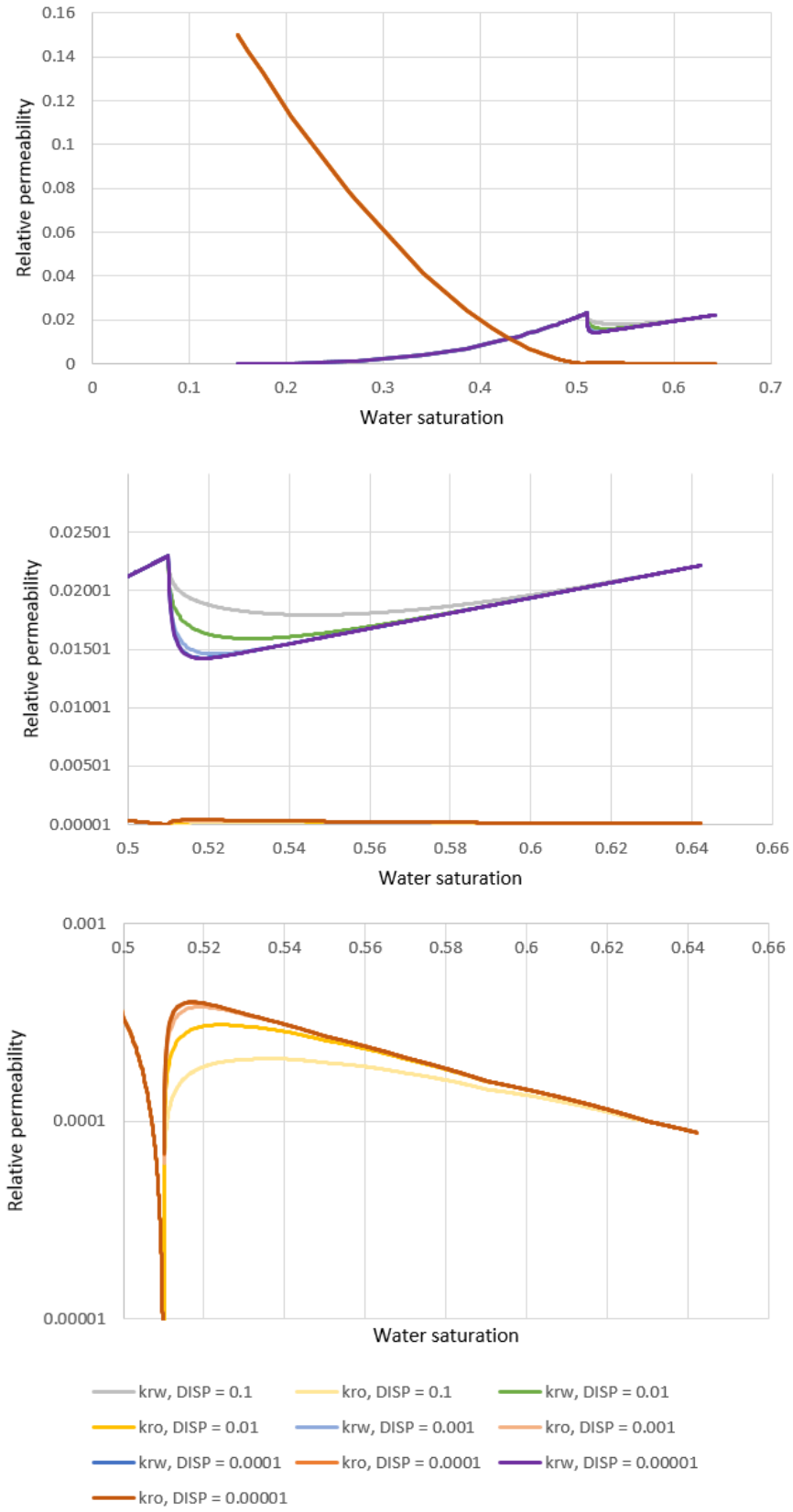

Figure 6.9: The effect of dispersion on relative permeability curves for cell 1,1,1. The two bottom graphs are zoomed in on water- and oil relative permeability respectively. Note the logarithmic y- axis scale of zoomed in oil relative permeability.

Because salt concentration is used in interpolation of relative permeability, this too will be affected by dispersion. Figure 6.9 shows that higher dispersion coefficients will cause LS relative permeability to be more equal HS relative permeability. As dispersion coefficients lower the interpolation approaches relative permeability defined for low salinity, in the model. In addition, the trends of increased smearing with length can be observed for relative permeability as well.

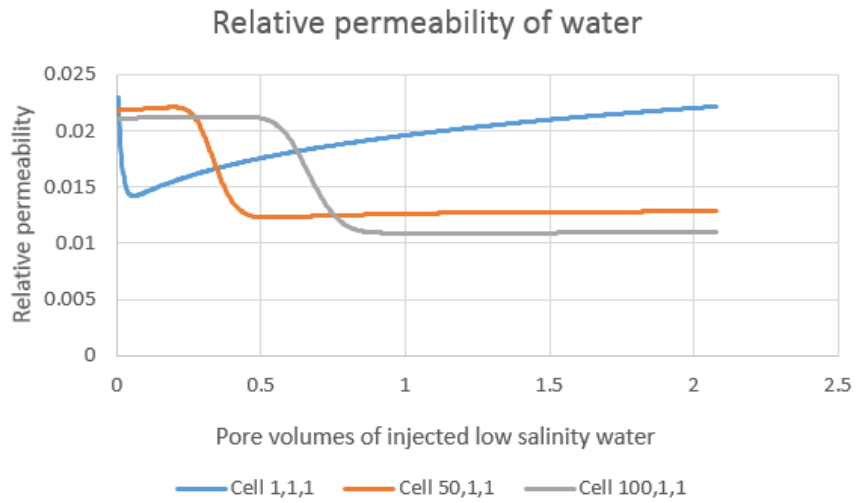

Figure 6.10: Effect of length on low salinity, relative permeability interpolation. Dispersion = 0.00001 cm^2/min

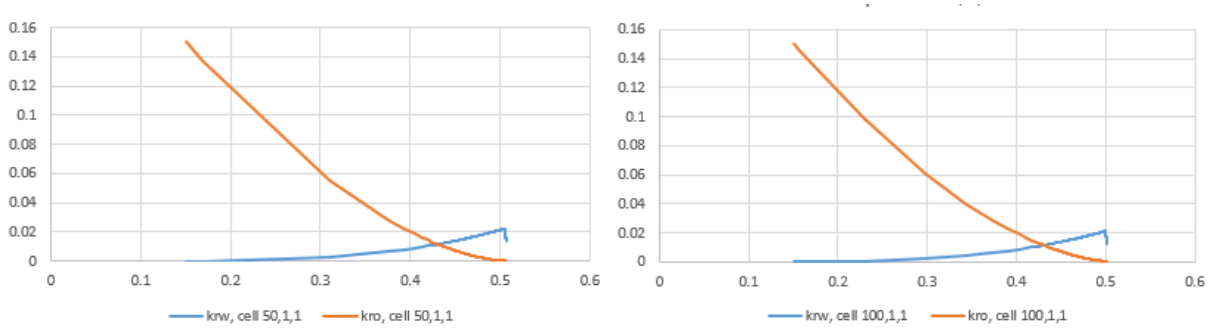

Figure 6.11: Relative permeability curves of cells 50,1,1 and 100,1,1. Dispersion = 0.00001 cm2/min

Since residual oil saturation is different between the cells. The trend of increasing relative permeability of water in cell 1,1,1 is not observed in cells 50,1,1 or 100,1,1. Comparing graphs in figures 6.9 and 6.11 this becomes apparent.

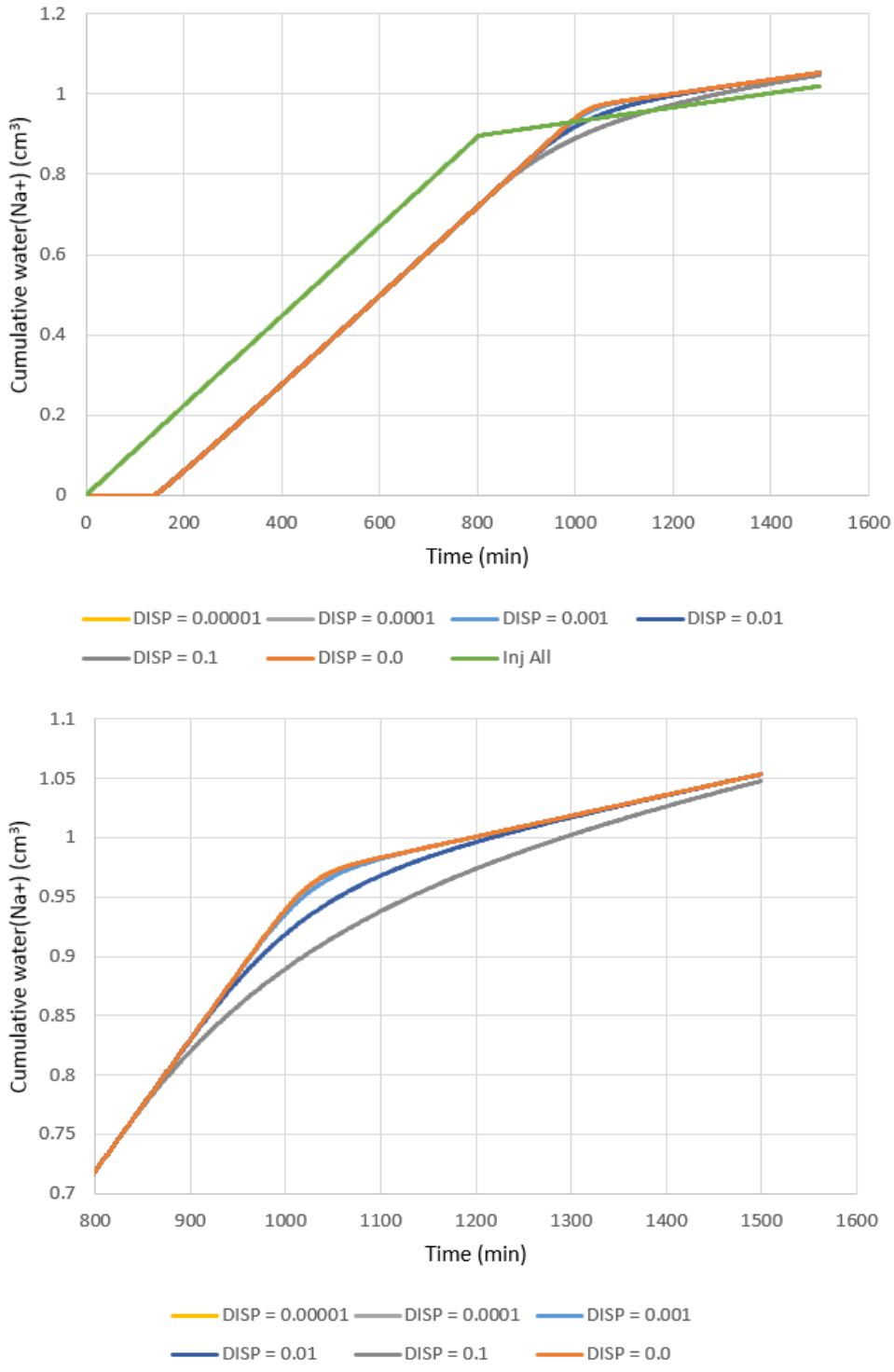

Figure 6.12: Produced- and injected volumes of Na+. Lower graph is zoomed in on injected volumes.

When observing the amount of salt in the effluent it becomes clear that dispersion causes disparities in these results as well. Initial and injected amounts of salt are equal for all runs. 2.39 pore volumes of synthetic seawater is injected before injecting 1.0 pore volumes of low salinity

water. Salt concentrations in the producer rises after water breakthrough and increases consistently until breakthrough of the low salinity flood. Na^+ production then stabilizes at a value equaling that of injected Na^+ in the low salinity flood. Fig. 6.12 shows that dispersion not only can cause earlier breakthrough [67], but also that salt, and potentially other miscible components, might become distributed differently in the core. This could also mean there is a deviation from the material balance equation in the STARS simulator that happens without the user receiving any warnings or errors. In this case, the maximum difference in produced salt was 0.54%.

6.3. R10 – Low Salinity Surfactant injection, LSS

0.50 pore volumes of an anionic, sulfonate surfactant, called XOF25S, was injected together with a low salinity brine. Since salinity was constant before, during and after surfactant flooding simulations, a type II(-) system was modelled. Interfacial tension- tables were simplified to not be salinity dependent because of the constant salinity. It was assumed that no surfactant was present in the oil phase during experiments and K value- tables were left out of the model. Experimental values of surfactant are given in table 6.4.

Table 6.6: Experimental values of 1wt% XOF25S.

Molecular weight (g/mol)	Injected mole fraction	Interfacial tension at zero surfactant (mN/m)*	Interfacial tension at max surfactant (mN/m)*
426	$4.27 \cdot 10^{-4}$	30.00	0.02

*with 4500ppm salinity brine

6.3.1 LSS - Relative Permeability Interpolation

Modelling of surfactant was done by adding micro emulsion viscosity, IFT- tables, physical dispersion, adsorption and relative permeability curves to the model

Adding surfactant, and therefore IFT- tables, into the modell forces interpolation parameter DTRAPW/N to be defined through Log_{10} of the capillary number. Modeling salinity dependent relative permeability curves using capillary number as an interpolation parameter is potentially tricky. The reduced salt concentration should lead to a decrease in IFT and therefore increase

in capillary number sufficient enough to separate high salinity and low salinity floods. In addition, relative permeability sets innfluence each other to a greater degree when interpolated based on capillary number, as will be discussed later in this chapter. To be able to interpolate based on salt concentration a second rock type, together with keyword RPT_INTRP, was defined. Figure 6.13 illustrates how relative permeability curves were handeled.

Rock type 1: Surfactant curves
- Set 1: High salinity, no surfactant
  - DTRAPW = $\text{Log}(N_c)$
- Set 2: Low salinity, max surfactant
  - DTRAPW = $\text{Log}(N_c)$

Rock type 2: Salinity curves
- Set 1: High salinity, no surfactant
  - DTRAPW = $x_{Na+,\ high}$
- Set 2: Low salinity, no surfactant
  - DTRAPW = $x_{Na+,\ low}$

Figure 6.13: Illustration of the interpolation setup used in modeling salinity and surfactant relative permeability.

Rock type 1 was used for interpolation purposes only by assigning rock type 2 relative permeabilities to the grid using keyword KRTYPE CON 2. This together with the ordering of the curves was found to be important for STARS to correctly handle the interpolation.

When using RPT_INTRP, upper and lower boundaries of Na^+ concentration were assigned to RPT 2 and 1 respectilvely. This meant that interpolation based on salinity now took place both inside and between rock types. The resulting relative permeability changes were not major and was only observed during low salinity injection. Still it had a significant impact on differential pressure.

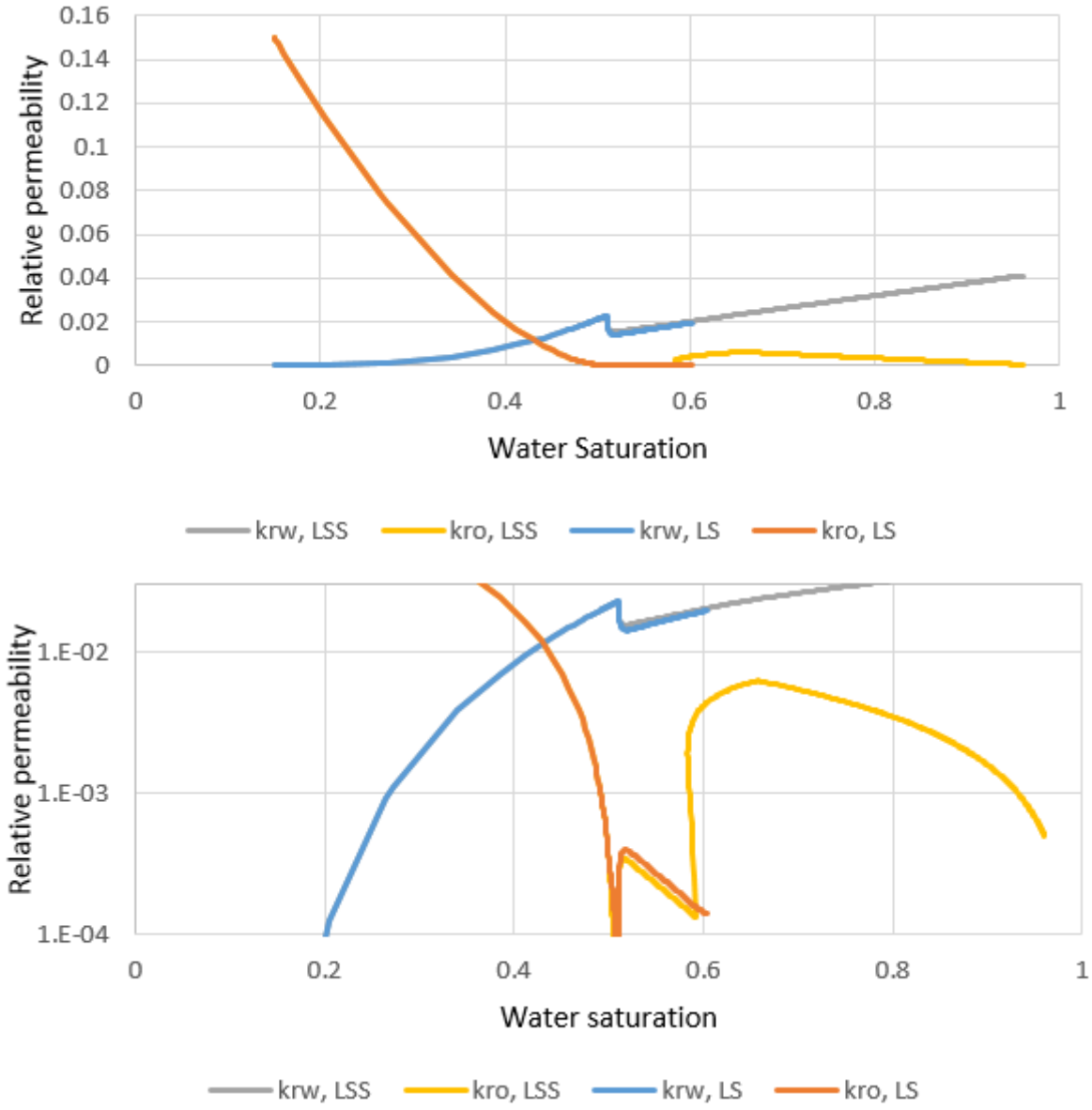

Figure 6.14: Simulated relative permeabiltiy of low salinity- and low salinity and surfactant-floods. Lower graph has a logarithmic scale on the y- aksis.

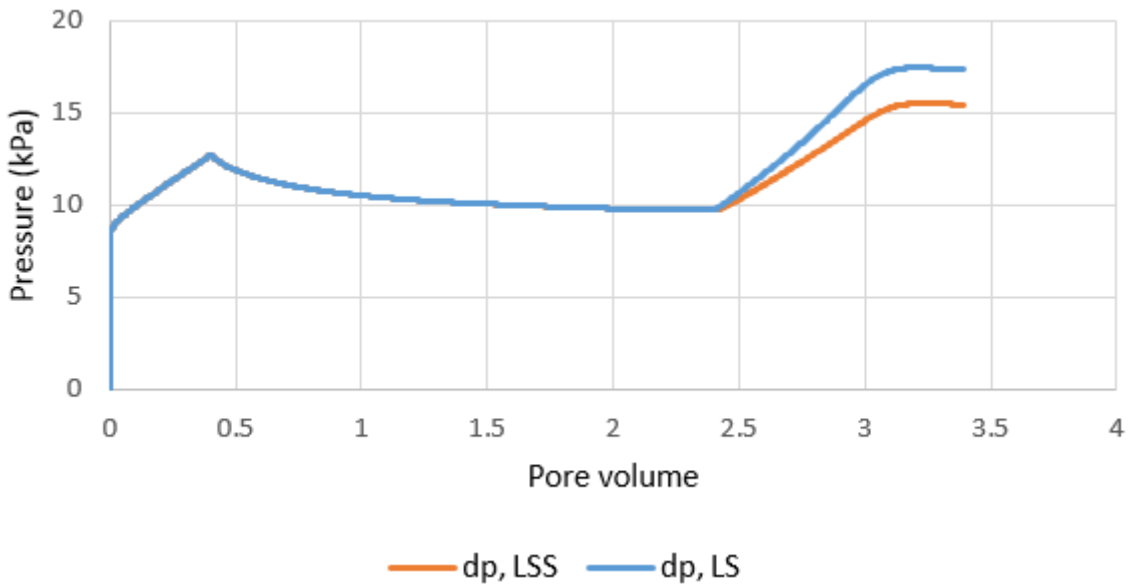

Figure 6.15: Simulated differential pressures of high and low salinity injection when surfactant is present(LSS) and not present(LS) in the model.

Small variations in relative permeability lead to significant changes in pressure. New relative permeability curves were therefore constructed to adjust for the new interpolation routine. Because of the presence of low salinity water during surfactant and polymer injection, the respective relative permeability curves would be affected by the LS curves during these injection sequences as well. Since there was no oil production during low salinity injection, but for subsequent injections (including the second low salinity flood) the relative permeability curves of LS had to be extended.

Initially, oil had no mobility (k_{ro}=0) beyond 0.51 water saturation. Surfactant had its own dedicated relative permeability curves with relative permeability above zero until water saturation reached 0.99. Oil would therefore be mobile during LSS because of interpolation between the curves. This was not the case for polymer- nor the second low salinity flood. In STARS relative permeability curves must be uniformly increasing or decreasing. This meant that low salinity oil permeability had to be altered for saturation values below 0.51 to be able to render oil mobility beyond this saturation. This could potentially affect results of the first low salinity injection. Relative permeability curves were defined to have minimal effect on the initial injection sequences while still yielding increased oil recovery.

Table 6.7: New Corey parameters used in modeling

	S_{wi}	S_{or}	n_w	$k_{rw}(S_{orw})$	n_o	$k_{ro}(S_{wi})$
LS, initial	0.15	0.49	6	0.012	3.0	0.15
LS, extended	-	0.99	1	0.055	1	-

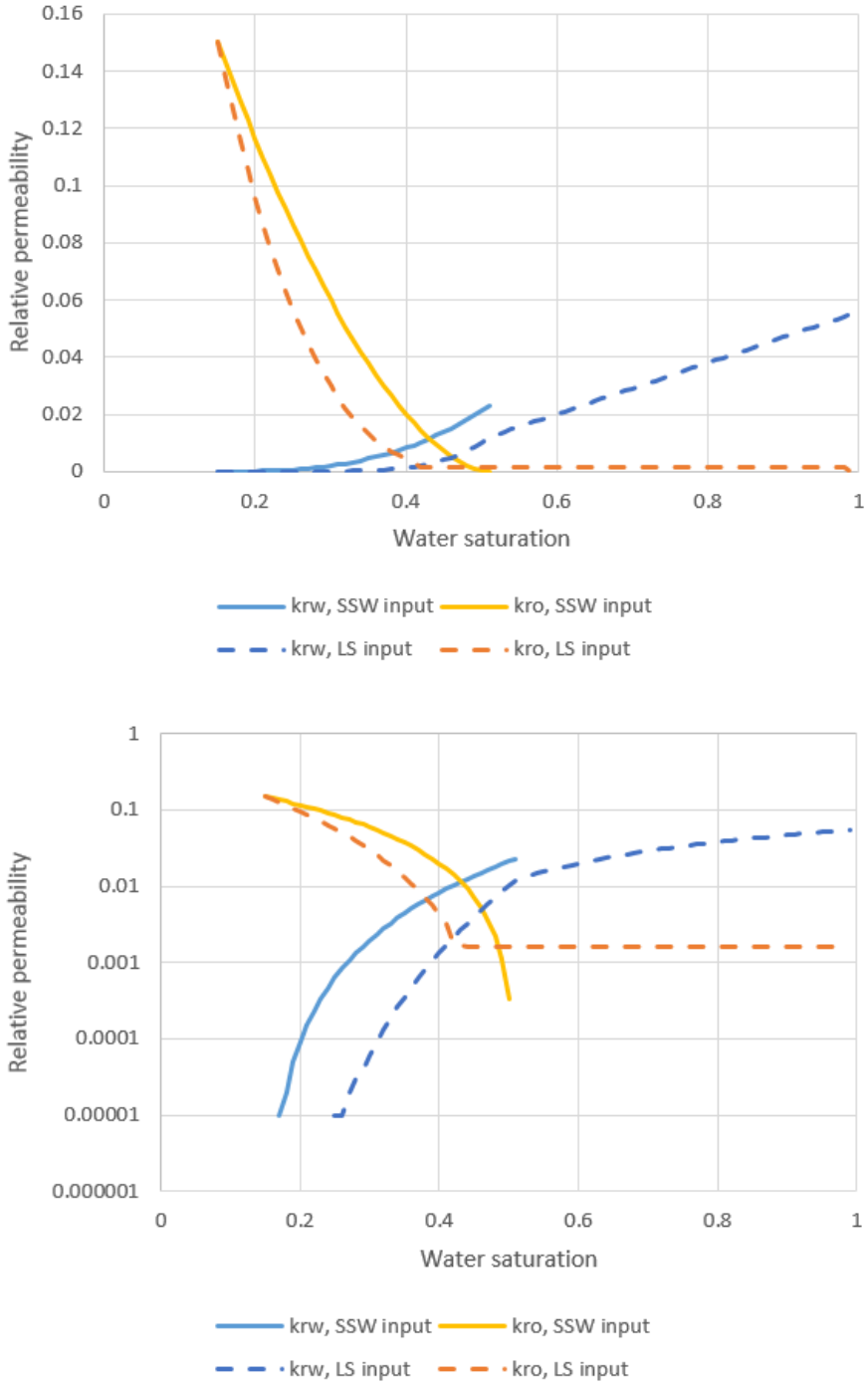

Figure 6.16: Relative permeability curves of synthetic seawater- and low salinity injection as defined in the model. The lower graph has a logarithmic scale on the y- axis.

In STARS the capillary number is calculated using equation (4,7). Since capillary number can be measured differently in the lab from how it is calculated in the simulator, it is important to adjust laboratory values to fit the simulator. As observed in Drønen 2015 [57], capillary number in the simulator, when surfactant is not present during primary injection, deviates by several orders of magnitude from calculated values. This might be a result of the transitioning interpolation routines, but the true cause is unknown. Capillary number values used as input in DTRAPW were therefore adjusted to make sure the relative permeability curves were represented properly.

Table 6.8: Values used in relative permeability interpolation routines of the first three flooding sequences.

High salinity DTRAPW = $Log_{10}(N_c)$	Surfactant DTRAPW = $Log_{10}(N_c)$	High salinity DTRAPW = x_{Na+}	Low Salinity DTRAPW x_{Na+}
-12.47	-9.47	0.00885	0.00139

```
IFTTABLE

**      cift            SIGIFT
        0       30
        0.000001    0.1
        0.000005    0.05
        0.00001     0.02
        0.00005     0.02
        0.00026     0.02
        0.000427    0.02
        0.05        0.02
```

Figure 6.17: Interfacial tension- table in model. It shows interfacial tension (right column) as a function of surfactant concentration (left column).

High surfactant concentrations and ultra- low interfacial tension values lower residual saturations and results in straightened relative permeability curves [70] [71]. Straight curves were tried initially, but could not adequately describe the pressure increase and oil production.

Table 6.9: Corey parameters used in modeling surfactant relative permeability curves.

S_{wi}	S_{or}	n_w	$k_{rw}(S_{orw})$	n_o	$k_{ro}(S_{wi})$
0.15	0.01	3	0.45	5	0.4

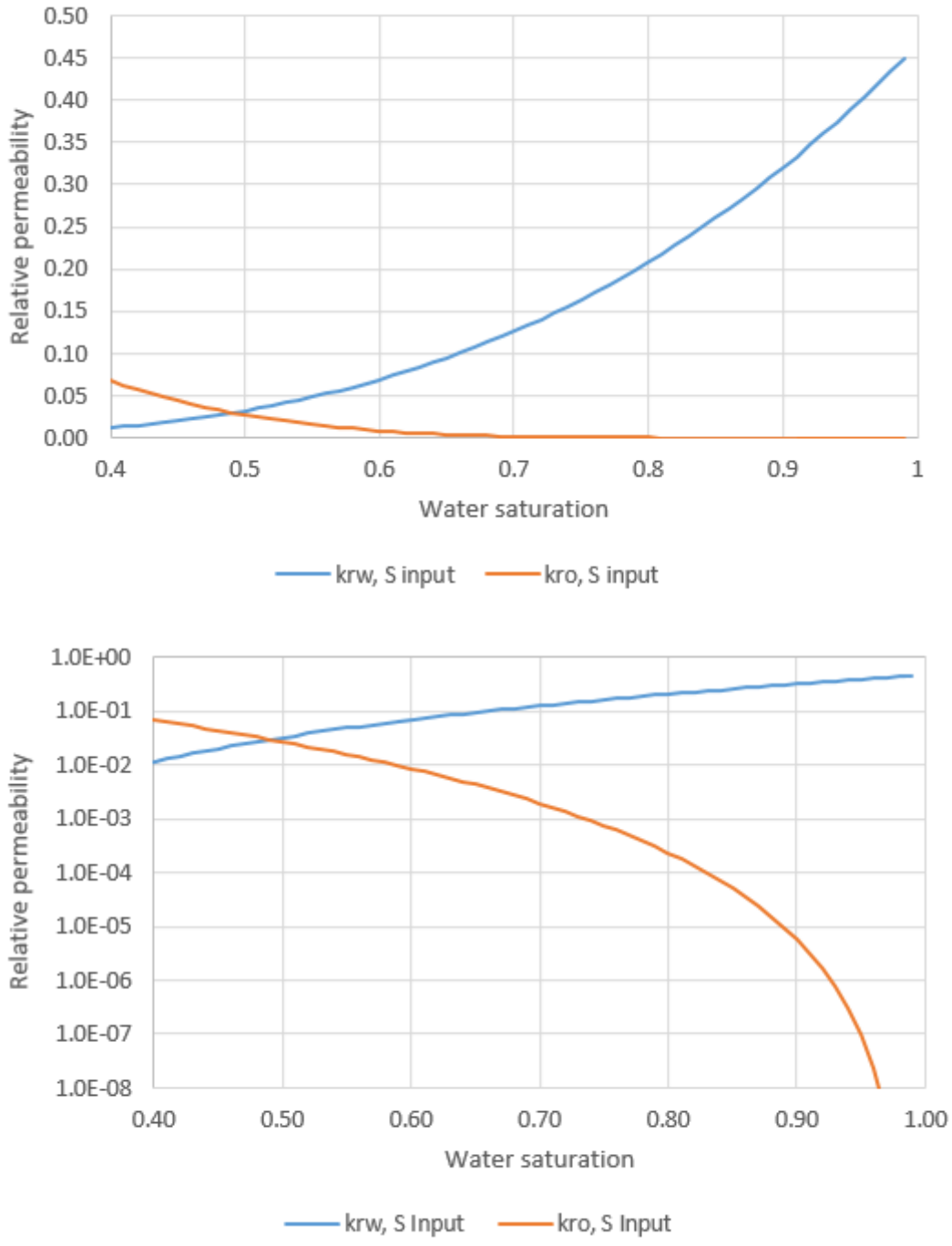

Figure 6.18. Effective range of surfactant relative permeability curves. Bottom graph has a logarithmic y- axis.

The Corey parameters from table 6.9 do not suggest straightened curves, but observing the relative permeability curves in their effective range does.

Decreasing dispersion to match the pressure had the effect of extending the surfactant response into subsequent flooding sequences. A surfactant dispersion of 0.01 cm^2/min was found to yield the best match.

6.3.2. Surfactant - Micro- emulsion viscosity

With the addition of surfactant, and later polymer, came the use of non- linear viscosity mixing keywords. Calculations take into account viscosity of pure component (μ_i), described by keyword AVISC, and component concentration values (x_i). Keyword VSMIXCOMP specifies the component assigned to the current mixing function. VSMIXENDP is used to define minimum and maximum mole fraction of which the viscosity is concentration dependent. Keyword VSMIXFUNC has eleven entries that determine the component viscosity at eleven concentrations evenly distributed between, and including, minimum and maximum mole fractions. The values used in the current model are defined to yield an exponential increase in viscosity with increasing component concentration. The linear logarithmic mixing rule is defined as follows [60]:

$$\ln \mu = \sum_i x_i \ln \mu_i \tag{6,1}$$

For nonlinear viscosity mixing, the mixing option discriminates key components specified by VSMIXCOMP (i=S) from those that are not (i≠S). Mole fractions of these groups sum to 1;

$$\sum_{i=S} x_i + \sum_{i \neq S} x_i = 1 \tag{6,2}$$

Nonlinear mixing is performed by replacing x_i with weighting factors $f_i(x_i)$ for i=S and $N \cdot x_i$ for i≠S. N is a normalizing factor derived by input of weighting factors in equation 6.1:

$$\sum_{i=S} f_i(x_i) + N \cdot \sum_{i \neq S} x_i = 1 \quad (6,3)$$

$$N = [1 - \sum_{i=S} f_i(x_i)] \,/\, [\sum_{i \neq S} x_i] \quad (6,4)$$

Equation (6,1) can now be altered to handle nonlinear logarithmic viscosity mixing:

$$\ln(\mu) = \sum_{i=S} f_i(x_i) \cdot \ln(\mu_i) + N \cdot \sum_{i \neq S} x_i \cdot \ln(\mu_i) \quad (6,5)$$

After adding surfactant to the model, it was observed that water viscosity during low salinity injection was not equal to 0.5cP as defined through AVISC. Although salt components were defined with the same viscosities, this was still the case. It was found that the nonlinear mixing function of surfactant was the cause of this discrepancy. To clarify, simulations previously mentioned and the simulations to come are run without this error.

```
AVISC
**'H2O' 'Na' 'Cl' 'SURF' 'DEAD_OIL'
0.5   0.5   0.5     5.0   3.0
```

Figure 6.19: Viscosities of pure components as defined during initial simulations.

```
VSMIXCOMP 'SURF'
VSMIXENDP   0.0 0.000427
VSMIXFUNC   0.07 0.21 0.34 0.46 0.56 0.66 0.74 0.82 0.90 0.97 1.0
```

Figure 6.20: Code showing initial input of nonlinear viscosity mixing function of surfactant.

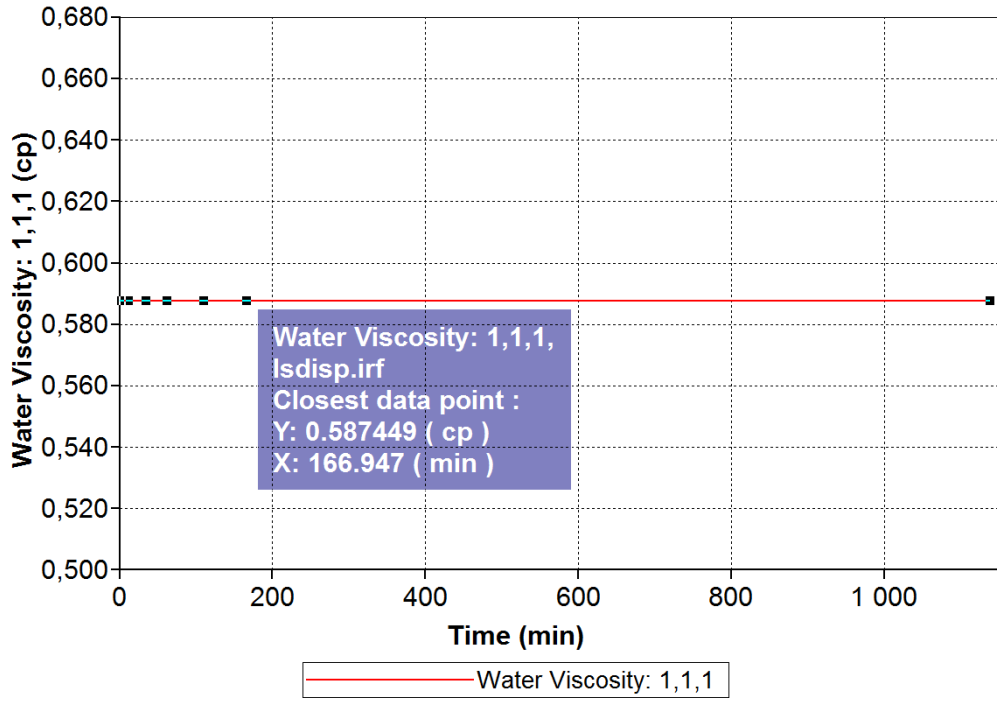

Figure 6.21: Snapshot of the Results Graph window showing constant water viscosity in cell 1,1,1. No other components but salt and water were injected.

Great care should be taken when generating values for the nonlinear mixing function. Calculations of $f_i(x_i)$ are only dependent on x_i, and the weighting factor must therefore be generated independently of other key components. Thus, for component "a", with viscosity function $f_a(x_a)$, mole fraction x_a and pure- component viscosity μ_a, it is implied that:

$$\sum_{i \neq S} x_i = 1 - x_a \tag{6,7}$$

and

$$\sum_{i=S} f_i(x_i) = f_a(x_a) \tag{6,8}$$

N can now be substituted into the mixing rule equation and solved for $f_a(x_a)$ to get:

$$f_a(x_a) = [\ln(\mu) - M] \,/\, [\ln(\mu_a) - M] \tag{6,9}$$

where μ is the mixed phase viscosity and $M = [\sum_{i \neq S} x_i \cdot \ln(\mu_i)] / (1 - x_a)$. As defined in appendix D.5 of the STARS manual [60]: When there is only one components "a" present in solute "b", $x_b = 1 - x_a$ and equation (6,9) can be written as:

$$f_a(x_a) = [\ln(\mu) - \ln(\mu_b)] / [\ln(\mu_a) - \ln(\mu_b)] \quad (6,10)$$

This implies that the mixed phase viscosity can be calculated through:

$$\mu = \exp[\, f_a(x_a) \cdot [\ln(\mu_a) - \ln(\mu_b)] + \ln(\mu_b)] \quad (6,11)$$

Entering μ_a as pure surfactant('SURF') viscosity and μ_b as pure water('H20') viscosity, the nonlinear viscosity mixing rule for surfactant was calculated using values of figure 6.19 and 6.20. Results are given in table 6.10.

Table 6.10: Calculated nonlinear logarithmic viscosity mixing of surfactant.

Nr.	x_a	$f_a(x_a)$	Phase viscosity μ (cP), water
1	0	0.07	0.587449
2	0.0000776	0.21	0.810905
3	0.0001165	0.34	1.093881
4	0.0001553	0.46	1.442016
5	0.0001941	0.56	1.815390
6	0.0002329	0.66	2.285441
7	0.0002717	0.74	2.747704
8	0.0003105	0.82	3.303467
9	0.0003494	0.9	3.971641
10	0.0003882	0.97	4.666272
11	0.0004270	1	5.000000

Looking at water viscosity in table 6.10 it becomes clear that surfactant has an impact even when concentration is zero. This corresponds with the observation made in figure 6.21. In STARS the mole fraction, x_a, is not directly used in calculations of phase viscosity. This is because $f_a(x_a)$ is already defined through mole fraction. In this case the calculated phase viscosity at $f_a(x_a) = 0.07$ is paired with the table entry $x_a = 0$ implying that surfactant has an effect on viscosity without being present in the core.

To avoid this, $x_a = 0$ should be paired with $f_a(x_a) = 0$, or the parameters should be defined such that an extrapolation of the curve will yield $(x_a, f_a(x_a)) = (0, 0)$. These observations were taken into account when adding polymer into the model.

Micro- emulsion viscosity was limited to two times the water viscosity. The initial increase in differential pressure suggested that maximum micro- emulsion viscosity (1.0cP) was a proper estimation.

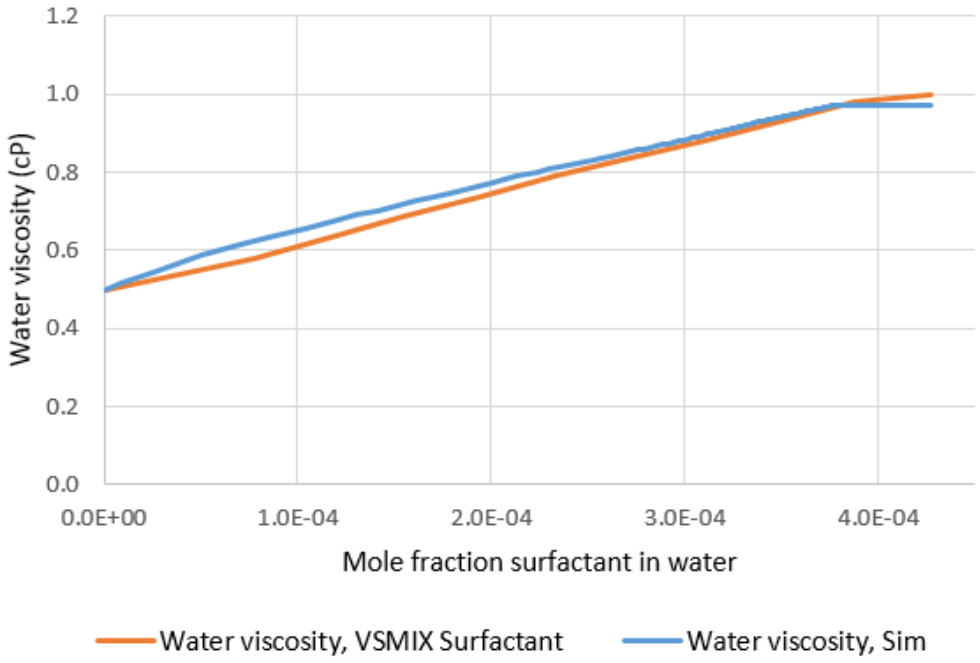

Figure 6.22: Comparison of simulated and input values (VSMIX) for water viscosity as a function of surfactant concentration.

Figure 6.22 shows that simulated viscosity deviates slightly from input values. Since salt components are present, with viscosity equal to 0.5cP, it would be natural to believe simulation of water phase viscosity to be lower than the input values of the nonlinear mixing function of surfactant. Why the STARS simulation shows the opposite trend is unknown, but it might be a result of adsorption. The deviation however is small and simulations are considered valid.

6.3.3. LSS - Adsorption

For core R10, adsorption of surfactant of 0.2mg/g_r (milligrams adsorbed component per gram rock) was found to yield the best match. This corresponds well with literature values as seen in figure 6.23 for brine salinity of 1 wt%.

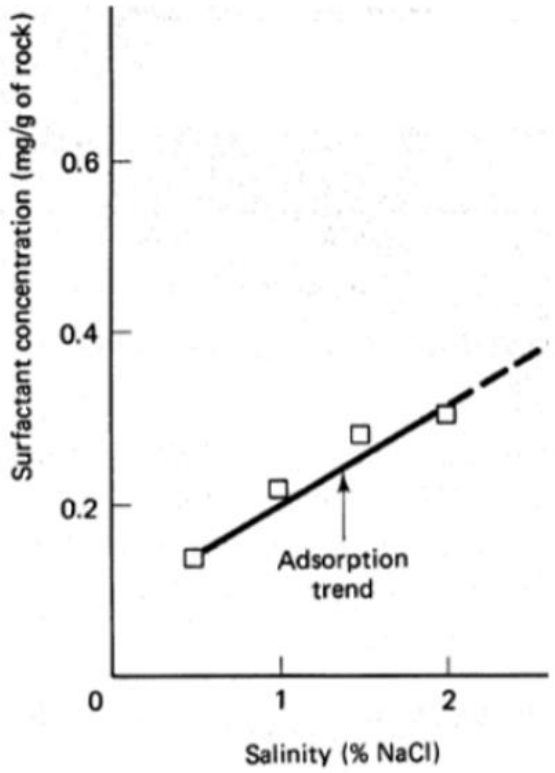

Figure 6.23: Surfactant adsorption as a function of brine salinity. Modified from Lake (1989) [6].

Adsorption values in STARS are given in mol/cm^3. Conversion was performed using the following equation [60]:

$$\mathrm{Ads_i}\left(\frac{\mathrm{mol}}{\mathrm{cm^3}}\right) = \mathrm{Ads_i}\left(\frac{\mathrm{mg}}{\mathrm{g_r}}\right) \cdot 10^3 \cdot \frac{(1-\varphi)\cdot\rho_\mathrm{r}\left(\frac{\mathrm{g_r}}{\mathrm{cm^3}}\right)}{\varphi} \cdot \frac{1}{\mathrm{M_W}\left(\frac{\mathrm{g}}{\mathrm{mol}}\right)} \qquad (6,12)$$

where $\mathrm{Ads_i}$ is adsorption of component i, φ is porosity of the rock, ρ_r is rock density and M_W is molecular weight of component i.

The Langmuir parameters (described in chapter 4.1.3) were defined to render a reasonable Langmuir adsorption isotherm with a maximum adsorption ADMAXT = Ads_i (mol/cm^3).

Table 6.11: Surfactant adsorption parameters.

Ads (mol/cm^3)	Ads (mg/g)	tad1(mol/cm^3)	tad2(mol/cm^3)	tad3
$3.372 \cdot 10^{-6}$	0.200	20500	0	100200

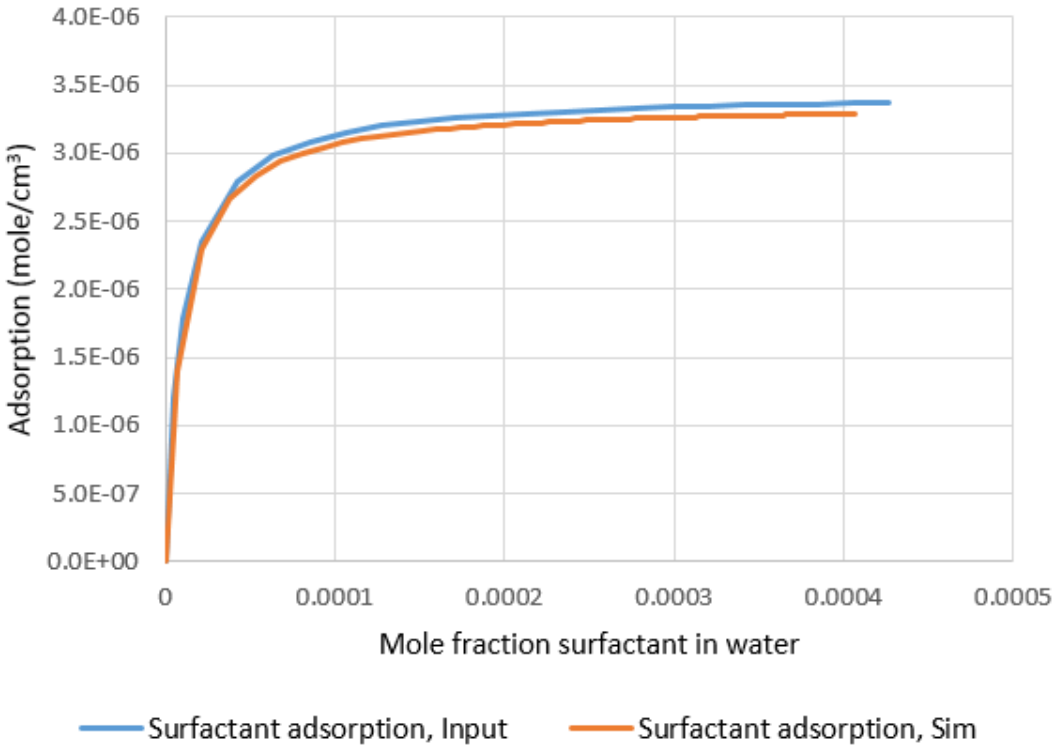

Figure 6.24: Comparison of simulated and input values of surfactant adsorption.

Results show a maximum deviation of 3.1% between simulated and input values of adsorption. This was considered acceptable and subsequent simulations were deemed valid.

6.3. R10 - Low Salinity Polymer injection, LSP

Since the multiple relative permeability interpolation (described in chapter 5) was found to be, in this case, unachievable for polymer, it was not assigned any relative permeability curves. Instead, the production history was matched by viscosity, adsorption, inaccessible pore volume and the extended low salinity relative permeability curve.

Polymer concentrations are often very low, and using correct values of molecular weight may cause numerical computation errors. This problem was avoided by reducing molecular weight of polymer by three orders of magnitude and increasing concentration proportionally. Since the main influence of molecular weight is on polymer viscosity, this approach still honors the effects of polymer when injected concentration and adsorption is adjusted accordingly. Downscaling molecular weight is therefore considered to be a valid method of modeling.

6.3.1. LSP – Polymer Viscosity

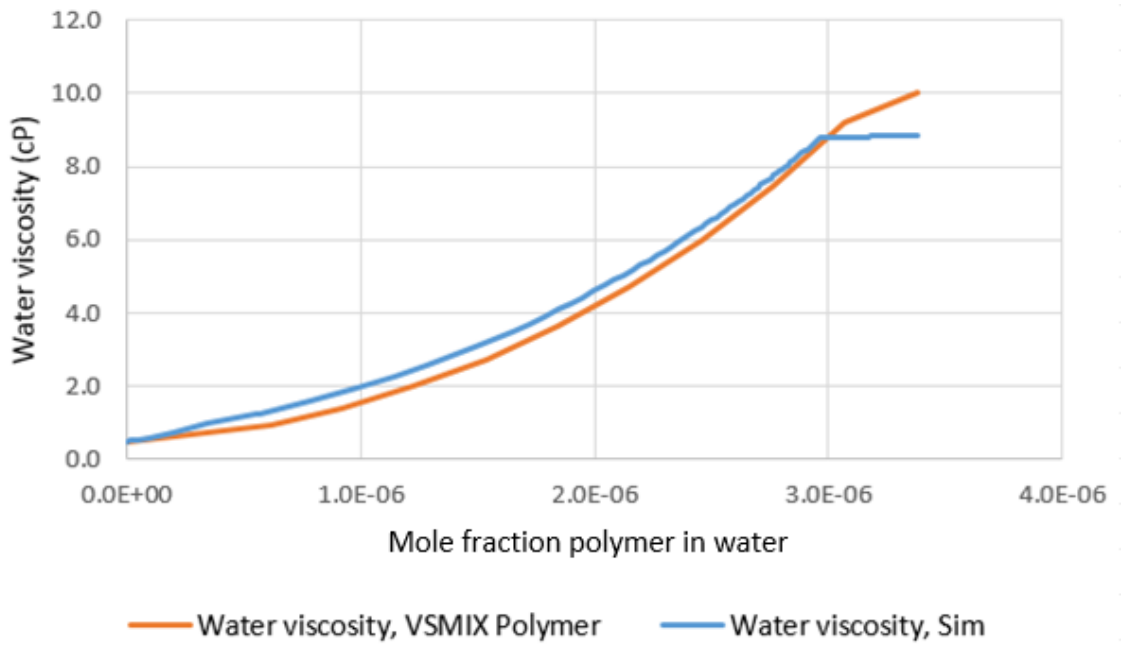

Figure 6.25: Comparison of simulated and input values (VSMIX) for water viscosity as a function of polymer concentration.

The same viscosity trends observed for micro- emulsions can also be viewed for polymer. Water viscosity follows the nonlinear mixing function with a slight deviation. For the simulation, when polymer concentration approaches max value, water viscosity stops increasing earlier and

to a greater degree than what is defined through the mixing function. Water viscosity was expected to be lower for all concentrations during simulation runs, because of the added weighting factors of salt components. The cause of this is likely to be adsorption (see figure 6.26), meaning adsorbed polymer does not contribute to increased water viscosity. This does not explain the trend deviation at high polymer concentrations. However, water viscosity at these concentrations are more in line with the added weighting factors of salt components. Since polymer concentration increases rapidly during injection, this deviation is negligible. Viscosity follows polymer concentration in a satisfactory manner, as observed in figure 6.26.

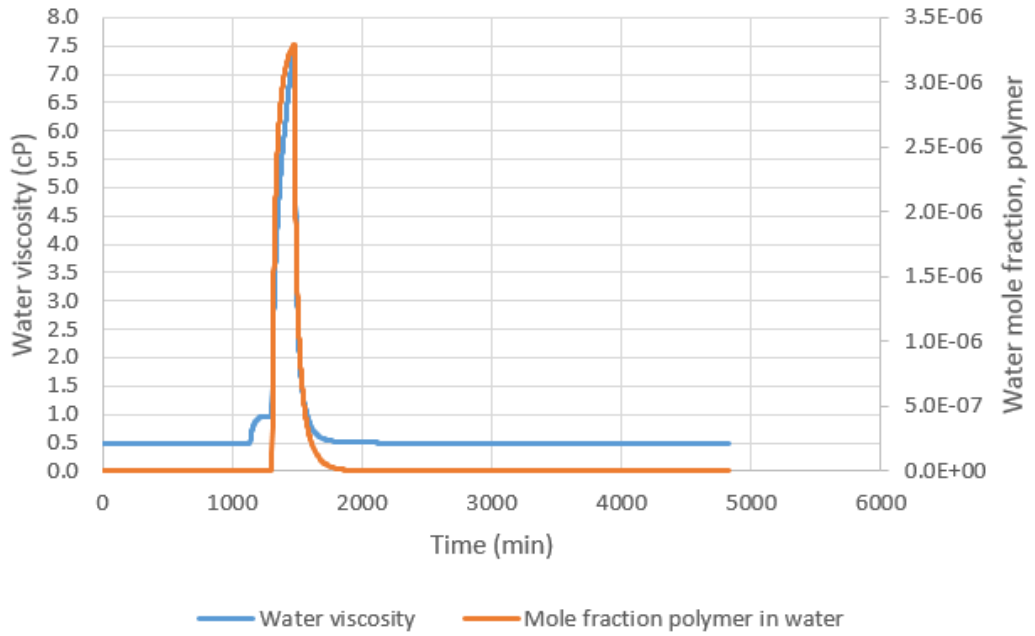

Figure 6.26: Water viscosity and polymer concentration.

A shear table describing phase velocity as a function of Darcy velocity was added to the model. Because injection velocity was constant at 0.1 cm^3/min it was assumed that the shear interval was constant during flooding. This meant that viscosity would only be dependent on polymer concentration.

```
SHEARTAB
** Darcy velocity    Viscosity
** (cm/min)          (cP)
0.00001              10.0
0.0001               10.0
0.001                10.0
0.01                 10.0
0.1                  10.0
```

Figure 6.27: Code showing viscosity as a function of Darcy velocity.

6.3.2. LSP – Polymer Adsorption

The polymer adsorption yielding the best match was found to be 10 µg/g. As for simulation of surfactant adsorption, a good correlation between simulated and input values of polymer adsorption was found. Polymer adsorption is known to be largely irreversible[72] and was modelled as such.

Table 6.12: Polymer adsorption parameters.

Ads (mol/cm^3)	Ads (mg/g)	tad1(mol/cm^3)	tad2(mol/cm^3)	tad3
$8.977 \cdot 10^{-9}$	0.01	102960	0	$1.00 \cdot 10^{-7}$

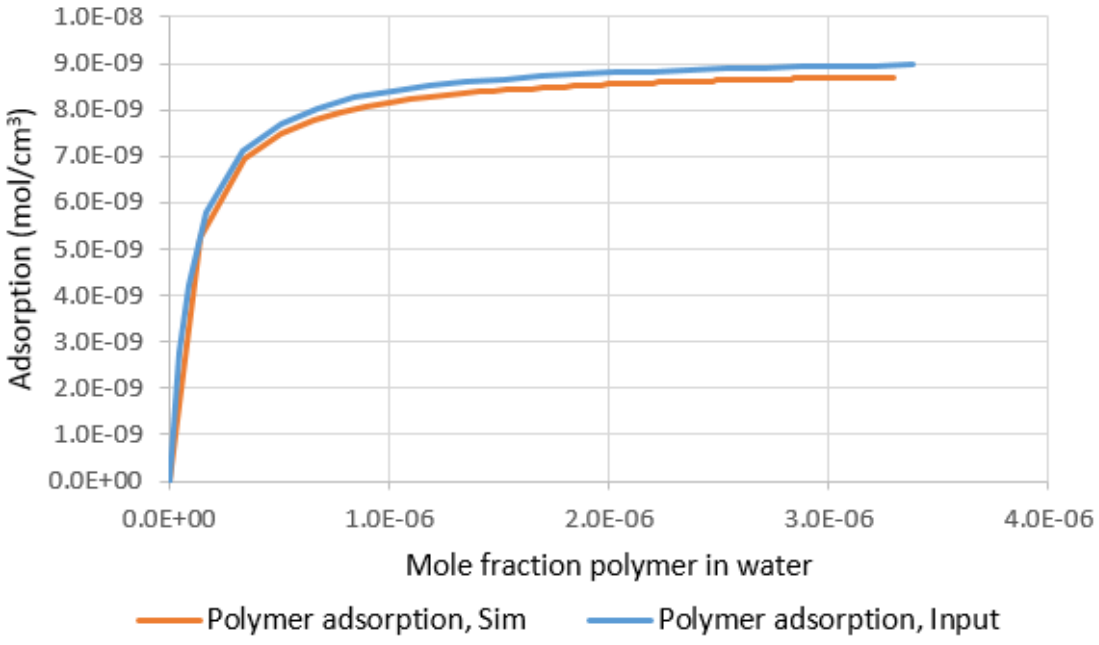

Figure 6.28: Comparison of simulated and input values of polymer adsorption.

Due to the large size of polymer molecules, some pores will be inaccessible. This is called inaccessible pore volume, IPV, and is usually in the range of 1-30% [4]. Dawson and Lantz (1972) [73] presented data showing that polymer propagation could be significantly affected when polymers did not occupy all of the connected pore volumes in the porous media. In STARS, this can be modeled using keyword PORFT, which defines accessible pore volume. The pressure response of polymer injection, that carried out into 2nd LS injection, could be minimized by increasing IPV in the model. This lead to a lower oil production, which could be managed by altering adsorption. To match the pressure interval and subsequent oil production, an inaccessible pore volume of 80% and an extremely low adsorption were set. This is far beyond what is observed in the literature and is an argument for dedicated relative permeability curves for both the polymer flood and second low salinity flood. A more reasonable IPV of 20% was chosen in the final model.

Table 6.13: Summary of matching parameters used in the simulation model of R10

Injection process	Parameter	Value
Low salinity	Viscosity	0.5 cP
	Physical dispersion	0.0001 cm^2/min
Surfactant	Micro- emulsion viscosity	1.0 cP
	Physical dispersion	0.01 cm^2/min
	Adsorption	0.2 mg/g
Polymer	Molecular weight	8000 g/mol
	Viscosity	10.0 cP
	Physical dispersion	0.01 cm^2/min
	Adsorption	10 μg/g
	Inaccessible pore volume	20 %

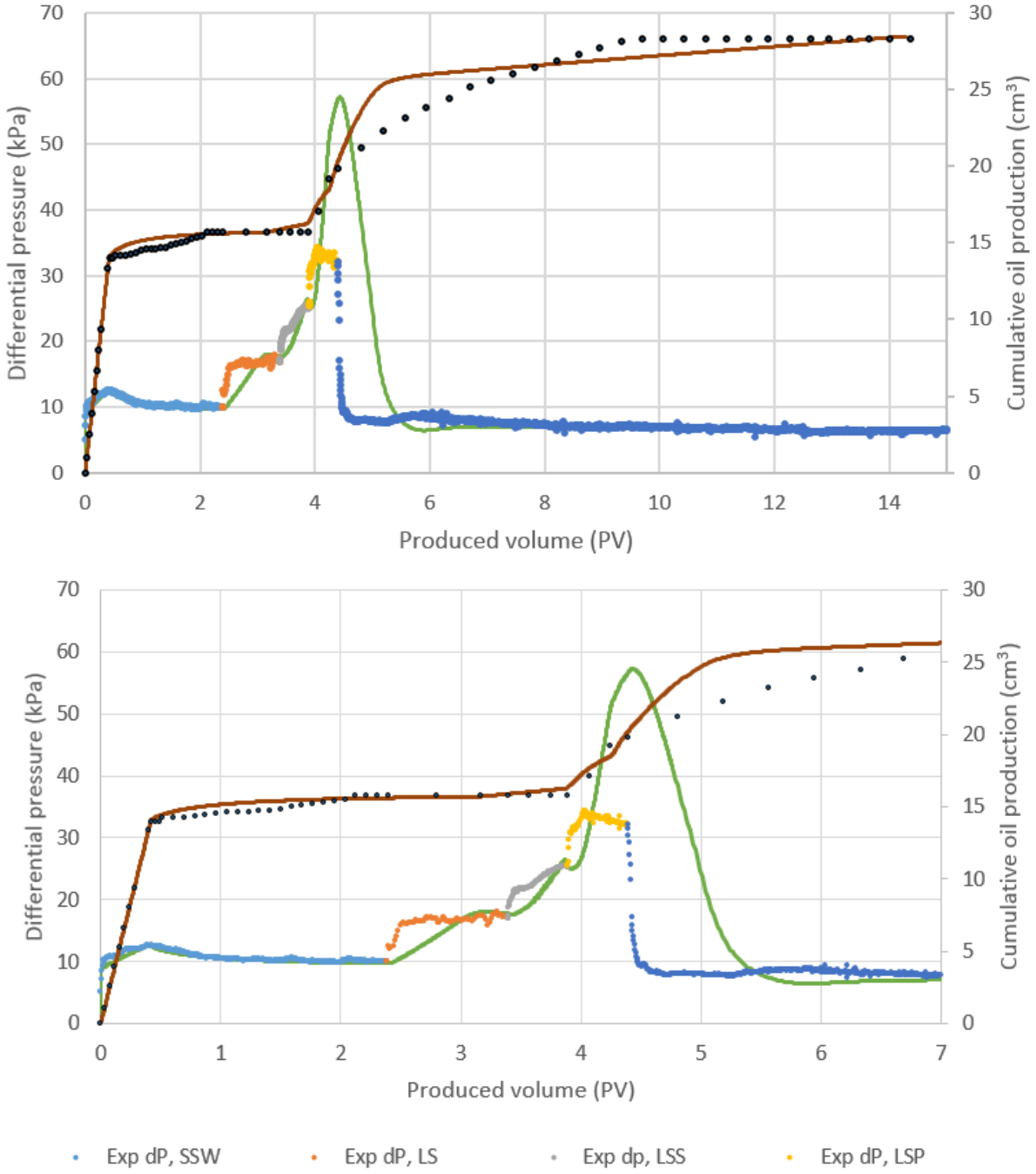

Figure 6.29: History match of differential pressure and oil production for the total flooding process. Bottom graph has a zoomed in x- axis.

7. Summary and Conclusion

Presented in chapter 4 was a wettability study, focusing on relative permeability, in the STARS simulator. Most results were found to be described accurately by the literature. Altering relative permeability curves for oil exhibited the most significant impact on oil production. This was the result of oil possessing a significantly higher viscosity than water, thus having a greater effect on mobility ratio and fractional flow. STARS was found to adequately render wettability changes through the use of relative permeability curves.

A multiple interpolation routine was investigated in chapter 5. Most of the methods used were found to work properly when k value- tables were altered. This was due to issues with concentration dependent parameters being defined by concentrations in the water phase alone. The new routine for multiple interpolation of relative permeability was found to be impractical. The relative permeability interpolation routine did not describe the exact behavior of polymer, but rendered the combined process of LSSP. The current approach of history matching each injection process separately makes the use of this interpolation routine unnecessarily complex.

Presented in chapter 6 was a history match performed utilizing established and newly investigated methods. Some explanations and demonstrations of best practice were presented with regards to numerical dispersion, relative permeability, interpolation parameter DTRAPW and the nonlinear viscosity mixing function. Polymer was modelled without relative permeability curves, but through the effects of viscosity, adsorption, IPV and dispersion alone.

Initial pressure responses for all injection sequences succeeding SSW were delayed in the simulations. Several efforts were made, but a pressure match could not be achieved without negatively affecting production. Additionally, a poor match of oil production during the second low salinity injection could be observed. Oil production during polymer flooding was heavily influenced by adsorption. Polymer adsorption can cause a delay in oil recovery [51] and it is therefore believed that the initial oil production during the second LS injection was too high because of it. The addition of polymer, relative permeability curves would likely solve this problem.

During modeling, several parameters were regarded as adjustable. This implies that the current history match is non- unique and another set of parameters could yield an identical result. Still, the underlying mechanisms of LS and LSP injection were found to be inadequately rendered by the current STARS model.

8. Further Work

In this thesis, an investigation into mechanistic modeling based on multiple interpolation of relative permeability was performed. This gave rise to several ideas for further work:

1. Modelling the transition between micro- emulsion systems, by defining concentration dependent parameters through component concentrations in both the oil and water phase.
2. Modeling of LSSP with the addition of unique relative permeability curves for both polymer and the 2nd low salinity injection. Alternatively, represent wettability alteration through cation exchange and/or other proposed mechanisms of low salinity(see point 4). This could potentially render both low salinity injections without the need for a second relative permeability set (or any).
3. Since interpolation was performed between near unique relative permeability curves during the polymer injection in chapter 5, this interpolation routine was not completely verified. Even though the method was deemed impractical for the current approach to history matching, it might still be viable tool for future multiple interpolation routines.
4. Utilizing untested options for complex chemical modeling in STARS to better represent the mechanisms behind low salinity water injection.
5. The addition of capillary pressure curves and hysteresis functions.
6. Upscaling of the aforementioned hybrid EOR methods. Topics like numerical and physical dispersion, reservoir heterogeneity, wettability, hysteresis, component degradation and in-situ rheology could be evaluated.

9. Appendix

This appendix contains the STARS input files used in the thesis.

Most of the timesteps have been removed from the input files to reduce code length. The files still honor the original start- and end- times of injection processes, but timesteps have to be added to render an adequate resolution.

A.a. Stars Input File – Wettability Study

```
** ============= INUT/OUTPUT CONTROL =============
TITLE1 'Wettability study'
INUNIT LAB
INTERRUPT *STOP
WSRF WELL 1
WSRF GRID TIME
WSRF SECTOR TIME

OUTSRF GRID VOL ADSORP MASS ADSORP MOLE ADSORP CMPVISW PPM KRO
KRW PRES SG SHEARW SO SW
        TEMP VISCVELW VISW VISWCOM W X Y
OUTSRF SPECIAL DELPBLK 2 1 1 99 1 1
OUTSRF SPECIAL DELPBLK 1 1 1 100 1 1
OUTSRF SPECIAL DELP 'INJ' 'PRODN'
OUTSRF SPECIAL MOLEFRAC 'PRODN' 'SALT'
OUTSRF SPECIAL MASSFRAC 'PRODN' 'SALT'
OUTSRF GRID ALL
OUTSRF WELL LAYER NONE

WPRN GRID 0
OUTPRN GRID POREVOL
OUTPRN RES NONE
WPRN ITER 1
OUTPRN ITER NEWTON

PARTCLSIZE 1e-017
** ============== GRID AND RESERVOIR DEFINITION ================
GRID CART 100 1 1
KDIR DOWN
DI CON 1
DJ CON 1
```

```
DK CON 1

NULL CON 1

POR 0.999 98*0.25 0.999

PERMI ALL
20000 98*2000 20000
PERMJ CON 2000
PERMK CON 200

PINCHOUTARRAY CON 1
END-GRID
** ================== COMPONENT PROPERTIES ======================
MODEL 3 3 3 2
COMPNAME 'WATER' 'SALT' 'DEAD_OIL'
CMM 0.018 0.058 0.4
PCRIT 0 0 0
TCRIT 0 0 0
CP 0 0 0
MASSDEN 0.0010 0.0019 0.00010
AVISC 1 5 13.8
BVISC 0 0 0

VSMIXCOMP 'SALT'
VSMIXENDP 0.0015 0.0400
VSMIXFUNC 0.003208333 0.006416667 0.009625 0.012833333 0.016041667 0.01925
0.022458333 0.025666667 0.028875 0.032083333 0.035291667

SOLID_DEN 'SALT' 0.0182482 0 0

PRSR 2528.25
TEMR 31
PSURF 101
TSURF 31
** ================== ROCK-FLUID DATA ================== **
ROCKFLUID
RPT 1 WATWET

INTCOMP 'SALT' WATER
** Set #1: High-sal. water injection
** ---------------------------------------------
KRINTRP 1
DTRAPW 0.0400
```

SWT
SMOOTHEND QUAD
** sw krw kro
0.2 0.000000 1.0000000
0.226 0.0008112 0.8987040
0.252 0.0032448 0.8028160
0.278 0.0073008 0.7123360
0.304 0.0129792 0.6272640
0.33 0.020280 0.5476000
0.356 0.0292032 0.4733440
0.382 0.0397488 0.4044960
0.408 0.0519168 0.3410560
0.434 0.0657072 0.2830240
0.46 0.081120 0.2304000
0.486 0.0981552 0.1831840
0.512 0.1168128 0.1413760
0.538 0.1370928 0.1049760
0.564 0.1589952 0.0739840
0.59 0.182520 0.0484000
0.616 0.2076672 0.0282240
0.642 0.2344368 0.0134560
0.668 0.2628288 0.0040960
0.70 0.300000 0.0000000

** Set #2: Low-sal. water injection
** ----------
KRINTRP 2
DTRAPW 0.0015
SWT
SMOOTHEND QUAD
** sw krw kro
0.2 0 1.0000000
0.226 0.000670413 0.9076893
0.252 0.002681653 0.8198479
0.278 0.006033719 0.7364760
0.304 0.010726612 0.6575736
0.33 0.016760331 0.5831405
0.356 0.024134876 0.5131769
0.382 0.032850248 0.4476826
0.408 0.042906446 0.3866579
0.434 0.054303471 0.3301025
0.46 0.067041322 0.2780165
0.486 0.081120 0.2304000
0.512 0.096539504 0.1872529

```
0.538   0.113299835   0.1485752
0.564   0.131400992   0.1143669
0.59    0.150842975   0.0846281
0.616   0.171625785   0.0593587
0.642   0.193749421   0.0385587
0.668   0.217213884   0.0222281
0.694   0.242019174   0.0103669
0.72    0.268165289   0.0029752
0.75    0.3       0.0000000

DISPI_WAT 'SALT' *CON 0.05
DISPJ_WAT 'SALT' *CON 0.01
DISPK_WAT 'SALT' *CON 0.01

** ================= INITIAL CONDITIONS ====== ============== **
INITIAL
VERTICAL OFF

INITREGION 1
PRES CON 101
TEMP CON 31

SW ALL
1 98*0 1

MFRAC_OIL 'DEAD_OIL' CON 1.0
MFRAC_WAT 'SALT' CON 0.0400
MFRAC_WAT 'WATER' CON 0.9600

** ================= NUMERICAL CONTROL ====================== **
NUMERICAL
TFORM SXY
ISOTHERMAL

** ================= RECURRENT DATA ====================== **
RUN

TIME 0
DTWELL 0.001

WELL 'INJ'
INJECTOR MOBWEIGHT 'INJ'
INCOMP WATER 0.9600 0.0400 0
OPERATE MAX STW 0.1 CONT
GEOMETRY K 0.01 0.2 1.0 0.0
```

```
PERF TUBE-END 'INJ'
1 1 1 1. OPEN FLOW-FROM 'SURFACE'

WELL 'PRODN'
PRODUCER 'PRODN'
OPERATE MIN BHP 101.1 CONT REPEAT
GEOMETRY K 0.01 0.2 1.0 0.0
PERF GEO 'PRODN'
100 1 1 1. OPEN FLOW-TO 'SURFACE'

TIME 20000

WELL 'INJ'
INJECTOR MOBWEIGHT 'INJ'

INCOMP WATER 0.9985 0.0015 0
OPERATE MAX STW 0.1 CONT

TIME 100000
STOP
```

A.b – Multiple Interpolation, LSSP

Note that parameters are defined with “SI” units and not “LAB” units as for the other files. See STARS manual [60] for complete explanation.

** 2016-10-19, 1:45:27 PM, erykah

** 2017-10-22, 5:34:04 PM, fraser

RESULTS SIMULATOR STARS 201710

INUNIT SI

WSRF WELL 1

WSRF GRID TIME

WSRF SECTOR TIME

OUTSRF GRID ADSORP ADSPCMP AQ-SP CAPN IFT KRO KRW LOGCAPN MASDENO MASDENW MOLDENO

MOLDENW PHAQ PRES RFO RFW SG SLD-SP SO SW TEMP VELOCRC

VISO VISW W X KRINTER

OUTSRF WELL MASS COMPONENT ALL

SHEAREFFEC SHR

WPRN GRID 0

OUTPRN GRID NONE

OUTPRN RES NONE

** Distance units: m

RESULTS XOFFSET 0.0000

RESULTS YOFFSET 0.0000

RESULTS ROTATION 0.0000 ** (DEGREES)

RESULTS AXES-DIRECTIONS 1.0 -1.0 1.0

**

****

** Definition of fundamental cartesian grid

**

****

```
GRID VARI 101 1 1
KDIR DOWN
DI IVAR
 0.0009075 99*0.001875 0.0009075
DJ JVAR
 0.033375
DK ALL
 101*0.03338623
DTOP
 101*1000
PERMI CON         2591
**  0 = null block, 1 = active block
NULL CON           1
POR CON       0.2494
PERMK  EQUALSI
**  0 = pinched block, 1 = active block
PINCHOUTARRAY CON           1
PERMJ  EQUALSI
END-GRID
** Model and number of components
MODEL 5 5 5 4
COMPNAME 'Water' 'Polymer' 'Surfact' 'NaCl' 'Dead_Oil'
CMM
0 8 0.427 0.0584428 0.4
PCRIT
0 0 0 0 0
TCRIT
0 0 0 0 0
```

```
LIQLIQKV
KVTABLIM 80 100000 10 500
KVKEYCOMP 'NaCl' Z 0 0.003 **0.00750386
** Liquid-liquid K Value tables
KVTABLE 'Surfact'
KEYCOMP
**
        0       0
        0       0
KEYCOMP
**
        0       0
        0       0
KEYCOMP
**
        0       0
        0       0
KEYCOMP
**
      1000     1000
      1000     1000
KEYCOMP
**
    1000000  1000000
    1000000  1000000

PRSR 100
TEMR 31
PSURF 100
```

TSURF 31

MASSDEN

0 0 3791.47 0 869.2

WATPHASE

AVISC

.8177 10.8 .8177 .8177 10.94

BVISC

0 0 0 0 0

VSMIXCOMP 'Polymer'

VSMIXENDP 0 1.69064e-006

VSMIXFUNC 0 0.140913 0.281826 0.422739 0.563502 0.621024 0.678546 0.745246 0.830164 0.915082 1

SHEARTAB

** velocity viscosity

0.01 10.8

0.1 10.584

1 6.48

3 4.86

6 4.32

10 4.212

*VSSALTCMP 'NaCl' 0.000308549 -0.428836

OILPHASE

**ME viscosity increase to 15 cp when surfactant is in the oil phase

AVISC

.8177 10.8 15.0 .8177 10.94

BVISC

0 0 0 0 0

VSMIXCOMP 'Surfact'

VSMIXENDP 0 0.001

VSMIXFUNC 0 0.1 0.2 0.3 0.4 0.5 0.6 0.7 0.8 0.9 1

** Reaction specification

STOREAC

0 1 0 0 0

STOPROD

443.951 0 0 0 0

RPHASE

0 1 0 0 0

RORDER

0 1 0 0 0

EACT 0

FREQFAC 0.000666488

ROCKFLUID

RPT 1 WATWET

**Curves with polymer concentration=2.25713011e-006

INTCOMP 'NaCl' WATER

IFTTABLE

** Weight percent Surfact = 0

2CMPW 1e-007

** Composition of component/phase Interfacial tension

0.001547029274	23.4 ** Salinity(NaCl), ppm = 5000
0.00310483332	5.163 ** Salinity(NaCl), ppm = 10000
0.003887811122	4.356 ** Salinity(NaCl), ppm = 12500
0.004673525099	3.715 ** Salinity(NaCl), ppm = 15000
0.00546198962	4.102 ** Salinity(NaCl), ppm = 17500
0.006253219154	3.805 ** Salinity(NaCl), ppm = 20000

0.007047228271 3.521 ** Salinity(NaCl), ppm = 22500

0.007844031643 2.953 ** Salinity(NaCl), ppm = 25000

** Weight percent Surfact = 0.11

2CMPW 4.64705e-005

** Composition of component/phase Interfacial tension

0.001547029274 0.17 ** Salinity(NaCl), ppm = 5000

0.00310483332 0.011 ** Salinity(NaCl), ppm = 10000

0.003887811122 0.005 ** Salinity(NaCl), ppm = 12500

0.004673525099 0.007 ** Salinity(NaCl), ppm = 15000

0.00546198962 0.007 ** Salinity(NaCl), ppm = 17500

0.006253219154 0.056 ** Salinity(NaCl), ppm = 20000

0.007047228271 0.097 ** Salinity(NaCl), ppm = 22500

0.007844031643 0.098 ** Salinity(NaCl), ppm = 25000

INTLOG

INTCOMP2 'Surfact'

KRINTRP 1

DTRAPW -5

DTRAPN -5

** Sw krw krow

SWT

0.306 0 0.9062

0.329813 4.03958e-005 0.746686

0.353625 0.000323167 0.607083

0.377437 0.00109069 0.486065

0.40125 0.00258533 0.382303

0.425063 0.00504948 0.294471

0.448875 0.0087255 0.22124

0.472688 0.0138558 0.161284

0.4965 0.0206827 0.113275

0.520313 0.0294486 0.0758854

0.544125 0.0403958 0.0477879

0.567937 0.0537669 0.027655

0.59175 0.069804 0.0141594

0.615563 0.0887496 0.00597349

0.639375 0.110846 0.00176992

0.663188 0.136336 0.00022124

0.687 0.165461 0

0.8435 0.464576 0

0.999 1 0

** Sl krg krog

SLT

0.6 0.7 0

0.625 0.576782 0.00022124

0.65 0.468945 0.00176992

0.675 0.375464 0.00597349

0.7 0.295312 0.0141594

0.725 0.227466 0.027655

0.75 0.170898 0.0477879

0.775 0.124585 0.0758854

0.8 0.0875 0.113275

0.825 0.0586182 0.161284

0.85 0.0369141 0.22124

0.875 0.0213623 0.294471

0.9 0.0109375 0.382303

0.925 0.00461426 0.486065

0.95 0.00136719 0.607083

```
      0.975  0.000170898    0.746686
        1           0      0.9062
KRINTRP 2 COPY 1 1
DTRAPW -3.5
DTRAPN -3.5
SORW 0.156

KRINTRP 3
DTRAPW -2
DTRAPN -2
**       Sw       krw      krow
SWT

      0.306         0    0.9062
      0.999         1         0
        1         1         0
**       Sl         krg        krog
SLT

       0.6         0.7           0
      0.625     0.576782  0.00022124
       0.65     0.468945  0.00176992
      0.675     0.375464  0.00597349
        0.7     0.295312   0.0141594
      0.725     0.227466    0.027655
       0.75     0.170898   0.0477879
      0.775     0.124585   0.0758854
        0.8       0.0875    0.113275
      0.825    0.0586182    0.161284
```

```
        0.85    0.0369141     0.22124
       0.875    0.0213623    0.294471
         0.9    0.0109375    0.382303
       0.925   0.00461426    0.486065
        0.95   0.00136719    0.607083
       0.975  0.000170898    0.746686
           1            0      0.9062

RPT 2 WATWET
**Interpolation between RPT types
RPT_INTRP
   COMP 'Polymer' WATER
   LOWER_BOUND 0.0
   UPPER_BOUND 2.25713011e-006   ** Max 'Polymer' concentration
   UPPERB_RPT 1

**Curves without polymer
INTCOMP 'NaCl' WATER
IFTTABLE
** Weight percent Surfact = 0
2CMPW 1e-007
**  Composition of component/phase  Interfacial tension
                0.001547029274             23.4  ** Salinity(NaCl), ppm = 5000
                 0.00310483332            5.163  ** Salinity(NaCl), ppm = 10000
                0.003887811122            4.356  ** Salinity(NaCl), ppm = 12500
                0.004673525099            3.715  ** Salinity(NaCl), ppm = 15000
                 0.00546198962            4.102  ** Salinity(NaCl), ppm = 17500
                0.006253219154            3.805  ** Salinity(NaCl), ppm = 20000
                0.007047228271            3.521  ** Salinity(NaCl), ppm = 22500
```

0.007844031643 2.953 ** Salinity(NaCl), ppm = 25000

** Weight percent Surfact = 0.11

2CMPW 4.64705e-005

** Composition of component/phase Interfacial tension

0.001547029274 0.17 ** Salinity(NaCl), ppm = 5000

0.00310483332 0.011 ** Salinity(NaCl), ppm = 10000

0.003887811122 0.005 ** Salinity(NaCl), ppm = 12500

0.004673525099 0.007 ** Salinity(NaCl), ppm = 15000

0.00546198962 0.007 ** Salinity(NaCl), ppm = 17500

0.006253219154 0.056 ** Salinity(NaCl), ppm = 20000

0.007047228271 0.097 ** Salinity(NaCl), ppm = 22500

0.007844031643 0.098 ** Salinity(NaCl), ppm = 25000

INTLOG

INTCOMP2 'Surfact'

KRINTRP 1

DTRAPW -5

DTRAPN -5

** Sw krw krow

SWT

0.306 0 0.9062

0.329813 4.03958e-005 0.746686

0.353625 0.000323167 0.607083

0.377437 0.00109069 0.486065

0.40125 0.00258533 0.382303

0.425063 0.00504948 0.294471

0.448875 0.0087255 0.22124

0.472688 0.0138558 0.161284

0.4965 0.0206827 0.113275

0.520313 0.0294486 0.0758854

0.544125 0.0403958 0.0477879

0.567937 0.0537669 0.027655

0.59175 0.069804 0.0141594

0.615563 0.0887496 0.00597349

0.639375 0.110846 0.00176992

0.663188 0.136336 0.00022124

0.687 0.165461 0

0.8435 0.464576 0

0.999 1 0

** Sl krg krog

SLT

0.6 0.7 0

0.625 0.576782 0.00022124

0.65 0.468945 0.00176992

0.675 0.375464 0.00597349

0.7 0.295312 0.0141594

0.725 0.227466 0.027655

0.75 0.170898 0.0477879

0.775 0.124585 0.0758854

0.8 0.0875 0.113275

0.825 0.0586182 0.161284

0.85 0.0369141 0.22124

0.875 0.0213623 0.294471

0.9 0.0109375 0.382303

0.925 0.00461426 0.486065

0.95 0.00136719 0.607083

0.975 0.000170898 0.746686

```
        1           0      0.9062
KRINTRP 2 COPY 2 1
DTRAPW -3.5
DTRAPN -3.5
SORW 0.20

KRINTRP 3
DTRAPW -2
DTRAPN -2
**       Sw       krw      krow
SWT

      0.306         0    0.9062
      0.999         1         0
          1         1         0
**       Sl         krg        krog
SLT

        0.6         0.7           0
      0.625    0.576782  0.00022124
       0.65    0.468945  0.00176992
      0.675    0.375464  0.00597349
        0.7    0.295312   0.0141594
      0.725    0.227466    0.027655
       0.75    0.170898   0.0477879
      0.775    0.124585   0.0758854
        0.8      0.0875    0.113275
      0.825   0.0586182    0.161284
       0.85  0.0369141     0.22124
```

0.875 0.0213623 0.294471

0.9 0.0109375 0.382303

0.925 0.00461426 0.486065

0.95 0.00136719 0.607083

0.975 0.000170898 0.746686

1 0 0.9062

KRTYPE CON 2

**Adsorption data

ADSCOMP 'Surfact' WATER

ADMAXT 5.13645

ADSTABLE

** Mole Fraction Adsorbed moles per unit pore volume

0 0

4.224186435e-005 5.136446911

ADSCOMP 'Polymer' WATER

RRFT 2

PORFT 0.9

ADRT 0.00747703

ADMAXT 0.299081

ADSPHBLK W

ADSTABLE

** Mole Fraction Adsorbed moles per unit pore volume

0 0

2.254749671e-006 0.2990812951

INTERP_ENDS ON

INITIAL

```
VERTICAL OFF

INITREGION 1
PRES CON          100
TEMP CON           31
MFRAC_WAT 'NaCl' CON   0.00944608
MFRAC_WAT 'Water' CON     0.990554
NUMERICAL
TFORM ZT
ISOTHERMAL
RUN
DATE 2012 1 1

DTWELL 0.001
**
WELL  'INJTR'
INJECTOR MOBWEIGHT IMPLICIT 'INJTR'
INCOMP  WATER  1.0  0.0  0.0  0.0  0.0
OPERATE  MAX  STW  0.00024  CONT REPEAT
**          rad  geofac  wfrac  skin
GEOMETRY  K  0.002  0.249  1.0  0.0
     PERF      GEOA  'INJTR'
** UBA             ff          Status  Connection
   1 1 1         10.0  OPEN    FLOW-FROM  'SURFACE'
**
WELL  'PRODN'
PRODUCER 'PRODN'
OPERATE  MIN  BHP  100.0  CONT REPEAT
**          rad  geofac  wfrac  skin
```

```
GEOMETRY  K  0.002  0.249  1.0  0.0
     PERF      GEOA  'PRODN'
** UBA              ff          Status  Connection
   101 1 1         10.0  OPEN    FLOW-TO  'SURFACE'

DATE 2012 1  2.14449

INJECTOR MOBWEIGHT IMPLICIT 'INJTR'
**INCOMP  WATER  0.995277703  2.25713011e-006  4.65169671e-005  0.00467352271
0.0
INCOMP  WATER  0.995278703  1.25713011e-006  4.65169671e-005  0.00467352271  0.0
OPERATE  MAX  STW  0.00024  CONT REPEAT

DATE 2012 1  2.88266

INJECTOR MOBWEIGHT IMPLICIT 'INJTR'
INCOMP  WATER  1.0  0.0  0.0  0.0  0.0
OPERATE  MAX  STW  0.00024  CONT REPEAT

DATE 2012 1  6.91699
STOP
RESULTS PROCESSWIZ PROCESS 2
RESULTS PROCESSWIZ FOAMYOILMODEL -1
RESULTS PROCESSWIZ SGC 0.15
RESULTS PROCESSWIZ KRGCW 0.0001
RESULTS PROCESSWIZ COALESCENCE -99999 FALSE
RESULTS PROCESSWIZ BUBBLEPT -99999
RESULTS PROCESSWIZ MINPRESSURE -99999 FALSE
RESULTS PROCESSWIZ NUMSETSFOAMY 2
RESULTS PROCESSWIZ PRODTIME 2.95849
```

RESULTS PROCESSWIZ FOAMYREACTIONS 1.82525 338.01 0.33801 3.3801 0.033801

RESULTS PROCESSWIZ VELOCITYFOAMY TRUE

RESULTS PROCESSWIZ CHEMMODEL 4

RESULTS PROCESSWIZ CHEMDATA1 TRUE FALSE TRUE TRUE TRUE 2 3 FALSE FALSE FALSE FALSE TRUE FALSE

RESULTS PROCESSWIZ CHEMDATA2 0.1 0.02 0.000308549 -0.428836 0 2 0.9 1040 21.88 5 5

RESULTS PROCESSWIZ CHEMDATA3 2.65 0 0.1 0.1 0.11 0.1 1 -99999

RESULTS PROCESSWIZ ASPRPT 0.5 2 1 1

RESULTS PROCESSWIZ FOAMDATA FALSE TRUE FALSE 80 100 31 1.386 0.693 693 13.86 0 0.02 0.35 -99999 6 2 FALSE

RESULTS PROCESSWIZ FOAMDATA1 0.2 1 -99999 -99999 0.5 2 0.01 0.4 1000 50000 1 5 0.0001 1 0.1 3 1e-006 1e-005 0.2 1 1 100000

RESULTS PROCESSWIZ TABLEFOAMVISC 0 0.02 0 1 0.1 20 0.2 40 0.3 45 0.4 48 0.5 49 0.6 15 0.7 10 0.8 5 0.9 2 1 0.02

RESULTS PROCESSWIZ TABLEFOAMVISC 0 0.1 0 1 0.1 160 0.2 170 0.3 180 0.4 205 0.5 210 0.6 220 0.7 150 0.8 48 0.9 20 1 15

RESULTS PROCESSWIZ TABLEFOAMVISC 0 0.2 0 1 0.1 235 0.2 255 0.3 345 0.4 380 0.5 415 0.6 335 0.7 255 0.8 180 0.9 125 1 40

RESULTS PROCESSWIZ FOAMVISCWEIGHT 1 0.1 0.4 1

RESULTS PROCESSWIZ FOAMVISCPERM -99999 -99999 -99999 -99999

RESULTS PROCESSWIZ IFTALKALI_WOR 0

RESULTS PROCESSWIZ TABLEIFT 0 18.2

RESULTS PROCESSWIZ TABLEIFT 0.05 0.5

RESULTS PROCESSWIZ TABLEIFT 0.1 0.028

RESULTS PROCESSWIZ TABLEIFT 0.2 0.028

RESULTS PROCESSWIZ TABLEIFT 0.4 0.0057

RESULTS PROCESSWIZ TABLEIFT 0.6 0.00121

RESULTS PROCESSWIZ TABLEIFT 0.8 0.00037

RESULTS PROCESSWIZ TABLEIFT 1 0.5

RESULTS PROCESSWIZ IFTSURFACTANT 1 9 0 0.3

RESULTS PROCESSWIZ IFTSURFACTANTSALINITY FALSE 8

RESULTS PROCESSWIZ IFTALKALI_SURFACT 0 0.11

RESULTS PROCESSWIZ TABLEIFTSSALINITY 5000 23.4

RESULTS PROCESSWIZ TABLEIFTSSALINITY 10000 5.163

RESULTS PROCESSWIZ TABLEIFTSSALINITY 12500 4.356

RESULTS PROCESSWIZ TABLEIFTSSALINITY 15000 3.715

RESULTS PROCESSWIZ TABLEIFTSSALINITY 17500 4.102

RESULTS PROCESSWIZ TABLEIFTSSALINITY 20000 3.805

RESULTS PROCESSWIZ TABLEIFTSSALINITY 22500 3.521

RESULTS PROCESSWIZ TABLEIFTSSALINITY 25000 2.953

RESULTS PROCESSWIZ TABLEIFTSSALINITY 5000 0.17

RESULTS PROCESSWIZ TABLEIFTSSALINITY 10000 0.011

RESULTS PROCESSWIZ TABLEIFTSSALINITY 12500 0.005

RESULTS PROCESSWIZ TABLEIFTSSALINITY 15000 0.007

RESULTS PROCESSWIZ TABLEIFTSSALINITY 17500 0.007

RESULTS PROCESSWIZ TABLEIFTSSALINITY 20000 0.056

RESULTS PROCESSWIZ TABLEIFTSSALINITY 22500 0.097

RESULTS PROCESSWIZ TABLEIFTSSALINITY 25000 0.098

RESULTS PROCESSWIZ IFTALKALI_SALINITY 10000

RESULTS PROCESSWIZ IFTALKALI_SALINITY_AQUEOUSCOMP 0 'Na+' 10000 'Na2CO3' 1 'NaOH' 0

RESULTS PROCESSWIZ IFTALKALI_TABLE 0 23.4

RESULTS PROCESSWIZ IFTALKALI_TABLE 0.025 18.21

RESULTS PROCESSWIZ IFTALKALI_TABLE 0.05 15.54

RESULTS PROCESSWIZ IFTALKALI_TABLE 0.1 12.21

RESULTS PROCESSWIZ IFTALKALI_TABLE 0.15 9.11

RESULTS PROCESSWIZ IFTALKALI_TABLE 0.2 7.25

RESULTS PROCESSWIZ IFTALKALI_TABLE 0.3 5.023

RESULTS PROCESSWIZ IFTALKALI_TABLE 0.4 4.535

RESULTS PROCESSWIZ IFTALKALI_TABLE 0.5 5.12

RESULTS PROCESSWIZ IFTALKALI_TABLE 0 18.2

RESULTS PROCESSWIZ IFTALKALI_TABLE 0.025 0.5

RESULTS PROCESSWIZ IFTALKALI_TABLE 0.05 0.028

RESULTS PROCESSWIZ IFTALKALI_TABLE 0.1 0.003

RESULTS PROCESSWIZ IFTALKALI_TABLE 0.15 0.006

RESULTS PROCESSWIZ IFTALKALI_TABLE 0.2 0.055

RESULTS PROCESSWIZ IFTALKALI_TABLE 0.3 0.082

RESULTS PROCESSWIZ IFTALKALI_TABLE 0.4 0.3

RESULTS PROCESSWIZ IFTALKALI_TABLE 0.5 1.2

RESULTS PROCESSWIZ SOAP 2 1 1 -99999 23.4 1 1 800 -5500

RESULTS PROCESSWIZ TOPSAL_SFT 0.001 14311 0

RESULTS PROCESSWIZ TOPSAL_SFT 873.4 14311 0

RESULTS PROCESSWIZ TOPSAL_SFT 4368.9 21496 0

RESULTS PROCESSWIZ ADSORPTION TRUE TRUE FALSE TRUE 2 FALSE -1

RESULTS PROCESSWIZ ADSPOR 0.2494 0.2494 0.2494

RESULTS PROCESSWIZ ADSSURF 0 0

RESULTS PROCESSWIZ ADSSURF 0.1 27.5

RESULTS PROCESSWIZ ADSALK 0 0

RESULTS PROCESSWIZ ADSALK 0.1 50

RESULTS PROCESSWIZ ADSPOLYMER 0 0

RESULTS PROCESSWIZ ADSPOLYMER 0.1 30

RESULTS PROCESSWIZ ALKALINECONC 0 0.3 0.6

RESULTS PROCESSWIZ ADSSURF2 0 0

RESULTS PROCESSWIZ ADSSURF2 0.1 27.5

RESULTS PROCESSWIZ ADSSURF2 0 0

RESULTS PROCESSWIZ ADSSURF2 0.1 39.5

RESULTS PROCESSWIZ ADSSURF2 0 0

RESULTS PROCESSWIZ ADSSURF2 0.1 51

RESULTS PROCESSWIZ ADSPOLY2 0 0

RESULTS PROCESSWIZ ADSPOLY2 0.1 50

RESULTS PROCESSWIZ ADSPOLY2 0 0

RESULTS PROCESSWIZ ADSPOLY2 0.1 50

RESULTS PROCESSWIZ ADSPOLY2 0 0

RESULTS PROCESSWIZ ADSPOLY2 0.1 50

RESULTS PROCESSWIZ ADSALK2 0 0

RESULTS PROCESSWIZ ADSALK2 0.1 50

RESULTS PROCESSWIZ ADSALK2 0 0

RESULTS PROCESSWIZ ADSALK2 0.1 50

RESULTS PROCESSWIZ ADSALK2 0 0

RESULTS PROCESSWIZ ADSALK2 0.1 50

RESULTS PROCESSWIZ SALINITYPPM 0 30000 60000

RESULTS PROCESSWIZ ADSSURF3 0 0

RESULTS PROCESSWIZ ADSSURF3 0.1 27.5

RESULTS PROCESSWIZ ADSSURF3 0 0

RESULTS PROCESSWIZ ADSSURF3 0.1 39.5

RESULTS PROCESSWIZ ADSSURF3 0 0

RESULTS PROCESSWIZ ADSSURF3 0.1 51

RESULTS PROCESSWIZ ADSPOLY3 0 0

RESULTS PROCESSWIZ ADSPOLY3 0.1 50

RESULTS PROCESSWIZ ADSPOLY3 0 0

RESULTS PROCESSWIZ ADSPOLY3 0.1 50

RESULTS PROCESSWIZ ADSPOLY3 0 0

RESULTS PROCESSWIZ ADSPOLY3 0.1 50

RESULTS PROCESSWIZ ADSALK3 0 0

RESULTS PROCESSWIZ ADSALK3 0.1 50

RESULTS PROCESSWIZ ADSALK3 0 0

RESULTS PROCESSWIZ ADSALK3 0.1 50

RESULTS PROCESSWIZ ADSALK3 0 0

RESULTS PROCESSWIZ ADSALK3 0.1 50

RESULTS PROCESSWIZ VELOCITY 0.01 0.1 1 3 6 10

RESULTS PROCESSWIZ SALINITY 1000 10000

RESULTS PROCESSWIZ COMPPOLY 0 0.03 0.05 0.075

RESULTS PROCESSWIZ POLYVISC 0.8177 3.5 5.2 10.8

RESULTS PROCESSWIZ POLYVISC 0.8177 3.43 5.096 10.584

RESULTS PROCESSWIZ POLYVISC 0.8177 2.1 3.12 6.48

RESULTS PROCESSWIZ POLYVISC 0.8177 1.575 2.34 4.86

RESULTS PROCESSWIZ POLYVISC 0.8177 1.4 2.08 4.32

RESULTS PROCESSWIZ POLYVISC 0.8177 1.365 2.028 4.212

RESULTS PROCESSWIZ POLYVISC 0.8177 1.30037 1.93198 4.01258

RESULTS PROCESSWIZ POLYVISC 0.8177 1.27437 1.89334 3.93233

RESULTS PROCESSWIZ POLYVISC 0.8177 0.780224 1.15919 2.40755

RESULTS PROCESSWIZ POLYVISC 0.8177 0.585168 0.869392 1.80566

RESULTS PROCESSWIZ POLYVISC 0.8177 0.520149 0.772793 1.60503

RESULTS PROCESSWIZ POLYVISC 0.8177 0.507146 0.753473 1.56491

RESULTS PROCESSWIZ COMPSALINITY 0 0.03 0.05 0.075

RESULTS PROCESSWIZ SALINITYVISC 0.8177 3.5 5.2 10.8

RESULTS PROCESSWIZ SALINITYVISC 0.8177 1.30037 1.93198 4.01258

RESULTS PROCESSWIZ SALINITY_INITIAL 30000

RESULTS PROCESSWIZ FINES 10000 8000 86.5556 15000 500 50 10 5000 0.0001 0.0624279 FALSE FALSE

RESULTS PROCESSWIZ LSWI 50 0.19 0.5 0 2 2 'Ca-X2'

RESULTS PROCESSWIZ LSWIREACT FALSE FALSE FALSE FALSE TRUE TRUE TRUE TRUE FALSE FALSE FALSE FALSE FALSE 0.9999 FALSE FALSE

RESULTS PROCESSWIZ LSWIREACTAQ

RESULTS PROCESSWIZ LSWIREACTMIN

RESULTS PROCESSWIZ LSWIREACTAQMINTEQ

RESULTS PROCESSWIZ LSWIREACTMINMINTEQ

RESULTS PROCESSWIZ LSWIRPT

RESULTS PROCESSWIZ LSWIRPTCHG FALSE 0.001 2 4 TRUE 0.3 0.1 0.1 FALSE 0.05 0.7

RESULTS PROCESSWIZ LSWIAQINJ 'H+' 0.000101

RESULTS PROCESSWIZ LSWIAQINIT

RESULTS PROCESSWIZ LSWIMIN

RESULTS PROCESSWIZ SALINITYCOMPS

RESULTS PROCESSWIZ ISCMODEL -1 FALSE FALSE FALSE FALSE FALSE FALSE FALSE

RESULTS PROCESSWIZ ISCDATA 10000 0.4 9 9.4 0.065 0.708108 0.065 0.708108

RESULTS PROCESSWIZ REACTO2 0 1

RESULTS PROCESSWIZ BURN 0 1

RESULTS PROCESSWIZ CRACK 0 1

RESULTS PROCESSWIZ COMPNAMES

RESULTS PROCESSWIZ BLOCKAGE FALSE 4

RESULTS PROCESSWIZ END

RESULTS RELPERMCORR NUMROCKTYPE 1

RESULTS RELPERMCORR CORRVALS 0.306 0.306 0 0.313 0.294 0.294 0 0

RESULTS RELPERMCORR CORRVALS 0.9062 1 0.7 -99999 3 3 3 3

RESULTS RELPERMCORR CORRVALS_HONARPOUR -99999 -99999 -99999 -99999 -99999 -99999 -99999 -99999

RESULTS RELPERMCORR NOSWC false

RESULTS RELPERMCORR CALINDEX 0

RESULTS RELPERMCORR STOP

RESULTS RELPERMCORR NUMROCKTYPE 1

RESULTS RELPERMCORR NUMISET 2

RESULTS RELPERMCORR NOSWC false

RESULTS RELPERMCORR CALINDEX 0

RESULTS RELPERMCORR STOP

RESULTS RELPERMCORR NUMROCKTYPE 1

RESULTS RELPERMCORR NUMISET 3

RESULTS RELPERMCORR NOSWC false

RESULTS RELPERMCORR CALINDEX 0

RESULTS RELPERMCORR STOP

RESULTS SPEC 'Porosity'

RESULTS SPEC SPECNOTCALCVAL -99999

RESULTS SPEC REGION 'All Layers (Whole Grid)'

RESULTS SPEC REGIONTYPE 'REGION_WHOLEGRID'

RESULTS SPEC LAYERNUMB 0

RESULTS SPEC PORTYPE 1

RESULTS SPEC CON 0.2494

RESULTS SPEC SPECKEEPMOD 'YES'

RESULTS SPEC STOP

RESULTS SPEC 'Permeability J'

RESULTS SPEC SPECNOTCALCVAL -99999

RESULTS SPEC REGION 'All Layers (Whole Grid)'

RESULTS SPEC REGIONTYPE 'REGION_WHOLEGRID'

RESULTS SPEC LAYERNUMB 0

RESULTS SPEC PORTYPE 1

RESULTS SPEC EQUALSI 0 1

RESULTS SPEC SPECKEEPMOD 'YES'

RESULTS SPEC STOP

RESULTS SPEC 'Permeability I'

RESULTS SPEC SPECNOTCALCVAL -99999

RESULTS SPEC REGION 'All Layers (Whole Grid)'

RESULTS SPEC REGIONTYPE 'REGION_WHOLEGRID'

RESULTS SPEC LAYERNUMB 0

RESULTS SPEC PORTYPE 1

RESULTS SPEC CON 2591

RESULTS SPEC SPECKEEPMOD 'YES'

RESULTS SPEC STOP

RESULTS SPEC 'Permeability K'

RESULTS SPEC SPECNOTCALCVAL -99999

RESULTS SPEC REGION 'All Layers (Whole Grid)'

RESULTS SPEC REGIONTYPE 'REGION_WHOLEGRID'

RESULTS SPEC LAYERNUMB 0

RESULTS SPEC PORTYPE 1

RESULTS SPEC EQUALSI 0 1

RESULTS SPEC SPECKEEPMOD 'YES'

RESULTS SPEC STOP

RESULTS SPEC 'Pressure'

RESULTS SPEC SPECNOTCALCVAL -99999

RESULTS SPEC REGION 'All Layers (Whole Grid)'

RESULTS SPEC REGIONTYPE 'REGION_WHOLEGRID'

RESULTS SPEC LAYERNUMB 0

RESULTS SPEC PORTYPE 1

RESULTS SPEC CON 100

RESULTS SPEC SPECKEEPMOD 'YES'

RESULTS SPEC STOP

RESULTS SPEC 'Temperature'

RESULTS SPEC SPECNOTCALCVAL -99999

RESULTS SPEC REGION 'All Layers (Whole Grid)'

RESULTS SPEC REGIONTYPE 'REGION_WHOLEGRID'

RESULTS SPEC LAYERNUMB 0

RESULTS SPEC PORTYPE 1

RESULTS SPEC CON 31

RESULTS SPEC SPECKEEPMOD 'YES'

RESULTS SPEC STOP

RESULTS SPEC 'Grid Top'

RESULTS SPEC SPECNOTCALCVAL -99999

RESULTS SPEC REGION 'Layer 1 - Whole layer'

RESULTS SPEC REGIONTYPE 'REGION_LAYER'

RESULTS SPEC LAYERNUMB 1

RESULTS SPEC PORTYPE 1

RESULTS SPEC CON 1000

RESULTS SPEC SPECKEEPMOD 'YES'

RESULTS SPEC STOP

RESULTS SPEC 'Grid Thickness'

RESULTS SPEC SPECNOTCALCVAL -99999

RESULTS SPEC REGION 'All Layers (Whole Grid)'

RESULTS SPEC REGIONTYPE 'REGION_WHOLEGRID'

RESULTS SPEC LAYERNUMB 0

RESULTS SPEC PORTYPE 1

RESULTS SPEC CON 0.033375

RESULTS SPEC SPECKEEPMOD 'YES'

RESULTS SPEC STOP

A.c. STARS Input File - R10

```
RESULTS SIMULATOR STARS 201210


** history match of lab experiment R10
** sequence HS - LS - LSS - LSP - LS
**
INUNIT LAB
WSRF WELL 1
WSRF GRID 1
WSRF SECTOR 1
OUTSRF GRID ADSORP ADSPCMP CAPN IFT KRO KRW LOGCAPN MASDENO
MASDENW MOLDENO MOLDENW
      PRES RFO RFW SG SO SW TEMP VELOCRC VISO VISW W KRSETN
KRINTER VELCAPN OILPOT
      X
OUTSRF GRID ALL
OUTSRF WELL MASS COMPONENT ALL
OUTSRF WELL MASS COMPONENT 'Na'
OUTSRF SPECIAL MASSFRAC 'INJTR' 'Na'
OUTSRF SPECIAL MOLEFRAC 'INJTR' 'Na'
OUTSRF SPECIAL MASSFRAC 'PRODN' 'Na'
OUTSRF SPECIAL MOLEFRAC 'PRODN' 'Na'
OUTSRF SPECIAL MASSFRAC 'PRODN' 'Cl'
OUTSRF SPECIAL MOLEFRAC 'PRODN' 'SURF'
OUTSRF SPECIAL MASSFRAC 'PRODN' 'SURF'
OUTSRF SPECIAL MOLEFRAC 'PRODN' 'POLYMER'
OUTSRF SPECIAL MASSFRAC 'PRODN' 'POLYMER'
OUTSRF SPECIAL VOLFRAC 'PRODN' 'Na'
OUTSRF SPECIAL DELPBLK 2 1 1 99 1 1
**$
**************************************************************************
```

```
**$ Definition of fundamental cartesian grid
**$
*****************************************************************************

**  ==============  GRID AND RESERVOIR DEFINITION  ================
GRID CART 100 1 1
KDIR DOWN

DI IVAR
**0.0033667 ft = 0.10262 cm
0.056 98*0.136 0.056

DJ
100*3.8

DK
100*3.8

DTOP
100*1

POR ALL
0.999 98*0.2205 0.999

PERMI
100000 98*360 100000

PERMJ EQUALSI
PERMK EQUALSI

END-GRID
** ==================  ROCK THERMAL PROPERTIES ==================
```

PRPOR 1000

CPOR 2.96e-8

** ================== COMPONENT PROPERTIES ============== **

MODEL 6 6 6 5

COMPNAME 'H2O' 'Na' 'Cl' 'SURF' 'POLYMER' 'DEAD_OIL'

CMM

0.018 0.02299 0.035453 0.426 8 0.4

PCRIT

0 0 0 0 0 0

TCRIT

0 0 0 0 0 0

PRSR 1000

TEMR 70

PSURF 101.1

TSURF 25

MASSDEN

0.001 0.001 0.001 0.001 0.001 0.0008784

AVISC

**'H2O' 'Na' 'Cl' 'SURF' 'POLYMER' 'DEAD_OIL'

0.5 0.5 0.5 1.0 10 3.0

VSMIXCOMP 'Na'

VSMIXENDP 0 0.00885

VSMIXFUNC 0 0 0.075 0.166 0.255 0.345 0.43 0.515 0.6 0.683 0.764

VSMIXCOMP 'SURF'

VSMIXENDP 0.0 0.000427

VSMIXFUNC

0.00

0.21

0.34

0.46

0.56

0.66

0.74

0.82

0.90

0.97

1.0

VSMIXCOMP 'POLYMER'

VSMIXENDP 0.0 3.38E-06

VSMIXFUNC

0.0

0.218370153

0.347982965

0.463303551

0.567173163

0.661661883

0.748324694

0.828359366

0.902708128

0.972125557

1.0

SHEARTAB

** Darcy velocity (cm/min)	Viscosity (cP)
0.00001	10.0
0.0001	10.0
0.001	10.0
0.01	10.0
0.1	10.0

SOLID_DEN 'Na' 0.001 0 0

SOLID_DEN 'Cl' 0.001 0 0

SOLID_DEN 'SURF' 0.001 0 0

SOLID_DEN 'POLYMER' 0.001 0 0

** ========== ROCK-FLUID DATA ========== **

ROCKFLUID

DISPI_WAT 'Na' CON 0.0001

DISPJ_WAT 'Na' CON 0.0001

DISPK_WAT 'Na' CON 0.0001

DISPI_WAT 'Cl' CON 0.0001

DISPJ_WAT 'Cl' CON 0.0001

DISPK_WAT 'Cl' CON 0.0001

DISPI_WAT 'SURF' CON 0.01

DISPJ_WAT 'SURF' CON 0.01

DISPK_WAT 'SURF' CON 0.01

DISPI_WAT 'POLYMER' CON 0.01

DISPJ_WAT 'POLYMER' CON 0.01

DISPK_WAT 'POLYMER' CON 0.01

RPT 1 WATWET

INTCOMP 'SURF' WATER

IFTTABLE

**	cift	SIGIFT
	0	30
	0.000001	0.1
	0.000005	0.05
	0.00001	0.02
	0.00005	0.02
	0.00026	0.02
	0.000427	0.02
	0.05	0.02

INTCOMP 'SURF' WATER

KRINTRP 1

DTRAPW -12.47

SWT

SMOOTHEND QUAD

**Sw	krw	kro
0.15	0.00000	0.15000
0.16	0.00000	0.14299
0.17	0.00001	0.13611
0.18	0.00002	0.12938
0.19	0.00005	0.12278
0.20	0.00009	0.11633

0.21	0.00015	0.11002
0.22	0.00023	0.10386
0.23	0.00034	0.09785
0.24	0.00047	0.09198
0.25	0.00064	0.08626
0.26	0.00083	0.08070
0.27	0.00106	0.07529
0.28	0.00133	0.07003
0.29	0.00163	0.06494
0.30	0.00198	0.06000
0.31	0.00237	0.05522
0.32	0.00281	0.05061
0.33	0.00330	0.04617
0.34	0.00384	0.04189
0.35	0.00444	0.03779
0.36	0.00509	0.03386
0.37	0.00579	0.03012
0.38	0.00656	0.02655
0.39	0.00739	0.02317
0.40	0.00829	0.01999
0.41	0.00925	0.01700
0.42	0.01028	0.01421
0.43	0.01138	0.01163
0.44	0.01255	0.00927
0.45	0.01380	0.00713
0.46	0.01513	0.00523
0.47	0.01654	0.00358
0.48	0.01803	0.00220
0.49	0.01960	0.00110
0.50	0.02126	0.00034
0.51	0.02300	0.00000

INTCOMP 'SURF' WATER

KRINTRP 2

DTRAPW -9.47

SWT

SMOOTHEND QUAD

**Sw	krw	kro
0.15	0.00000	0.40000
0.16	0.00000	0.37675
0.17	0.00001	0.35460
0.18	0.00002	0.33349
0.19	0.00005	0.31341
0.20	0.00009	0.29431
0.21	0.00016	0.27614
0.22	0.00026	0.25889
0.23	0.00039	0.24251
0.24	0.00055	0.22697
0.25	0.00076	0.21224
0.26	0.00101	0.19828
0.27	0.00131	0.18507
0.28	0.00167	0.17257
0.29	0.00208	0.16075
0.30	0.00256	0.14959
0.31	0.00311	0.13906
0.32	0.00373	0.12913
0.33	0.00443	0.11978
0.34	0.00521	0.11098
0.35	0.00607	0.10270
0.36	0.00703	0.09492
0.37	0.00808	0.08762
0.38	0.00924	0.08078
0.39	0.01050	0.07437

0.40	0.01186	0.06838
0.41	0.01334	0.06278
0.42	0.01494	0.05755
0.43	0.01667	0.05267
0.44	0.01852	0.04814
0.45	0.02050	0.04392
0.46	0.02262	0.04000
0.47	0.02488	0.03636
0.48	0.02728	0.03300
0.49	0.02984	0.02989
0.50	0.03255	0.02702
0.51	0.03542	0.02437
0.52	0.03846	0.02194
0.53	0.04166	0.01970
0.54	0.04504	0.01765
0.55	0.04859	0.01577
0.56	0.05233	0.01406
0.57	0.05625	0.01250
0.58	0.06036	0.01108
0.59	0.06467	0.00979
0.60	0.06919	0.00863
0.61	0.07390	0.00758
0.62	0.07883	0.00663
0.63	0.08397	0.00578
0.64	0.08932	0.00502
0.65	0.09490	0.00435
0.66	0.10071	0.00374
0.67	0.10675	0.00321
0.68	0.11303	0.00274
0.69	0.11955	0.00232
0.70	0.12632	0.00196
0.71	0.13333	0.00165

0.72	0.14060	0.00137
0.73	0.14814	0.00114
0.74	0.15593	0.00093
0.75	0.16399	0.00076
0.76	0.17233	0.00062
0.77	0.18095	0.00049
0.78	0.18984	0.00039
0.79	0.19903	0.00031
0.80	0.20850	0.00024
0.81	0.21828	0.00018
0.82	0.22835	0.00014
0.83	0.23873	0.00010
0.84	0.24941	0.00007
0.85	0.26042	0.00005
0.86	0.27174	0.00004
0.87	0.28338	0.00002
0.88	0.29535	0.00002
0.89	0.30766	0.00001
0.90	0.32030	0.00001
0.91	0.33328	0.00000
0.92	0.34661	0.00000
0.93	0.36030	0.00000
0.94	0.37433	0.00000
0.95	0.38873	0.00000
0.96	0.40349	0.00000
0.97	0.41862	0.00000
0.98	0.43412	0.00000
0.99	0.45000	0.00000

** ----------

RPT 2 WATWET

RPT_INTRP

COMP 'Na' WATER

LOWER_BOUND 0.00139

UPPER_BOUND 0.00885

UPPERB_RPT 1

INTCOMP 'Na' WATER

KRINTRP 1

DTRAPW 0.00885

SWT

SMOOTHEND QUAD

**Sw	krw	kro
0.15	0.00000	0.15000
0.16	0.00000	0.14299
0.17	0.00001	0.13611
0.18	0.00002	0.12938
0.19	0.00005	0.12278
0.20	0.00009	0.11633
0.21	0.00015	0.11002
0.22	0.00023	0.10386
0.23	0.00034	0.09785
0.24	0.00047	0.09198
0.25	0.00064	0.08626
0.26	0.00083	0.08070
0.27	0.00106	0.07529
0.28	0.00133	0.07003
0.29	0.00163	0.06494
0.30	0.00198	0.06000
0.31	0.00237	0.05522
0.32	0.00281	0.05061

0.33	0.00330	0.04617
0.34	0.00384	0.04189
0.35	0.00444	0.03779
0.36	0.00509	0.03386
0.37	0.00579	0.03012
0.38	0.00656	0.02655
0.39	0.00739	0.02317
0.40	0.00829	0.01999
0.41	0.00925	0.01700
0.42	0.01028	0.01421
0.43	0.01138	0.01163
0.44	0.01255	0.00927
0.45	0.01380	0.00713
0.46	0.01513	0.00523
0.47	0.01654	0.00358
0.48	0.01803	0.00220
0.49	0.01960	0.00110
0.50	0.02126	0.00034
0.51	0.02300	0.00000

KRINTRP 2

DTRAPW 0.00139

SWT

**Sw	krw	kro
0.15	0.00000	0.15000
0.16	0.00000	0.13784
0.17	0.00000	0.12636
0.18	0.00000	0.11554
0.19	0.00000	0.10535
0.20	0.00000	0.09578
0.21	0.00000	0.08681

0.22	0.00000	0.07841
0.23	0.00000	0.07058
0.24	0.00000	0.06328
0.25	0.00001	0.05651
0.26	0.00001	0.05023
0.27	0.00002	0.04444
0.28	0.00003	0.03912
0.29	0.00004	0.03423
0.30	0.00006	0.02977
0.31	0.00009	0.02572
0.32	0.00013	0.02205
0.33	0.00019	0.01875
0.34	0.00026	0.01580
0.35	0.00035	0.01317
0.36	0.00047	0.01085
0.37	0.00063	0.00882
0.38	0.00082	0.00706
0.39	0.00105	0.00556
0.40	0.00135	0.00428
0.41	0.00170	0.00322
0.42	0.00214	0.00165
0.43	0.00266	0.00165
0.44	0.00328	0.00160
0.45	0.00402	0.00160
0.46	0.00489	0.00160
0.47	0.00592	0.00160
0.48	0.00712	0.00160
0.49	0.00852	0.00160
0.50	0.01013	0.00160
0.51	0.01200	0.00160
0.52	0.01289	0.00160
0.53	0.01379	0.00160

0.54	0.01469	0.00160
0.55	0.01558	0.00160
0.56	0.01648	0.00160
0.57	0.01737	0.00160
0.58	0.01827	0.00160
0.59	0.01916	0.00160
0.60	0.02006	0.00160
0.61	0.02096	0.00160
0.62	0.02185	0.00160
0.63	0.02275	0.00160
0.64	0.02364	0.00160
0.65	0.02454	0.00160
0.66	0.02544	0.00160
0.67	0.02633	0.00160
0.68	0.02723	0.00160
0.69	0.02812	0.00160
0.70	0.02902	0.00160
0.71	0.02991	0.00160
0.72	0.03081	0.00160
0.73	0.03171	0.00160
0.74	0.03260	0.00160
0.75	0.03350	0.00160
0.76	0.03439	0.00160
0.77	0.03529	0.00160
0.78	0.03619	0.00160
0.79	0.03708	0.00160
0.80	0.03798	0.00160
0.81	0.03887	0.00160
0.82	0.03977	0.00160
0.83	0.04066	0.00160
0.84	0.04156	0.00160
0.85	0.04246	0.00160

0.86 0.04335 0.00160
0.87 0.04425 0.00160
0.88 0.04514 0.00160
0.89 0.04604 0.00160
0.90 0.04694 0.00160
0.91 0.04783 0.00160
0.92 0.04873 0.00160
0.93 0.04962 0.00160
0.94 0.05052 0.00160
0.95 0.05141 0.00160
0.96 0.05231 0.00160
0.97 0.05321 0.00160
0.98 0.05410 0.00160
0.99 0.05500 0.00000

KRTYPE CON 2

** ----------

** Adsorption Data
** ----------

ADSCOMP 'SURF' WATER
ADSLANG
20500 0 100200

ADMAXT
3.37E-6

ADRT
3.37E-6

```
ADSCOMP 'POLYMER' WATER
ADSLANG
102960          0          1.00E+07

ADMAXT
8.97747E-09

ADRT
8.97747E-09

PORFT 0.8

** ================= INITIAL CONDITIONS ====== ============== **
INITIAL
VERTICAL OFF

**INITREGION 1
PRES CON 1200
TEMP CON 70

** Initial saturation

SW CON
0.15

SO CON
0.85

MFRAC_OIL 'DEAD_OIL' CON 1
MFRAC_WAT 'H2O' CON 0.98079
MFRAC_WAT 'Na' CON 0.00885
MFRAC_WAT 'Cl' CON 0.01036
```

```
MFRAC_WAT 'SURF' CON 0
MFRAC_WAT 'POLYMER' CON 0


** ================= NUMERICAL CONTROL ====================== **

NUMERICAL
TFORM SXY
ISOTHERMAL



** ================  RECURRENT DATA  ====================== **

RUN
TIME 0
DTWELL 0.01
DTMAX 1

WELL 'INJTR'
INJECTOR UNWEIGHT 'INJTR'
**                 'H2O' 'Na' 'Cl' 'SURF' 'POLYMER  'DEAD_OIL'
INCOMP WATER 0.98079  0.00885          0.01036          0 0  0
OPERATE MAX STW 0.10 CONT

**      rad  geofac  wfrac  skin
GEOMETRY  K  0.01  0.249  1.  0.
PERF  TUBE-END  'INJTR'
** UBA    ff  Status  Connection
   1 1 1  1.  OPEN    FLOW-FROM  'SURFACE'

WELL 'PRODN'
```

```
PRODUCER 'PRODN'
OPERATE MIN BHP 1200 CONT REPEAT

**      rad  geofac  wfrac  skin
GEOMETRY  K  0.01  0.249  1.  0.
PERF  TUBE-END  'PRODN'
** UBA      ff  Status  Connection
   100 1 1  1.  OPEN    FLOW-TO  'SURFACE'

TIME 1
TIME 803

WELL 'INJTR'
INJECTOR UNWEIGHT 'INJTR'
**                'H2O' 'Na' 'Cl' 'SURF'  'POLYMER'   'DEAD_OIL'
INCOMP WATER 0.997220 0.00139 0.00139 0   0   0
OPERATE MAX STW 0.10 CONT

TIME 1139

WELL 'INJTR'
INJECTOR UNWEIGHT 'INJTR'
**                'H2O' 'Na' 'Cl' 'SURF'  'POLYMER'   'DEAD_OIL'
INCOMP WATER 0.996793 0.00139 0.00139 0.000427   0   0
OPERATE MAX STW 0.1 CONT

TIME 1307

WELL 'INJTR'
INJECTOR UNWEIGHT 'INJTR'
**                'H2O' 'Na' 'Cl' 'SURF'  'POLYMER'   'DEAD_OIL'
INCOMP WATER 0.99721662 0.00139 0.00139 0  3.38E-06   0
```

```
OPERATE MAX STW 0.1 CONT

TIME 1478.36

WELL 'INJTR'
INJECTOR UNWEIGHT 'INJTR'
**                'H2O' 'Na' 'Cl' 'SURF'  'POLYMER'   'DEAD_OIL'
INCOMP WATER 0.997220 0.00139 0.00139 0   0   0
OPERATE MAX STW 0.1 CONT

TIME 4831
STOP
```

References

1. Teigland, R. and J. Kleppe, *EOR Survey in the North Sea*, in *SPE/DOE Symposium on Improved Oil Recovery, 22-26 April, Tulsa, Oklahoma, USA*. 2006, Society of Petroleum Engineers, doi.org/10.2118/99546-MS.
2. Lien, J.R., M. Jakobsen, and A. Skauge, *PTEK100, Introduksjon til petroleums- og prosessteknologi*. 2007, Bergen: University of Bergen. 99.
3. Craig, F.F., *The reservoir engineering aspects of waterflooding*. Henry L. Doherty series. Vol. 3. 1971, New York: Henry L. Doherty Memorial Fund of AIME.
4. Zolotukhin, A.B.a.U., J.R., *Introduction to Petroleum Reservoir Engineering*. 2000: Høyskoleforlaget, Norwegian Academic Press.
5. Anderson, W.G., *Wettability Literature Survey- Part 4: Effects of Wettability on Capillary Pressure.* 1987. **39**(10): p. 1,283 - 1,300, doi.org/10.2118/15271-PA.
6. Lake, L.W., *Enhanced Oil Recovey*. 1989: Englewood Cliffs, N.J., Prentice Hall.
7. Willhite, G.P., *Waterflooding*, ed. S.o.P. Engineers. Vol. v.3. 1986, Richardson, TX: Society of Petroleum Engineers. 326, Print ISBN: 9781555630058.
8. Skarestad, M. and A. Skauge, *PTEK213 Reservoarteknikk II*. 2012, Bergen: University of Bergen. 220.
9. Brownell, L.E. and D.L. Katz, *Flow of Fluids Through Porous Media, Part II, Simultaneous Flow of Two Homogeneous Phases.* Chem. Eng. Progr., 1947. **43**: p. 601-612.
10. Stegemeier, G.L., *MECHANISMS OF ENTRAPMENT AND MOBILIZATION OF OIL IN POROUS MEDIA - SHAH, D.O*, in *Improved Oil Recovery by Surfactant and Polymer Flooding*, R.S. Schechter, Editor. 1977, Academic Press. p. 55-91, https://doi.org/10.1016/B978-0-12-641750-0.50007-4.
11. Chatzis, I. and N.R. Morrow, *Correlation of Capillary Number Relationships for Sandstone.* 1984. **24**(05): p. 555 - 562, doi.org/10.2118/10114-PA.
12. Mohanty, K.K., *Multiphase Flow in Porous Media: III. Oil Mobilization, Transverse Dispersion, and Wettability*, in *SPE Annual Technical Conference and Exhibition, 5-8 October, San Francisco, California*. 1983, Society of Petroleum Engineers, https://doi.org/10.2118/12127-MS.
13. Gupta, S.P. and S.P. Trushenski, *Micellar Flooding - Compositional Effects on Oil Displacement.* 1979. **19**(02): p. 116 - 128, https://doi.org/10.2118/7063-PA.

14. Smith, K.W., *Brines as Flooding Liquids.* Paper presented at 7th Annual Technical Meeting, Min. Ind. Expt. Sta., Penn. State College. , 1942.
15. Bernard, G.G., *Effect of Floodwater Salinity on Recovery Of Oil from Cores Containing Clays*, in *SPE California Regional Meeting, 26-27 October, Los Angeles, California*. 1967, Society of Petroleum Engineers, https://doi.org/10.2118/1725-MS.
16. Jadhunandan, P.P. and N.R. Morrow, *Effect of Wettability on Waterflood Recovery for Crude-Oil/Brine/Rock Systems.* 1995. **10**(01): p. 40 - 46, https://doi.org/10.2118/22597-PA.
17. Yildiz, H.O. and N.R. Morrow, *Effect of brine composition on recovery of Moutray crude oil by waterflooding.* Journal of Petroleum Science and Engineering, 1996. **14**(3): p. 159-168, doi.org/10.1016/0920-4105(95)00041-0.
18. Morrow, N.R., M. Valat, and H. Yidliz, *Effect of Brine Composition On Recovery of an Alaskan Crude Oil By Waterflooding*, in *Annual Technical Meeting, June 10 - 12, Calgary, Alberta*. 1996, Petroleum Society of Canada, https://doi.org/10.2118/96-94.
19. Yildiz, H.O., M. Valat, and N.R. Morrow, *Effect of Brine Composition On Wettability And Oil Recovery of a Prudhoe Bay Crude Oil.* 1999. **38**(01): p. https://doi.org/10.2118/99-01-02.
20. Tang, G.-Q. and N.R. Morrow, *Influence of brine composition and fines migration on crude oil/ brine/ rock interactions and oil recovery.* Journal of Petroleum Science and Engineering, 1999. **24**(2-4): p. 99-111, doi.org/10.1016/S0920-4105(99)00034-0.
21. Filoco, P.R. and M.M. Sharma, *Effect of Brine Salinity and Crude Oil Properties on Relative Permeabilities and Residual Saturations*, in *SPE Annual Technical Conference and Exhibition, 27-30 September, New Orleans, Louisiana*. 1998, Society of Petroleum Engineers, https://doi.org/10.2118/49320-MS.
22. Sharma, M.M. and P.R. Filoco, *Effect of Brine Salinity and Crude-Oil Properties on Oil Recovery and Residual Saturations.* 2000. **5**(03): p. 293 - 300, https://doi.org/10.2118/65402-PA.
23. Zhang, Y. and N.R. Morrow, *Comparison of Secondary and Tertiary Recovery With Change in Injection Brine Composition for Crude-Oil/Sandstone Combinations*, in *SPE/DOE Symposium on Improved Oil Recovery, 22-26 April, Tulsa, Oklahoma, USA*. 2006, Society of Petroleum Engineers, https://doi.org/10.2118/99757-MS.
24. Agbalaka, C., et al., *Coreflooding Studies to Evaluate the Impact of Salinity and Wettability on Oil Recovery Efficiency.* Transport in Porous Media, 2009. **76**(1): p. 77-94, doi.org/10.1007/s11242-008-9235-7.

25. Lager, A., et al., *Low Salinity Oil Recovery - An Experimental Investigation.* 2008. **49**(01): p. 28-35.
26. Shaker Shiran, B. and A. Skauge, *Wettability and Oil Recovery by Low Salinity Injection*, in *SPE EOR Conference at Oil and Gas West Asia, 16-18 April, Muscat, Oman*. 2012, Society of Petroleum Engineers, https://doi.org/10.2118/155651-MS.
27. Webb, K.J., C.J.J. Black, and H. Al-Ajeel, *Low Salinity Oil Recovery - Log-Inject-Log*, in *SPE/DOE Symposium on Improved Oil Recovery, 17-21 April, Tulsa, Oklahoma*. 2004, Society of Petroleum Engineers, https://doi.org/10.2118/89379-MS.
28. Tang, G.Q. and N.R. Morrow, *Salinity, Temperature, Oil Composition, and Oil Recovery by Waterflooding.* 1997. **12**(04): p. 269 - 276, https://doi.org/10.2118/36680-PA.
29. Morrow, N.R., et al., *Prospects of improved oil recovery related to wettability and brine composition.* Journal of Petroleum Science and Engineering, 1998. **20**(3): p. 267-276, https://doi.org/10.1016/S0920-4105(98)00030-8.
30. McGuire, P.L., et al., *Low Salinity Oil Recovery: An Exciting New EOR Opportunity for Alaska's North Slope*, in *SPE Western Regional Meeting, 30 March-1 April, Irvine, California*. 2005, Society of Petroleum Engineers, https://doi.org/10.2118/93903-MS.
31. Vledder, P., et al., *Low Salinity Water Flooding: Proof Of Wettability Alteration On A Field Wide Scale*, in *SPE Improved Oil Recovery Symposium, 24-28 April, Tulsa, Oklahoma, USA*. 2010, Society of Petroleum Engineers, https://doi.org/10.2118/129564-MS.
32. Seccombe, J., et al., *Demonstration of Low-Salinity EOR at Interwell Scale, Endicott Field, Alaska*, in *SPE Improved Oil Recovery Symposium, 24-28 April, Tulsa, Oklahoma, USA*. 2010, Society of Petroleum Engineers, https://doi.org/10.2118/129692-MS.
33. Jerauld, G.R., et al., *Modeling Low-Salinity Waterflooding*, in *SPE Annual Technical Conference and Exhibition*. 2006, Society of Petroleum Engineers: San Antonio, Texas, USA. p. 1,000 - 1,012, https://doi.org/10.2118/102239-PA.
34. Wu, Y.-S. and B. Bai, *Efficient Simulation for Low Salinity Waterflooding in Porous and Fractured Reservoirs*, in *SPE Reservoir Simulation Symposium, 2-4 February, The Woodlands, Texas*. 2009, Society of Petroleum Engineers, https://doi.org/10.2118/118830-MS.

35. Omekeh, A.V., et al., *Modeling of Ion-Exchange and Solubility in Low Salinity Water Flooding*, in *SPE Improved Oil Recovery Symposium, 14-18 April, Tulsa, Oklahoma, USA*. 2012, Society of Petroleum Engineers, https://doi.org/10.2118/154144-MS.
36. Dang, C.T.Q., et al., *Modeling Low Salinity Waterflooding: Ion Exchange, Geochemistry and Wettability Alteration*, in *SPE Annual Technical Conference and Exhibition, 30 September-2 October, New Orleans, Louisiana, USA*. 2013, Society of Petroleum Engineers, https://doi.org/10.2118/166447-MS.
37. Kazemi Nia Korrani, A., G.R. Jerauld, and K. Sepehrnoori, *Coupled Geochemical-Based Modeling of Low Salinity Waterflooding*, in *SPE Improved Oil Recovery Symposium, 12-16 April, Tulsa, Oklahoma, USA*. 2014, Society of Petroleum Engineers, https://doi.org/10.2118/169115-MS.
38. Berg, J.C., *An Introduction to Interfaces & Colloids, The Bridge to Nanoscience*. 4th ed. 2015: World Scientific Publishing Co. Pte. LTD. p. 30-37, 137-148.
39. Winsor, P.A., *Solvent properties of amphiphilic compounds*. 1954, London: Butterworth's Scientific Publications.
40. Reed, R.L. and R.N. Healy, *SOME PHYSICOCHEMICAL ASPECTS OF MICROEMULSION FLOODING: A REVIEW A*, in *Improved Oil Recovery by Surfactant and Polymer Flooding*, R.S. Schechter and D.O. SHAH, Editors. 1977, Academic Press. p. 383-437, doi.org/10.1016/B978-0-12-641750-0.50017-7.
41. Huh, C., *Interfacial tensions and solubilizing ability of a microemulsion phase that coexists with oil and brine.* Journal of Colloid and Interface Science, 1979. **71**(2): p. 408-426, doi.org/10.1016/0021-9797(79)90249-2.
42. Somasundaran, P. and H.S. Hanna, *PHYSICO–CHEMICAL ASPECTS OF ADSORPTION AT SOLID/LIQUID INTERFACES: I. Basic Principles A2 - SHAH, D.O*, in *Improved Oil Recovery by Surfactant and Polymer Flooding*, R.S. Schechter, Editor. 1977, Academic Press. p. 205-251, doi.org/10.1016/B978-0-12-641750-0.50012-8.
43. Sorbie, K.S., *Polymer-Improved Oil Recovery*. 1991, Boca Raton, Florida: CRC Press, Inc. 359.
44. Sheng, J.J., *Chapter 5 - Polymer Flooding*, in *Modern Chemical Enhanced Oil Recovery*. 2011, Gulf Professional Publishing: Boston. p. 101-206, doi.org/10.1016/B978-1-85617-745-0.00005-X.

45. Smith, F.W., *The Behavior of Partially Hydrolyzed Polyacrylamide Solutions in Porous Media.* Journal of Petroleum Technology, SPE-2422-PA, 1970. **22**(2): p. 148 - 156, https://doi.org/10.2118/2422-PA.
46. Alagic, E. and A. Skauge, *Combined Low Salinity Brine Injection and Surfactant Flooding in Mixed−Wet Sandstone Cores.* Energy & Fuels, 2010. **24**(6): p. 3551-3559, doi.org/10.1021/ef1000908.
47. Alagic, E., et al., *Effect of crude oil ageing on low salinity and low salinity surfactant flooding.* Journal of Petroleum Science and Engineering, 2011. **78**(2): p. 220-227, https://doi.org/10.1016/j.petrol.2011.06.021.
48. Spildo, K., A.M. Johannessen, and A. Skauge, *Low Salinity Waterflood at Reduced Capillarity*, in *SPE Improved Oil Recovery Symposium, 14-18 April, Tulsa, Oklahoma, USA*. 2012, Society of Petroleum Engineers, doi.org/10.2118/154236-MS. p. doi.org/10.2118/154236-MS.
49. Ayirala, S.C., et al., *A Designer Water Process for Offshore Low Salinity and Polymer Flooding Applications*, in *SPE Improved Oil Recovery Symposium, 24-28 April, Tulsa, Oklahoma, USA*. 2010, Society of Petroleum Engineers. p. 12, https://doi.org/10.2118/129926-MS.
50. Shaker Shiran, B. and A. Skauge, *Enhanced Oil Recovery (EOR) by Combined Low Salinity Water/Polymer Flooding.* Energy & Fuels, 2013. **27**(3): p. 1223-1235, doi.org/10.1021/ef301538e.
51. Vermolen, E.C.M., et al., *Low-Salinity Polymer Flooding: Improving Polymer Flooding Technical Feasibility and Economics by Using Low-Salinity Make-up Brine*, in *International Petroleum Technology Conference, 19-22 January, Doha, Qatar*. 2014, https://doi.org/10.2523/IPTC-17342-MS.
52. Kallevik, G.S., *Implementations of Methods for Modeling Low Salinity Waterflood and Low Salinity Surfactant Flooding*, in *Department of Chemistry*. 2010, University of Bergen: UNI Research CIPR. p. 143.
53. Skauge, A., Z. Ghorbani, and M. Delshad, *Simulation of Combined Low Salinity Brine and Surfactant Flooding*, in *16th European Symposium on Improved Oil Recovery, 12-14 April*. 2011, Cambridge, UK.
54. Mohammadi, H. and G. Jerauld, *Mechanistic Modeling of the Benefit of Combining Polymer with Low Salinity Water for Enhanced Oil Recovery*, in *SPE Improved Oil Recovery Symposium, 14-18 April, Tulsa, Oklahoma, USA*. 2012, Society of Petroleum Engineers, https://doi.org/10.2118/153161-MS.

55. Jerauld, G.R., et al., *Modeling Low-Salinity Waterflooding.* 2008. **11**(06): p. 1,000 - 1,012, doi.org/10.2118/102239-PA.
56. Skauge, A., *Modelling of Hybrid Waterflood EOR Processes.* 18th European Symposium on Improved Oil Recovery in Dresden, Germany, 16th April, 2015.
57. Drønen, I., *Modelling of Waterflood Hybrid EOR*, in *Department of Physics and Technology, Centre for Integrated Petroleum Research*. 2015, University of Bergen.
58. Tavassoli, S., et al., *Low-Salinity Surfactant Flooding—A Multimechanistic Enhanced-Oil-Recovery Method.* 2016. **21**(03): p. 744 - 760, https://doi.org/10.2118/173801-PA.
59. Khorsandi, S., C. Qiao, and R.T. Johns, *Displacement Efficiency for Low-Salinity Polymer Flooding Including Wettability Alteration.* 2017. **22**(02): p. 417 - 430, https://doi.org/10.2118/179695-PA.
60. *STARS User's Guide.* 2016.
61. Corey, A.T., *The interrelation between gas and oil relative permeabilities.* Producers monthly, 1954. **19**(1): p. 38-41.
62. Morrow, N.R., *Wettability and Its Effect on Oil Recovery.* 1990. **42**(12): p. 1,476 - 1,484, https://doi.org/10.2118/21621-PA.
63. Mungan, N., *Role of Wettability and Interfacial Tension in Water Flooding.* Society of Petroleum Engineers, 1964. **4**(02): p. 115 - 123, https://doi.org/10.2118/705-PA.
64. Anderson, W.G., *Wettability Literature Survey-Part 6: The Effects of Wettability on Waterflooding.* Journal of Petroleum Technology, 1987. **39**(12): p. 1,605 - 1,622, https://doi.org/10.2118/16471-PA.
65. Salathiel, R.A., *Oil Recovery by Surface Film Drainage In Mixed-Wettability Rocks.* Journal of Petroleum Technology, 1973. **25**(10): p. 1,216 - 1,224, https://doi.org/10.2118/4104-PA.
66. Zhang, Y., X. Xie, and N.R. Morrow, *Waterflood Performance By Injection Of Brine With Different Salinity For Reservoir Cores*, in *SPE Annual Technical Conference and Exhibition, 11-14 November, Anaheim, California, U.S.A.* 2007, Society of Petroleum Engineers, https://doi.org/10.2118/109849-MS.
67. Fanchi, J.R., *Multidimensional Numerical Dispersion.* 1983. **23**(01): p. 143 - 151, https://doi.org/10.2118/9018-PA.
68. Ewing, R.E. and R.F. Heinemann, *Incorporation of Mixed Finite Element Methods in Compositional Simulation for Reduction of Numerical Dispersion*, in *SPE Reservoir*

Simulation Symposium, 15-18 November, San Francisco, California. 1983, Society of Petroleum Engineers, https://doi.org/10.2118/12267-MS.

69. Mahadevan, J., L.W. Lake, and R.T. Johns, *Estimation of True Dispersivity in Field Scale Permeable Media*, in *SPE/DOE Improved Oil Recovery Symposium, 13-17 April, Tulsa, Oklahoma*. 2002, Society of Petroleum Engineers, https://doi.org/10.2118/75247-MS.
70. Van Quy, N. and J. Labrid, *A Numerical Study of Chemical Flooding Comparison With Experiments.* 1983. **23**(03): p. 461-474, https://doi.org/10.2118/10202-PA.
71. Amaefule, J.O. and L.L. Handy, *The Effect of Interfacial Tensions on Relative Oil/Water Permeabilities of Consolidated Porous Media.* 1982. **22**(03): p. 371-381, https://doi.org/10.2118/9783-PA.
72. Zaitoun, A. and N. Kohler, *The Role of Adsorption in Polymer Propagation Through Reservoir Rocks*, in *SPE International Symposium on Oilfield Chemistry, 4-6 February, San Antonio, Texas*. 1987, Society of Petroleum Engineers, https://doi.org/10.2118/16274-MS.
73. Dawson, R. and R.B. Lantz, *Inaccessible Pore Volume in Polymer Flooding.* 1972. **12**(05): p. 448 - 452, https://doi.org/10.2118/3522-PA.